

Grasp Stability Analysis with Passive Reactions

Maximilian Haas-Heger

Submitted in partial fulfillment of the
requirements for the degree of
Doctor of Philosophy
under the Executive Committee
of the Graduate School of Arts and Sciences

COLUMBIA UNIVERSITY

© 2021

Maximilian Haas-Heger

All Rights Reserved

Abstract

Grasp Stability Analysis with Passive Reactions

Maximilian Haas-Heger

Despite decades of research robotic manipulation systems outside of highly structured industrial applications are still far from ubiquitous. Perhaps particularly curious is the fact that there appears to be a large divide between the theoretical grasp modeling literature and the practical manipulation community. Specifically, it appears that the most successful approaches to tasks such as pick-and-place or grasping in clutter are those that have opted for simple grippers or even suction systems instead of dexterous multi-fingered platforms.

We argue that the reason for the success of these simple manipulation systems is what we call *passive stability*: passive phenomena due to nonbackdrivable joints or underactuation allow for robust grasping without complex sensor feedback or controller design. While these effects are being leveraged to great effect, it appears the practical manipulation community lacks the tools to analyze them. In fact, we argue that the traditional grasp modeling theory assumes a complexity that most robotic hands do not possess and is therefore of limited applicability to the robotic hands commonly used today.

We discuss these limitations of the existing grasp modeling literature and set out to develop our own tools for the analysis of passive effects in robotic grasping. We show that problems of this kind are difficult to solve due to the non-convexity of the *Maximum Dissipation Principle* (MDP), which is part of the Coulomb friction law. We show that for planar grasps the MDP can be decomposed into a number of piecewise convex problems, which can be solved for efficiently. We show that the number of these piecewise convex problems is quadratic in the number of contacts and develop a polynomial time algorithm for their enumeration. Thus, we present the first polynomial runtime algorithm for the determination of passive stability of planar grasps.

For the special case we present the first grasp model that captures passive effects due to non-backdrivable actuators and underactuation. Formulating the grasp model as a Mixed Integer Pro-

gram we illustrate that a consequence of omitting the maximum dissipation principle from this formulation is the introduction of solutions that violate energy conservation laws and are thus unphysical. We propose a physically motivated iterative scheme to mitigate this effect and thus provide the first algorithm that allows for the determination of passive stability for spacial grasps with both fully actuated and underactuated robotic hands. We verify the accuracy of our predictions with experimental data and illustrate practical applications of our algorithm.

We build upon this work and describe a convex relaxation of the Coulomb friction law and a successive hierarchical tightening approach that allows us to find solutions to the exact problem including the maximum dissipation principle. It is the first grasp stability method that allows for the efficient solution of the passive stability problem to arbitrary accuracy. The generality of our grasp model allows us to solve a wide variety of problems such as the computation of optimal actuator commands. This makes our framework a valuable tool for practical manipulation applications. Our work is relevant beyond robotic manipulation as it applies to the stability of any assembly of rigid bodies with frictional contacts, unilateral constraints and externally applied wrenches.

Finally, we argue that with the advent of data-driven methods as well as the emergence of a new generation of highly sensorized hands there are opportunities for the application of the traditional grasp modeling theory to fields such as robotic in-hand manipulation through model-free reinforcement learning. We present a method that applies traditional grasp models to maintain quasi-static stability throughout a nominally model-free reinforcement learning task. We suggest that such methods can potentially reduce the sample complexity of reinforcement learning for in-hand manipulation.

Table of Contents

Chapter 1: Introduction	1
1.1 Background	1
1.2 Contributions	4
1.3 Dissertation outline	5
Chapter 2: Related Work	6
2.1 Grasp force analysis	7
2.1.1 Force closure and stability	7
2.1.2 Methods assuming full contact wrench control	8
2.1.3 Compliance methods	10
2.1.4 Quality metrics	11
2.1.5 Discussion	12
2.2 Rigid body methods	14
2.2.1 Rigid body mechanics	14
2.2.2 Rigid body dynamics	16
2.2.3 Discussion	18
2.3 Dexterous in-hand manipulation	20
Chapter 3: Grasp stability analysis — Theory and Praxis	22

3.1	A representative example problem	26
Chapter 4: Grasp Stability Analysis in Two Dimensions and Polynomial Time		29
4.1	Introduction	29
4.2	Grasp model	31
4.3	Definition of stability	34
4.4	Solving for stability given contact states	35
4.5	Number of possible contact states	37
4.6	Contact state enumeration	41
4.7	Complete stability determination procedure	44
4.8	Applications to planar grasp stability analysis	45
4.9	Discussion	48
Chapter 5: Grasp Stability Analysis in Three Dimensions		52
5.1	Introduction	52
5.2	Grasp model	53
5.3	Formulation as a Mixed Integer Program	59
5.3.1	Unilaterality	59
5.3.2	Friction	61
5.4	Iterative solution approach	63
5.5	Application to grasp analysis in three dimensions	66
5.6	Discussion	75
Chapter 6: Grasp Stability Analysis with the Maximum Dissipation Principle		78

6.1	Introduction	78
6.2	A formulation using McCormick envelopes	80
6.3	Convex relaxation of the Coulomb friction law	82
6.4	Successive hierarchical refinement	87
6.5	Robustness to geometrical uncertainties	92
6.6	Application to grasp analysis in three dimensions	95
6.6.1	Existence problems	95
6.6.2	Space of resistible disturbances	97
6.6.3	Actuator command optimization	102
6.6.4	Computational performance	105
6.7	Discussion	111
Chapter 7: Grasp Stability Analysis for Reinforcement Learning of in-hand manipulation		114
7.1	Introduction	114
7.2	In-hand manipulation with pure reinforcement learning	116
7.2.1	Experimental design	116
7.2.2	Results	118
7.3	Islands and Bridges: An equivalent problem?	122
7.4	Constructing a shield for in-hand manipulation	128
7.4.1	Grasp stability constraints	128
7.4.2	Grasp model	129
7.4.3	Complete shield formulation	134
7.5	Future work	135

Chapter 8: Conclusions	137
8.1 Contributions	137
8.2 Potential impact	140
8.3 Challenges	141
8.4 Future work	142
References	145

Chapter 1: Introduction

1.1 Background

Since the introduction of the first robotic manipulation systems they have almost exclusively been confined to specialized spaces. This is true both in the physical space (as to guarantee the safety of humans in the vicinity) and the task space. The environments they work in are structured and engineers design the tools that robots use specifically for a single task. This allows for the application of robots in highly repetitive tasks where each task instance is exactly the same as every other instance.

This paradigm could not be farther removed from the environment us humans experience. Our everyday environments are complex, unstructured and cluttered. While some tasks may seem repetitive to a human, instances are never exactly alike. Attempting to bridge this divide and enabling robotic manipulators to become helpful in human spaces is perhaps the most important issue facing the field of robotic manipulation today.

While to date no manipulation system has found success in regular human environments, efforts at breaching the limitations and introducing functional robots to everyday environments and tasks are ongoing. The advent of soft robotics and passively compliant hands has enabled the grasping of isolated objects. Advances made in computer vision over the last two decades allowed for significant progress to be made towards solving pick-and-place tasks in clutter. However, there remains a distinct lack of dexterity. In fact it appears that the most successful methods for picking objects from clutter leverage suction grippers instead of multi-fingered hands [1][2][3][4]. These methods practically reduce the grasping problem to one of computer vision as they are concerned with identifying surfaces on which to place the suction gripper and do not require grasp planning or contact modeling.

The majority of works focusing on practical applications of multi-fingered hands view grasping as the task of placing contacts in order to fulfill a given task. Despite the advent of practical tactile sensing technology little attention is being paid to the explicit control of contact forces, which is a defining characteristic of the human manipulation experience. There is a wealth of work into the theoretical foundations and the mechanics of grasping that aim to provide the understanding of the intricate relationship between contact forces and actuation that is required for truly dexterous manipulation. However, none of the popular practical manipulation methods [5][6][7][8][9][10] make use of those theoretical works. In fact, interest in theoretical grasp modeling seems to have waned since the early 2000s.

It appears as though the most progress towards dexterous multi-fingered manipulation has been made in fields, which have only become established relatively recently compared to the bulk of the manipulation literature. The fields in question are those of Deep Learning and Reinforcement Learning. There is promising work indicating that neural network policies can be trained to process the vast amounts of sensor data and manipulate objects with more and more dexterity [11][12].

It strikes the author as fascinating, that the foundational works of grasp modeling appear to have been largely forgotten while large impact results are obtained using entirely model-free techniques. We believe there are two potential reasons for this:

1. The theoretical works on multi-fingered grasping and unilateral contact modeling did not capture some important aspect of grasping, made the wrong assumptions or are too computationally complex to be of practical use;
2. The theoretical works are unknown to the practitioners in the learning community or their usefulness has not yet been discovered.

We do believe that the first point above as to why the grasping theory has not been widely adopted by the manipulation community has at least some truth to it. In Chapter 2 we will discuss in detail the different theoretical approaches and their limitations in modeling modern robotic hands. In short the majority of the grasp modeling literature introduces the assumption that the

contact wrenches¹ of a grasp can be somehow actively controlled in real time and in reaction to disturbances applied to the grasped object.

In practice this assumptions means that the robotic hand must be fully actuated, highly articulated, and equipped with torque or tactile sensors. Robotic hands of such complexity are few in number and rarely used in practice. For reasons we will discuss in Chapter 3 the majority of robotic hands in use today either lack the kinematics, the actuation scheme or sensing ability to be able to actively modulate contact wrenches. This means that in practice we rarely explicitly reason about the contact wrenches when grasping objects with robotic hands. Instead, we rely on either of two entirely passive effects:

Firstly, there is passive compliance as showcased by underactuated hands or soft hands. While these hands are complex in their own right they trade off real-time control of contact wrenches in favor of a priori design complexity. The second effect is more subtle and applies to all hands with highly-g geared actuators and thus nonbackdrivable joints. Large gearing ratios between the actuators and the joints coupled with the friction present in the gearbox mean the fingers cannot be moved through forces applied externally to the finger. This means that fingers can provide potentially rigid constraints for the grasped object — namely when the object is being pushed against that finger by the applied wrench or contact wrenches from other fingers. While these passive effects greatly reduce the complexity of control for grasping tasks they cannot be analyzed using tools derived from the traditional grasping theory.

In Chapter 3 we will provide an explanation as to why the design of robotic hands has diverged so far from the theory developed in order to model robotic grasping. However, with the increased interest in machine learning for dexterous manipulation there is also renewed interest into highly complex hands. Reinforcement learning is a promising candidate for the synthesis of the highly complex controllers required for truly dexterous manipulation. Such controllers — or policies — require enormous amounts of data and thus robotic hands providing various modes of sensing technology are being developed. We believe that with these new hands much of the classical

¹A wrench is a contraction of a force and a torque.

grasping theory will become relevant again. However, it appears that its potential has not yet been realized by the learning community.

1.2 Contributions

As we argue above the lack of ability to model the passive effects provided by modern robotic hands is one of the most important limitations that have stymied the success of the grasping theory in practical robotic manipulation. To the best of the author’s knowledge there is no explicit mention of the implications of nonbackdrivable joints in the literature even though robotic hands with such properties appear in the majority of practical manipulation works. We thus develop our own methods of analyzing grasps with passive effects. Specifically, we are interested in predicting the stability of grasps as well as the contact forces that arise due to actuation forces or wrenches otherwise applied to the grasp.

- We begin by investigating the passive stability of planar grasps and develop a novel polynomial-time algorithm that makes use of results from computational geometry. We improve on previous approaches that did not incorporate accurate frictional constraints including the maximum dissipation principle. As such, we introduce the first 2D grasp model with Coulomb friction for grasp stability analysis that is solvable in provably polynomial time.
- Moving on to spacial grasps we show that omission of the maximum dissipation principle introduces unphysical solutions. We thus present a physically motivated iterative algorithm that mitigates this effect. While the algorithm is not guaranteed to converge, we verify its accuracy with empirical data.
- In order to obtain an algorithm that is guaranteed to converge we introduce a novel contact model that allows us to efficiently solve for contact forces obeying Coulomb friction including the maximum dissipation principle. Specifically, we introduce a convex relaxation of the Coulomb friction model and an algorithm for the hierarchical successive tightening of the

relaxation. Our method is guaranteed to converge to the exact solution and is sufficiently efficient for the analysis of practical grasps.

- We apply our algorithms to answer for the first time grasp stability queries that take into account the passive behavior of the robotic hand. These results provide examples of possible applications of our framework to practical manipulation tasks. We make implementations of the grasp models and algorithms for spacial grasps publicly available as part of the open source GraspIt! simulator [13].
- With the more recent drive towards more dexterous manipulation by the deep learning community, there is renewed demand for highly sensorized hands and we believe the rich grasping theory that has mostly been forgotten by the manipulation community is once again becoming relevant. Our final contribution is an excursion into a potential application of theoretical grasp models in ordinarily model-free reinforcement learning of in-hand manipulation.

1.3 Dissertation outline

We begin by providing a broad summary of the grasp models and theories developed by the manipulation community in Chapter 2, taking a closer look at some of these works, which we find to be most pertinent to the manipulation problems the field faces today. Furthermore, we will introduce some of the more recent work demonstrating dexterous manipulation - specifically reinforcement learning for in-hand manipulation.

What follows are the technical chapters of this dissertation. Beginning with our work on grasp modeling in two dimensions presented in Chapter 4 we then move our attention to problems in three dimensions in Chapters 5 & 6. We will discuss some preliminary results of our ongoing work investigating the applications of grasp stability analysis to reinforcement learning of in-hand manipulation tasks in Chapter 7.

Finally, we provide concluding remarks in Chapter 8.

Chapter 2: Related Work

Examining the problems the dexterous manipulation community is working on today — multi-fingered grasping, pick-and-place, in-hand manipulation, regrasping, teleoperation, etc. — they all share one requirement: the ability to move a grasped object in a desired manner. In manipulation this most often means maintaining a robust grasp on the object. Thus, the stability of a grasp is a foundational prerequisite to many forms of dexterous manipulation.

There is no singular agreed-upon definition of grasp stability in the literature [14][15]. Stability might be simply defined as the existence of equilibrium contact wrenches that obey some friction law. This is quite different from the notion of stability in control theory, which distinguishes between stable, unstable and marginally stable equilibria. In some works the notion of grasp stability also includes treatment of some region around an original equilibrium state and is thus similar to that of asymptotic stability commonly encountered in control theory, which denotes a system that returns to its original state after a small perturbation is applied in an equilibrium state. Other works use a broader definition of stability: Contacts may slip leading to the dissipation of energy such that a system will not, in general, return to its initial state after a small perturbation. Such a grasp may, however, still be considered stable if it reaches a new equilibrium point where the grasped object is relatively at rest with respect to the hand.

Furthermore, some works make use of the quasi-static assumption (all motions are assumed to be slow enough such that effects due to inertia can be neglected) while others use the full dynamic equations of motion in their treatment of grasp stability. The exact definition of grasp stability heavily depends on the context and the choices made by the researcher in modeling the grasp. However, they all have in common the study of contact forces and torques at the interfaces between a robotic hand and a grasped object.

2.1 Grasp force analysis

2.1.1 Force closure and stability

The class of *form closure* grasps is trivially stable as it consists of grasps in which the contacts totally immobilize the grasp object. Analysis of form closure grasps dates back to Reuleaux (1876) [16] who showed that for planar grasps a minimum of 4 frictionless contacts are required for form closure. For spacial form closure grasps Somov [17] and later Lakshminarayana [18] showed a minimum of 7 frictionless contacts are required. Another class of grasps is that of *force closure* grasps. These grasps are such that the hand can apply arbitrary wrenches to the object through the contacts. There is still disagreement over the exact definitions of the closures mentioned above. We choose to use the interpretation described by Bicchi and Kumar in their review on grasp and contact modeling [19].

Salisbury [20] proposed an analytical method to test for either form or force closure. However, perhaps the most commonly used method to test for force closure was introduced by Ferrari and Canny [21]. Their algorithm constructs the total space of possible resultant object wrenches that can be achieved by contact wrenches that obey (linearized) friction constraints and whose magnitudes sum to 1. They call this space the *Grasp Wrench Space* or GWS. The smallest distance from the origin to the convex hull of the wrenches making up the GWS is a measure of the magnitude of the contact wrenches required to balance a worst-case disturbance. Thus, it can also be used as a metric to quantify the *quality* of a grasp.

The characteristic of force closure is a necessary requirement for a grasp to be able to resist and therefore be stable with respect to arbitrary disturbances. Force closure is, however, by no means a sufficient condition — it just indicates the existence of contact wrenches that satisfy the friction laws that can balance arbitrary disturbances but does not guarantee they will arise [22]. The choice of specific grasp forces, or as Bicchi [23] calls it the *force distribution problem* is crucial for the stability of a grasp. Bicchi [23] defined two basic questions:

"a) when external forces act upon the manipulated object disturbing its equilibrium,

how do they distribute between the contacts, and

b) how can we modify the contact forces so as to achieve desirable values in spite of external disturbances."

2.1.2 Methods assuming full contact wrench control

A complicating factor in this analysis is the unilaterality of contacts in the context of robotic grasping — objects in contact may only 'push', not 'pull' on each other. Furthermore, contact wrenches are subject to friction laws such as the Coulomb friction model [24]; providing an upper bound to the ratio of friction force magnitude to normal force magnitude. If we can actively control the hand and its kinematics allow us to apply arbitrary wrenches at the contacts we can ensure that contact wrenches satisfy both unilaterality and the friction constraints at all times. Thus, this assumption greatly simplifies analysis and will be made by all of the works discussed in the rest of Chapter 2.1.2. In this context the question of grasp stability becomes that of finding contact wrenches that satisfy the friction law and equations of equilibrium.

A further complication is that in general robotic grasps are statically indeterminate (or hyperstatic). Even if a grasp has force closure it is difficult in general to synthesize stabilizing contact forces as there is an infinite number of internal stresses and hence equilibrium contact wrenches. Salisbury et al. [25] investigated the conditions for a grasp to become overconstrained for a variety of different contact types and was the first to express contact wrenches as the sum of a particular and a homogeneous solution. The physical interpretation of these solutions can respectively be described as the *manipulation forces* balancing the applied wrench and *internal forces* that do not directly contribute to resisting the applied wrench but cause internal stresses in the object. This decomposition allows for the synthesis of stabilizing contact wrenches given a grasp and an externally applied wrench. First, the particular solution must be computed. This can be done using a generalized inverse of the grasp map matrix relating contact wrenches to the overall resultant wrench the hand applies on the object. The computed manipulation forces will not in general satisfy unilaterality and friction constraints. Given the grasp has force closure an appropriate homogeneous

solution from the nullspace of the grasp map matrix can be added to obtain legal stabilizing contact wrenches.

This insight allowed Kerr et al. [26] to formulate the synthesis of contact wrenches as an optimization problem providing the foundation for the large body of work on grasp force optimization, which is concerned with finding optimal grasp forces in the space of contact forces possible under a friction law. Linearizing the friction constraints they propose solving a linear program in order to obtain contact wrenches that are as far as possible from violating the constraints already mentioned as well as additional constraints such as actuator torque limits or the dynamic range of tactile sensors. Nakamura et al. [27] used Lagrange multipliers to solve a nonlinear grasp force optimization problem. In contrast to Kerr et al. [26] they argue that contact wrenches should not be maximized for stability: As Cutkosky et al. [28] pointed out increasing grasp forces reduces the risk of slipping but may make the grasp less stable to disturbances. Therefore, they instead find the contact forces that minimize the internal forces but retain a certain level of contact robustness (i.e. are far enough from violating contact constraints.)

In order to avoid having to linearize the friction model Buss et al. [29] showed a different optimization formulation applicable when nonlinear friction constraints can be formulated as positive-definiteness constraints turning the optimization problem into a linear matrix inequality (LMI) problem. Their algorithm, however, requires a valid initial guess of contact wrenches and they do not discuss how to obtain such a guess. Han et al. [30] built upon this work and cast the grasp analysis problem as a set of convex optimization problems involving said LMIs thus eliminating the need for an initial guess. Boyd et al. [31] developed a custom interior-point algorithm that exploits the structure of force optimization problems and thus very efficiently solves such problems. In fact, the complexity of their algorithm is only linear in the number of contacts.

Jen et al. [14] take a control theoretic approach to grasp stability. Starting from a set of initial equilibrium contact wrenches they derive feedback controllers for the control of contact wrenches in response to motions of the grasped object such that the grasp remains asymptotically stable.

2.1.3 Compliance methods

An alternative method to resolve the static indeterminacy is to take into account the flexibility of the object and the elements of the hand. If we assume the hand to be a passive fixture we may solve for contact wrenches by taking into account the flexibility of the object and the fixture through constitutive equations. This also allows us to analyze grasps without the need to be able to control contact wrenches explicitly as we have in effect replaced unilaterality and the Coulomb friction law with a model linearly relating contact wrenches to displacements.

Salisbury [20] used this approach to develop a framework to test for the stability of a grasp. A grasp is stable if the stiffness matrix, which characterizes the behavior of the grasp under small perturbations is positive definite. Nguyen [32] modeled each contact as a spring (a method first introduced by Hanafusa et al. [33]) and showed that any force closure grasp can be made stable under this definition by choosing appropriate spring stiffnesses. Cutkosky et al. [34] extended this work to take into account the compliance of structural elements of the hand and object as well as effects due to changing geometry such as contact location changes due to rolling contacts. Adding also the compliance due to servo gains allows for active control of the overall grasp compliance.

Salisbury [35] pointed out that previous work had focused on manipulation using only the fingertips of the hand. They suggested using more of the surface of robotic manipulators, which Salisbury calls 'Whole Arm Manipulation'. Bicchi [36] noted that in such cases we cannot assume that the kinematics of the hand allow us to explicitly apply arbitrary contact wrenches. For enveloping grasps (Bicchi calls them "whole-limb" grasps) contacts occur on links with limited mobility such as proximal links or the palm of a robotic hand. In consequence we cannot freely choose internal forces in order to synthesize stable grasp forces — only a subset of the internal forces are actively controllable.

Similarly to the work by Nguyen [32] Bicchi models the contacts as springs but also uses the compliance matrix introduced by Cutkosky et al. [34] and the principle of virtual work to derive expressions for the subset of *active internal forces* (internal forces, which can be actively controlled by commanding the hand actuators) and the subset of *passive internal forces* (which cannot be

actively controlled and therefore will remain constant at their initial value). Demonstrating how a particular solution can be found from the compliance matrix weighted inverse of the grasp map matrix Bicchi proposes a method to find optimal contact wrenches, which are actually achievable with the kinematics in question [23]. This was a large step forwards as it allowed for the analysis of grasps commonly encountered in practice.

With these insights Bicchi proposed a new definition of the term 'force closure', which takes into account the kinematic capabilities of the grasping mechanism to actively control the contact wrenches [37]. He introduced an algorithm to test for force closure under this definition. A modification to this algorithm allows for a quantitative measure of how far a grasp with optimal contact wrenches is from violating contact constraints. Thus, the concept of a metric to quantify the quality of a grasp was extended from a purely geometric concept [21] to include the kinematic capabilities of the hand to apply optimal contact wrenches.

2.1.4 Quality metrics

Quality metrics are an essential component of the grasp planning problem, which can be described as the problem of computing appropriate contacts the hand should make on the object. Optimal grasp planning can be posed as a search over the space of possible grasps in order to find an instance that optimizes a given quality metric. It should come to no surprise that grasp quality metrics usually relate to the stability of the grasp. We have already introduced the metric derived from the grasp wrench space [21] and the metric by Bicchi, which takes into account the hand kinematics [37]. Note, that the objective value in grasp force optimization methods such as in [26] can be understood as a metric of grasp quality as well.

In many of the aforementioned works, the objective to be optimized (and hence the quantitative measure of grasp quality) is related to how far the contact wrenches are from violating contact constraints. Prattichizzo et al. [38] take a similar approach, however, similarly to Nakamura et al. [27] they relate the distance contact wrenches are from violating contact constraints to the magnitude of the external disturbance acting on the object. Given optimal contact wrenches the

magnitude of the smallest external disturbance that will cause a contact constraint violation is defined as the *Potential Contact Robustness* or PCR. In contrast to [27], however, contact forces are optimized over the space of active internal forces as defined by Bicchi [36][23][37] using the compliance analysis by Cutkosky et al. [34]

Another valuable contribution is founded on the insight that the robustness of individual contacts is not necessarily required for grasp stability. They argue that a grasp will remain stable even if some contact constraints are violated. Contacts may slip or detach entirely — as long as a sufficient set of contacts remain that satisfy contact constraints grasp stability may be maintained. Thus, PCR can be an overly conservative measure of stability. To achieve a less conservative grasp stability metric — the *Potential Grasp Robustness* or PGR — they make some simplifying assumptions in order to avoid modeling of the complex frictional behavior at the contacts. Specifically, they assume a slipping contact may not apply any frictional forces, which results in a stability measure that is still conservative, however less so than one based solely on contact robustness. A further disadvantage of this approach is that every potentially stable combination of contact states (rolling, slipping, detaching) must be considered. Therefore the computational complexity of this approach scales exponentially in the number of contacts, which can be prohibitive for real-time evaluation of enveloping grasps that make many contacts between the hand and grasped object.

2.1.5 Discussion

The methods introduced in Chapter 2.1.2 assume that we have some degree of control over the contact wrenches. They deem a grasp to be *potentially* stable if a solution to the equilibrium equations exists that also satisfies contact constraints. However, as we have noted before, force closure is no guarantee for stability. The existence of a solution to the equilibrium equations is no guarantee that it will arise. Instead, we must actuate the grasping mechanism accordingly in order to achieve the desired equilibrium contact wrenches. In Chapter 3 we will show that this assumption is of only limited applicability for the majority of robotic hands commonly used as they lack the capabilities to accurately control joint torques.

The works discussed in Chapters 2.1.3 and 2.1.4 introduce grasp models that do not necessarily presuppose the full control of contact wrenches. However, in order to do so they must introduce treatment of the compliance of the grasp and hence make another set of assumptions. Specifically, Bicchi [36] made use of the grasp compliance theory developed by Cutkosky et al. [34]. Assume the grasp is made up of deformable components such as series-elastic actuators or the contacts themselves are deformable due to an elastic skin covering the finger links. These deformable components would provide us with constitutive equations such that we can solve for displacements and hence contact wrenches given a specific external disturbance.

One obvious limitation of this approach is that the stiffness parameters can be difficult to obtain [39], particularly for very stiff hands. Another limitation was pointed out by Prattichizzo et al. [38]: When there is compliance in the grasp the presence of sliding or breaking contacts does not necessarily mean the grasp is unstable. Only a subset of contacts may be required for stability. This causes an issue as the contact wrench at a breaking or sliding contact is clearly not described by a compliance relation. At a breaking contact a compliance relation would lead to a negative normal force, which is impossible. At a sliding contact the contact force would depend linearly on the tangential displacement, which does not satisfy the Coulomb friction law. While Prattichizzo et al. find approximations that work well for their purposes, there is no computationally efficient and accurate way to apply an approach based on grasp compliance to a problem with potentially breaking or slipping contacts.

As all of the works discussed thus far do not model the friction forces at sliding contacts the Coulomb friction model is often reduced to the statement it makes about static contacts: The magnitude of the friction force may not exceed the magnitude of the normal force scaled by the coefficient of static friction. To the reader of the grasp force analysis literature it can often appear as though this statement was the complete Coulomb friction model. However, the Coulomb model also includes treatment of sliding contacts. Specifically, it includes the statement that the friction force, which arises at a sliding contact is the one, which dissipates the most energy. Thus, for isotropic friction the friction force must oppose tangential motion at a sliding contact.

By itself this is known as the *principle of maximum dissipation* or *Maximum Dissipation Principle* (MDP) [40]. For a more recent discussion of the MDP see the review by Stewart [41]. Although many readers will know the MDP to be part of the Coulomb model of friction, in this dissertation we will explicitly state when we make use of it due to its absence from much of the grasp force analysis literature.

2.2 Rigid body methods

A grasp can be viewed as a completely passive fixture. The grasp is made up of rigid bodies that are either fixed in space (like the 'grounded' base of the robot), free floating (like the grasped object) or connected by a kinematic chain (such as the manipulator links.) The bodies comprising the kinematic chains are connected to each other and — at least indirectly — the ground by bilateral constraints such as hinge joints. Contacts between bodies are unilateral constraints also satisfying a friction law such as Coulomb friction. All external forces acting on the bodies such as gravity or actuation wrenches are known. Such an arrangement is deemed stable if it remains at rest (all accelerations are zero) or as Palmer [42] puts it

"In the context of robotic assembly, we assume that objects are initially fixed in space, and say that they are stable if the force of gravity cannot cause the position of any object to change."

2.2.1 Rigid body mechanics

Palmer [42] investigated the stability of arrangements of rigid polygonal bodies under gravity and showed that the problem of determining stability is co-NP complete. However, they proposed a class of stability, which can efficiently be tested for using linear programming techniques: *Potential stability* is satisfied if contact wrenches exist within the contact constraints that also satisfy equilibrium. Mattikalli et al. [43] also noted the difficulty of determining the stability of assemblies of bodies with frictional contacts and used *potential stability* as defined by Palmer [42] as an indicator for stability. They point out that the existence of a solution to the contact constraints

and equilibrium equations is a necessary but not sufficient condition for stability and introduce conservative approximations of the friction law to mitigate this. Furthermore, they note that in the frictionless case a potentially stable arrangement is in fact guaranteed to be stable.

Erdmann [44] investigated the motion of rigid planar bodies in frictional contact given initial velocities. They note that in order to predict the motion of a body the relative motion of the contacts must be known. This apparent circularity stems from the different contact conditions due to unilaterality and the maximum dissipation principle. They consider each contact to be in one of several states: A contact can break, roll or slide. They propose solving the contact problem by first hypothesizing a combination of contacts states and then verifying that the resulting motion is consistent with the contact conditions. Thus, they propose enumerating all possible combinations of contact states, which provides an exponential complexity method of solving the rigid body contact problem. They note that the rigid body contact problem does not necessarily have a unique solution or may even have no solution at all.

Trinkle et al. [39] also advocate for a rigid body treatment in order to obtain accurate solutions without having to resort to computationally taxing finite elements methods to model compliance. They develop theory to predict the motion of rigid bodies in the plane under a quasistatic assumption (i.e. inertial effects are considered negligible.) and Coulomb friction. In their analysis the joints of the manipulator are assumed to be either position controlled or torque controlled.

Similarly to the work by Erdmann [44] their initial approach [39] requires the consideration of every possible combination of contact states where a contact can either roll, detach or slip in the tangential plane. While the number of feasible contact state combinations is quadratic in the number of contacts if the hand is immobile [45][46] they note that it is exponential in the number of bodies involved and hence in general the number of combinations is exponential in the number of contacts.

In further work Pang et al. [47] avoid this enumeration of contact state combinations by casting the contact constraints as an uncoupled complementarity problem (UCP). They show that problems of this type are NP-complete but present a bilinear programming approach to solving them. Trinkle

et al. [48] later extended this line of work to grasps in three dimensions.

2.2.2 Rigid body dynamics

Dropping the quasistatic assumption, Trinkle et al. [49] worked with the full dynamic equations instead. They showed that the Coulomb friction law with maximum dissipation can be cast as a mixed nonlinear complementarity problem (mixed NCP), which is difficult to solve. Therefore, they propose linearizing the friction cone by approximating it as a pyramid, which allows for a formulation of the friction constraint as a linear complementarity problem (LCP). While problems of this type can be solved with Lemke’s algorithm, a downside of this approximation is that the friction force will in general lie on the specific edge of the friction cone discretization, which maximizes the energy dissipation and therefore may not exactly oppose motion. An immensely influential time stepping scheme for the solution of multi-rigid-body dynamics with Coulomb friction that makes use of this framework became known as the Stewart-Trinkle formulation [50]. Another very influential time-stepping scheme — the Anitescu-Potra formulation [51] — can be obtained by omission of the constraint stabilization term from the Stewart-Trinkle formulation.

Pang et al. [52] point out that the equations of equilibrium are insufficient for the determination of stability of rigid body contact problems due to the possibility of false positives. Therefore they use the methodology developed in [49], which uses the dynamic equations instead with rigid bodies initially at rest and fixing the position of the elements making up the hand. Using this framework they build on the stability characterizations proposed by Palmer [42], which they describe as overly conservative. They define the class of *strongly stable loads* — disturbances which are guaranteed not to destabilize the grasp in their framework. They attribute the distinction between strongly and weakly stable loads (Palmer’s *potential stability*) to the nonuniqueness of the possible contact wrenches; there may be many solutions to the dynamic equations that satisfy the friction constraints but not all may be stable. Thus, they define the strongly stable loads as those, where every potential set of contact wrenches results in *nonpositive virtual work*.

If the solution is unique, then strong and weak stability are equivalent. Using the unique-

ness result from [49], they show that this is the case if the friction coefficient is below a certain bound. Unfortunately, this bound is not known and the authors expect it to be difficult to compute in general. Using the pyramidal linearization of the friction cone they do, however, present an exponential-time method to check if strong and weak stability are equivalent for a given grasp geometry. In those special cases strong stability can efficiently be determined as weak stability can be determined by solving a linear program.

Song et al. [53] attribute the nonuniqueness of solutions to both the statical indeterminacy of general grasping problems and the nonsmooth nature of the relationship between tangential forces and relative velocities. In order to overcome these difficulties they propose a compliant model of the contacts between nominally rigid bodies. Both normal and tangential contact forces are determined by viscoelastic constitutive relations coupling them to local deformations.

Anitescu and Tasora [54][55] showed that using the LCP formulation of the pyramidal friction cone approximation in general leads to non-convex solution sets. LCP problems with non-convex solution sets contain reformulated instances of the Knapsack problem and are therefore NP-hard. Thus, problems of this type are difficult to solve. The authors develop an iterative algorithm to solve them that converges to the solution of the original problem. They achieve this through successive convex relaxation effectively solving subproblems that have the form of strictly convex quadratic programs. They note that their algorithm is only guaranteed to converge for 'sufficiently small' friction coefficients but provide a lower bound for convergence.

In further work Anitescu et al. [56] argue that the computational burden of solving LCP based formulations of rigid body dynamics problems is too high for applications with large numbers of colliding bodies. They also point out that the linearization of the friction cone as a polygonal pyramid required for formulation as an LCP violates the assumption of isotropic friction. They instead propose a cone-complementarity approach and an iterative method that converges under fairly general conditions but may allow bodies to behave as if they were in contact although they have drifted apart, particularly at high tangential velocities [57].

Kaufman et al. [58] showed that solving for friction forces when normal forces are known can

be achieved by solving a quadratic program (QP). Similarly, the normal forces can be solved for when friction forces are known. However, problems where both are to be solved for simultaneously are non-convex. The solution of non-convex QPs is generally NP-hard [59]. The authors present an algorithm which iterates between the two convex QPs until a solution of the required accuracy is found. Although it works well in practice convergence is not guaranteed with their approach.

Todorov [60] takes a completely new approach by deriving nonlinear equations for the dynamic contact problem that implicitly satisfy the complementarity conditions. In order to solve the resulting nonlinear equations Todorov proposes a Gauss-Newton approach with specific adaptations such as a novel linesearch procedure. Todorov [61] and Drumwright et al. [62] independently developed formulations that are relaxing the complementarity conditions such that a convex optimization problem is recovered.

More recently, Pang et al. [63] showed that the LCP formulation for discretized friction cones first introduced by Trinkle [49] can be cast as a Mixed Integer Program instead. While this method still suffers from the same inaccuracies they demonstrated its applicability for the control of a robotic gripper in simulation.

An excellent starting point to some of the most influential works towards rigid body dynamics with frictional contacts is the comparative review by Horak and Trinkle [57], which elucidates some of the similarities and differences between many of the approaches listed above.

2.2.3 Discussion

We introduce the works discussed above because they can be applied to robotic grasps while making no assumption of active control of contact wrenches. In fact, the community focusing on the analysis of rigid bodies has developed very natural complementarity formulations that capture passively stable grasps. Furthermore, there are numerous relaxations available in order to improve efficiency.

In order to determine the stability of a grasp with respect to a given disturbance we could, for example, attempt to use any of the various dynamics solvers the field has produced to compute

contact forces and calculate a single time step. If all accelerations remain zero, we deem the grasp stable. Unfortunately, as we will now discuss, this approach will not give us definite results.

Any algorithm that makes use of relaxations also introduces artifacts as we are no longer solving the exact problem as outlined above. These artifacts are acceptable for the purposes of those algorithms: Dynamics simulation that is fast enough for use in time sensitive applications such as virtual reality or deep learning. In our application, however, these artifacts mean that we cannot rely on the simulation to produce exactly zero accelerations even for grasps that are truly stable.

Thus, we need to focus on the algorithms that solve the exact problem. Perhaps the best candidate is the formulation as a mixed nonlinear complementarity problem (mixed NCP) introduced by Trinkle et al. [49]. In a previous paper [64] Pang and Trinkle showed that in the case of systems initially at rest the existence of a solution is guaranteed. However, they also note a difficulty in using this formulation for stability analysis: One must show that *every* solution to the complementarity problem has a zero acceleration.

Generally, when using a complementarity formulation in a dynamics engine only one solution is required in order to step the simulation forward in time. This allows the application of solvers such as Lemke’s algorithm, which only finds a single solution — if one exists. The only algorithms that find all solutions to general complementarity problems are enumerative in nature [65] and therefore of exponential computational complexity.

To the best knowledge of the author, the work which comes closest to answering the question of stability under the above assumptions is that by Pang et al. [52], which makes use of the complementarity formulation due to Trinkle et al. [49]. In special cases, in which the solution is unique, there is no ambiguity due to multiple solutions and the single solution to the LCP determines stability. A framework that efficiently determines stability for general grasps under the rigid body assumption has not yet been found.

2.3 Dexterous in-hand manipulation

In-hand manipulation is the task of reorienting a grasped object with respect to the grasping robotic hand. One approach to problems of this kind is to make use of kinematic models of the hand and object and apply analytic methods from the realm of optimization and planning algorithms to compute an appropriate series of behaviors such as contact sliding, contact rolling and finger gaiting. These approaches (see for instance [66][67][68][69][70][71][72][73][74][75][76][77]) assume some knowledge of the grasped object geometry as well as the ability to model the dynamics and interactions at the contacts.

In contrast to these model-based methods the advent of efficient Reinforcement Learning (RL) algorithms has allowed researchers to investigate entirely model-free approaches. As such, the grasp is treated as a black box and Deep Reinforcement Learning (DRL) is used to train end-to-end policies directly mapping from sensor inputs to actuator commands. van Hoof et al. [78] demonstrated the viability of RL for in-hand manipulation with planar grasps. They used an underactuated hand for which devising analytical controllers is difficult and leveraged tactile sensors to provide features for the policy.

More recently results published by groups at OpenAI have garnered large publicity. They demonstrated reorientation of a block in the palm of a anthropomorphic robotic hand [11] using a scaled-up implementation of the Proximal Policy Optimization algorithm [79]. They train their policy in simulation and use domain randomization in order to achieve robust transfer to the real robotic hand. The reason they train in simulation is the sample complexity of their method: it takes approximately 100 years of simulated experience to train a policy that robustly transfers to the real hand. In later work they extended this work to the solving of Rubik's cubes in a similar experimental setup [12]. In order to improve sample efficiency Zhu et al. [80] as well as Rajeswaran et al.[81] leveraged Imitation Learning in combination with RL.

Li et al. [82] point out that none of the model-free approaches above require the hand to maintain a stable and robust grasp of the object throughout the grasp. The object is either supported

by a tabletop [78], the palm of the hand [11][12][81] or limited in its degree of freedoms through external supports [80]. In order to overcome this limitation Li et al. propose a hierarchical control structure instead of the monolithic end-to-end paradigm of DRL. They develop analytical torque controllers for three different manipulation primitives that are intrinsically designed for grasp stability. A higher level DRL policy is trained to choose the manipulation primitive as well as its parameters. Using this approach they achieve stable in-hand manipulation for planar grasps in simulation.

The idea of maintaining a stable grasp throughout an RL task has parallels in the 'Safe Reinforcement Learning' literature (see Garcia et al. [83] for a survey of Safe RL.) Avoiding unsafe states during training and execution of RL policies is similar to avoiding states that result in an unstable grasp during an in-hand manipulation task. Particularly interesting is the work of Dalal et al. [84] in which they append a 'safety layer' to their policy network that performs an action correction. The action correction is formulated as an optimization problem that uses a linearized model and thus allows for an analytic solution. The optimization computes the minimum perturbation to the action such that safety constraints are satisfied. Amos et al. [85] introduced 'OptNet': A neural network architecture that integrates optimization problems such that complex constraints can be captured.

Due to the relative novelty of DRL approaches to in-hand manipulation we believe there are many synergies yet to be discovered in the combination of the above ideas and approaches from the traditional grasp analysis theory.

Chapter 3: Grasp stability analysis — Theory and Praxis

In Chapter 2 we argued that the notion of a grasp’s stability is of foundational importance to the majority of manipulation tasks and hence many competing definitions of stability have been proposed by the grasp modeling community. In essence, all these definitions share a common goal: to maintain a grasp such that the grasped object remains relatively at rest with respect to the hand throughout the task. Motions in reaction to a disturbance that lead to another static equilibrium where again the object is at rest with respect to the hand may be allowed. We will use this informal definition of stability in the following general discussion of manipulation. In Chapter 4.3 we will provide a more precise definition of stability in the context of our own grasp model.

In practice, maintaining stability as defined above throughout a task requires maintaining stability with respect to every disturbance the grasp will encounter throughout that task. Determining the ability of a grasp to resist given disturbances, formulated as external wrenches applied to the grasped object, is equivalent to computing the stability of a multi-body system with frictional contacts under applied loads. Problems of this kind are thus pervasive in grasp analysis and may be encountered in many other scenarios that rely on the stability of assemblies of general rigid bodies with frictional contacts.

Inspired by the queries formulated by Bicchi [23] and quoted in Chapter 2.1 we formulate our own pair of queries. We argue that these queries are foundational to the majority of robotic manipulation tasks:

Given a set of actuator commands and an external disturbance will the system as described above remain stable?

We can also formulate the inverse query to obtain useful insight into how to control the hand:

Given an external disturbance, how must we command the actuators to guarantee the grasp remains stable?

In the context of robotic manipulations the ability to answer these queries is of great practical use. A grasp model that can answer these queries must capture the interplay of contact forces, joint torques and externally applied wrenches. It must be able to accurately predict how joint torques and external wrenches are transmitted through the object and distributed across the contacts taking into account the unilaterality of contacts, the specific actuation scheme of the hand as well as the nonlinear nature of friction laws. So why is there no 'grand unified theory of grasp stability'?

As discussed in 2.1 much of the existing grasp analysis literature makes the simplifying assumption that all contact wrenches are being actively controlled at all times. This can be done directly through commanding appropriate joint torques or more indirectly through setting controllable compliance parameters such as servo gains. This assumption allows the analysis of grasp stability through the equilibrium equations and friction laws alone and allow us to compute optimal contact forces and the joint torques necessary to balance them. This is incredibly powerful, as for any specific wrench applied to the object encountered throughout a task we can compute the specific optimal joint torques for stability.

In order to use this in practice, however, we have to make a string of assumptions:

1. We assume perfect knowledge of the disturbance to the object that must be balanced at all times;
2. We assume that we can actively control the contact wrenches at every contact;
3. We assume that we can actively control the joint torques required for equilibrium;
4. We assume that we can accurately control the torque output of the hand actuators.

In the majority of robotic manipulation tasks these assumptions do not hold. First, the exact wrench acting on an object is difficult to compute — it requires knowledge of the mass and inertial properties of the object as well as its exact trajectory. Any additional disturbance cannot be

accounted for unless the fingers are equipped with tactile sensors. Second, many robotic hands are kinematically deficient and contain links with limited mobility. This means that we cannot directly control (through controlling joint torques) the contact wrench at a contact on the palm of the hand for instance. Wrenches at such a contact can only arise passively by transmission of the disturbance on the grasped object or wrenches at other contacts through the object.

Third, the kinematics of the hand may not permit explicit control of the torques at every individual joint. This is the case for the class of underactuated hands, where joint torques by definition may not be independently controlled but are also a function of the kinematic composition and the pose of the hand. Finally, the actuation method of the hand may prevent accurate torque control at the joints. Most robotic hands use highly geared motors for instance, which makes accurate sensing and control of the torques at the hand joints all but impossible.

Therefore, in practice it is rarely the case that contact wrenches are actively controlled in response to disturbances to the grasp. Unfortunately, this means that the existence of contact wrenches that satisfy the equilibrium equations as well as friction constraints is a necessary but by no means sufficient condition for the ability of a grasp to resist a given disturbance. In general such contact wrenches will not arise, unless we are actively controlling the contact wrenches to that end.

Having discussed the limiting assumptions of the grasp analysis theory it is instructive to think about why robotic hands have not evolved in such a way as to fulfill the assumptions listed above. We discussed why these assumptions are difficult to satisfy in practice and why attempts to remove those assumptions introduce their own limitations. Still, it seems to not provide enough justification for the schism that separates the theory and the robotic hands commonly in use today. After all, why build hands that are so far removed from the theory that allows their analysis?

In order to answer this question we must revisit a concept, which we call *passive stability* or *passive resistance*. It denotes the ability of a grasp to resist a given applied wrench without active control of the hand, but through purely passive phenomena. In Chapter 1.1 we mentioned two such phenomena contributing to passive stability: underactuation and nonbackdrivability. Let

us for now focus on nonbackdrivability, which we believe to have had a large influence on the manipulation field despite the community being largely unaware of it.

Nonbackdrivability allows practitioners to greatly simplify robotic grasping. We can often apply actuator torques that close the fingers around the object without necessarily worrying if these will balance out once contact is made: the fingers jam as the hand squeezes the object, and the gearboxes between joints and actuators provide additional structural torques. If the grasp geometry is adequately chosen, the equilibrium joint torques arise passively when the fingers squeeze the object between them and a stable grasp arises.

For example, in the grasp in Fig. 3.1 it is sufficient to actively load the joints of one finger. The nonbackdrivability of the other finger means the object will be stably grasped and equilibrium joint torques arise passively in the non-actuated finger. The same phenomenon can allow a grasp to withstand a range of disturbances applied to the object without a change in the actuator commands. If chosen wisely, the initially applied actuator forces — called a *preload* — are sufficient to balance the object throughout the task and various corresponding different disturbances. Again, if the grasp geometry is adequately chosen, equilibrium joint torques arise passively when disturbance wrenches applied to the object push it against the fingers. This is the true power of passive resistance.

We believe this characteristic to be the reason why robotic manipulation without explicit real-time control of the hand actuators has become so commonplace. Reactions to disturbances arising passively due to nonbackdrivable actuators remove the need for complex hand control schemes and the high fidelity sensing they require. If the grasp geometry and actuator commands are chosen wisely the grasp will be passively stable to a range of disturbances greatly simplifying the control of the hand. We simply need to pick a constant command appropriate to the task. So the answer to the question as to why most robotic hands lack the complexity required for the application of the grasp theory is that practitioners can rely on passive stability instead. This allows them to form stable grasps, even though they lack the tools required to analyze them.

Underactuated hands provide similar advantages: These hands make use of their passive com-

pliance in order to conform around objects. Soft robotic hands take this approach to the extreme. Most of the hands commonly found in research labs today exhibit either underactuation, nonbackdrivability or both. They all have in common that their passive behavior greatly simplifies control, which explains their popularity.

3.1 A representative example problem

In order to illustrate the implications of passive stability on robotic manipulation let us consider the grasp in Fig. 3.1. Does the grasp remain stable if we apply either disturbance w_1 or w_2 to the grasped object? In order to resist those disturbances, contact forces must arise that balance them. Clearly in either case there exist contact forces that satisfy a simple friction law (illustrated by red friction cones) and balance the disturbance. In fact, this grasp has *force closure* and hence contact forces exist that could balance arbitrary disturbances.

In practice, however, this is not a sufficient criterion for grasp stability. It is clear that contact forces c_2 and c_4 will only arise if we have previously loaded the grasp such that there is sufficient normal force at contacts 2 and 4 to sustain the friction forces required: an appropriate preload is required, or the object will slip out. We could, for example apply actuator torques at the joints such that the hand 'squeezes' the object and hence provides such a preload.

We can make a similar argument about contact forces that balance disturbance w_2 , however if we assume that the joints on the robotic hand are nonbackdrivable (as is the case with most robotic hands in use today) contact forces c_1 and c_3 will arise entirely passively. The disturbance will push the object against the fingers, which due to the nonbackdrivability of the joints provide a rigid support. There is no need for us to apply any torques at the joints as the grasp will be stable regardless. The grasp provides *passive resistance* to the applied wrench.

As discussed in Chapter 2.1.5 none of the traditional grasp force analysis works discussed in Chapter 2.1 can accurately capture the passive behavior of this grasp. A perhaps more natural formulation for problems of this kind can be found in the rigid body dynamics literature discussed in Chapter 2.2. We mentioned the main complication in using such a formulation based on the

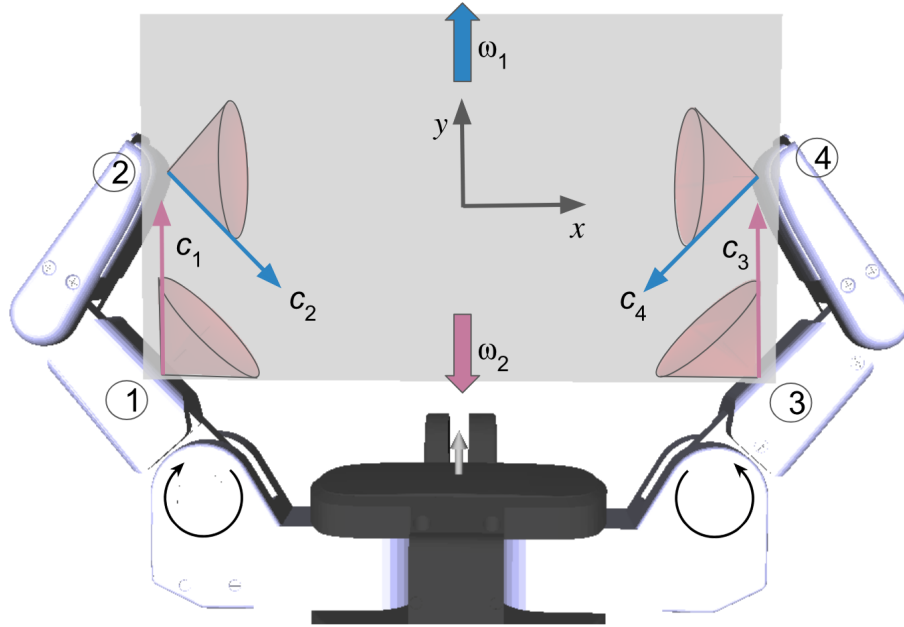


Figure 3.1: A grasping scenario where a hand establishes multiple frictional contacts (numbered 1-4) with a target object. External disturbance w_1 can be resisted by contact forces c_2 and c_4 ; w_2 by contact forces c_1 and c_3 .

dynamics equations and complementarities in Chapter 2.2.3. The nonuniqueness of solutions in the general case means that one has to find all solutions to the problem to show that all of them result in zero accelerations.

This ambiguity due to multiple solutions can be well illustrated using again the grasp in Fig. 3.1 assuming nonbackdrivable fingers: Consider the case of applying w_2 with a zero preload such that contact forces are zero prior to the application of w_2 . A formulation based on complementarities admits at least two solutions:

In solution 1 the box slides upward out of the grasp completely unhindered by the grasp, as it is not applying any contact forces. This is the intuitively correct solution to this grasp stability problem. If we do not preload the grasp it may not withstand w_2 .

In solution 2 contact forces arise at contacts 2 and 4 such that there is sufficient friction to maintain a stable grasp on the object. This can happen because, while the contacts are not previously loaded with contact forces, they are maintained and the complementarity condition for contact forces to arise is met. Due to the assumption of nonbackdrivability both fingers are rigidly

fixed in space, which allows for arbitrarily large contact forces to arise without the need to balance them with joint torques.

While this second solution is not useful in practice — we know it will never arise — it is a perfectly valid solution to the formulation used to model the grasp. It is simply a feature of the rigid body assumption. In reality, however, no body is truly rigid, which is why this second solution is never observed in practice. The existence of such solutions that are mathematically correct, but physically impossible is problematic. The second solution by itself would have us conclude the grasp is stable. Thus, in order to be able to conclude that a grasp is stable from a single solution we must derive a different formulation that relaxes the rigid body assumption.

The grasp shown in Fig. 3.1 is exceedingly simple but still representative of many robotic manipulation tasks. And yet we lack the means to analyze the passive effects that make these grasps so powerful. If we want to move beyond blindly using passive reactions and truly understand how to leverage them we must be able to model passive effects. We can then answer the stability queries we defined at the beginning of this chapter with our new understanding of the mechanics of grasping.

Chapter 4: Grasp Stability Analysis in Two Dimensions and Polynomial Time

4.1 Introduction

In Chapter 3 we argued that for a grasp model to be useful as a grasp stability analysis tool it must be able to predict the purely passive behavior of the grasp. In this chapter we will begin to investigate the modeling of such passive phenomena in the special case of planar grasps. This simplification is convenient when modeling friction forces under the maximum dissipation principle. The reason is that in the plane contacts can only slide in one of two directions. This is illustrated in the grasp in Fig. 4.1: there are no out of plane motions or forces to consider.

This grasp was constructed to exhibit passive characteristics very similar to those of the grasp in Fig. 3.1: External disturbance w_1 (left, pushing the object up) can be resisted by contact forces c_1 and c_3 , but only if contacts 1 and 3 have been actively pre-loaded with enough normal force to generate the corresponding friction forces. In contrast, disturbance w_2 (right, pushing the object down), regardless of its magnitude, will always be passively resisted by contact force c_2 . In this chapter we introduce a computationally efficient method to predict the stability of passive planar grasps such as the one in Fig. 4.1 when applying arbitrary wrenches to the grasped object.

As we are interested in passive stability we cannot make the simplifying assumption that we have any control over the contact forces. Thus, we take a similar approach to previous researchers, who leverage the compliance of the grasp to resolve the static indeterminacy [20][86][33][34][36][23][37][38]. Modeling the compliance of the grasp provides *constitutive equations* relating motion of the object to contact forces. This is a common approach in the solution of statically indeterminate systems, in which contact forces cannot be uniquely determined from the equations of equilibrium alone and are therefore difficult to solve. The contact forces are then fully deter-

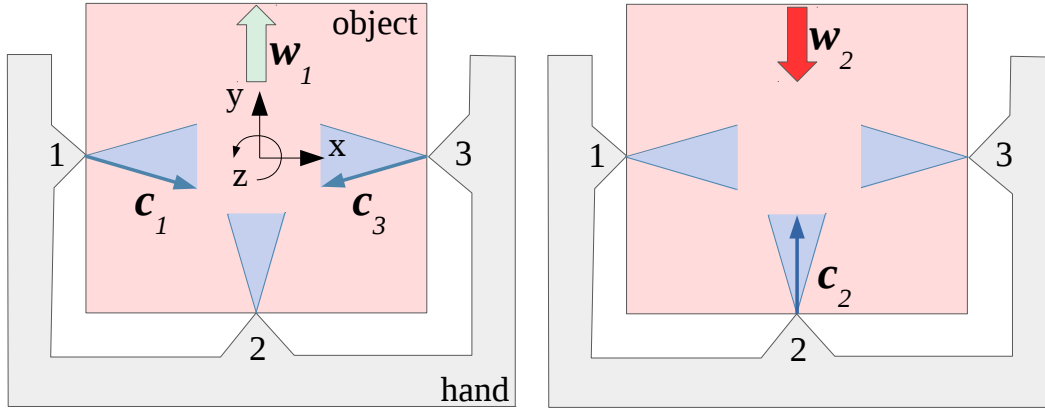


Figure 4.1: A planar grasping scenario where a hand establishes multiple frictional contacts (numbered 1-3) with a target object.

mined by the relative motion between the hand and the object — the system becomes statically determinate. These constitutive relations are desirable, as they are linear and therefore allow for very efficient solution.

However, as we described in Chapter 2.1.3 the unilaterality of contact normal forces as well as the the frictional components of contact wrenches cannot be accurately described by compliance relations. Thus, we choose to model only normal forces at persisting contacts with constitutive relations while modeling friction with the Coulomb friction model including the maximum dissipation principle (MDP) [40].

Initially, we assume all bodies making up the grasp to be at rest. Due to the compliance we introduced to resolve the static indeterminacy, we expect some motion once an external disturbance is applied to the grasped object. This may include breaking or sliding contacts. However, we assume all motion to be small such that we only have to account for first order effects and can ignore any higher order effects on the grasp geometry due to this motion. Assuming the grasp geometry to remain constant greatly simplifies the grasp model and is a reasonable assumption for relatively stiff hands and objects as the motions observed are indeed very small.

Furthermore, we assume that all dynamic effects are negligible. As such, when we speak of the motion of a body we really mean the displacement it undergoes when a wrench is applied to it. As is common when dealing with rigid body motion we will consider a displacement to include both

the translation and the rotation of the body.

4.2 Grasp model

We first introduce the general framework of our grasp model. Consider a rigid robotic hand that makes m contacts with a grasped object. The system is initially at rest. Each contact is defined by a location on the surface of the grasped object and a normal direction determined by the local geometry of the bodies in contact. We choose the *Point Contact with Friction* model to describe the possible contact wrenches that may arise at the interfaces between the hand and the object. Therefore we only consider contact forces and do not allow for frictional torques. This is a reasonable assumption for contacts between smooth and relatively stiff bodies. For any contact specific vector such as contact force or contact motion we will use subscripts n and t respectively to denote the components lying in the contact normal and contact tangent directions. We use the vector $\mathbf{c} \in \mathbb{R}^{2m}$ to denote contact forces, where $\mathbf{c}_i \in \mathbb{R}^2$ is the force at the i -th contact. Using the notation above, $c_{i,n} \in \mathbb{R}$ is the normal component of this force, and $c_{i,t} \in \mathbb{R}$ is its tangential (i.e. frictional) component.

Equilibrium: Let us define the grasp map matrix $\mathbf{G} \in \mathbb{R}^{3 \times 2m}$, which maps contact forces into a frame fixed to the grasped object. We can now write the equilibrium equations for the grasped object where we collect all disturbances externally applied to the object (such as gravitational forces for instance) in $\mathbf{w} \in \mathbb{R}^3$.

$$\mathbf{G}\mathbf{c} + \mathbf{w} = 0 \tag{4.1}$$

The transpose of matrix \mathbf{G} also maps object motion $\mathbf{r} \in \mathbb{R}^3$ to translational motion of the contacts in the contact frame $\mathbf{d} \in \mathbb{R}^{2m}$. Recall that in the context of our grasp model by motion we mean the displacement of the object and this relation is only valid for small displacements.

$$\mathbf{G}^T \mathbf{r} = \mathbf{d} \tag{4.2}$$

Note that as we assume a constant grasp geometry matrix \mathbf{G} is also constant.

Normal forces: Due to the unilaterality of contacts — we do not concern ourselves with adhesion or similar effects — a contact may only push on an object but can never pull. Thus, the normal force at a contact must be strictly non-negative. Furthermore, if the contact detaches the contact force must be zero. We model the normal forces by placing virtual linear springs along the contact normals such that normal forces will only arise through object motions that compress these springs. As we have assumed all motions to be small such that grasp geometries are invariant we are not interested in actually computing the real magnitude of the displacements of the grasped object. Instead, we can think of the motion as entirely virtual; it is simply a tool to resolve static indeterminacy and enforce contact constraints and thus we can forgo having to identify the true compliance parameters of the hand. To simplify notation we choose the virtual springs to be of unity stiffness. The result is a compliant version of the *Signorini Fichera Condition*.

$$\begin{cases} c_{i,n} = -d_{i,n} & \text{if } d_{i,n} \leq 0 \\ c_{i,n} = 0 & \text{if } d_{i,n} > 0 \end{cases} \quad (4.3a)$$

$$\begin{cases} c_{i,n} = -d_{i,n} & \text{if } d_{i,n} \leq 0 \\ c_{i,n} = 0 & \text{if } d_{i,n} > 0 \end{cases} \quad (4.3b)$$

We are here implicitly assuming that all contacts are of equal stiffness. For grasps with very dissimilar contact compliances it may be necessary to choose spring stiffnesses with appropriate ratios with respect to each other. Nonetheless, the absolute magnitude of the spring stiffnesses is irrelevant as object motion scales inversely proportional to spring stiffness and hence contact forces are invariant with respect to spring stiffnesses.

Of course only one of the two pairs of constraints in (4.3) can be active at any contact, the choice of which depends on if the contact breaks or not. As the object motion is part of the solution we seek it is unknown which pair of constraints is active. However, these constraints can also be formulated in terms of two linear inequalities and a non-convex quadratic constraint that must all be satisfied in either case:

$$c_{i,n} \geq 0 \quad (4.4)$$

$$c_{i,n} + d_{i,n} \geq 0 \quad (4.5)$$

$$c_{i,n} \cdot (c_{i,n} + d_{i,n}) = 0 \quad (4.6)$$

If re-posed as a Linear Complementarity Problem the matrix relating the vectors of unknowns is non-positive definite and therefore problems including such constraints are difficult to solve. We can instead construct a system of equations for each possible combination of contact constraints and search for solutions in all such problems. This way a problem contains only the active pair of linear equality and inequality constraints and can thus be readily solved. Of course we must now solve multiple simpler problems instead of one complex one, but as we will see we can make use of the structure of the problem to arrive at an algorithm of polynomial complexity as opposed to a direct approach to the LCP, which would be worst-case exponential.

We will therefore work directly with the formulation of the normal force constraints in (4.3) after adding one more detail: We may be interested in grasps where we assume a certain level of contact normal forces is already present before the application of any external wrench. The virtual springs in such a grasp are pre-stressed in order to achieve the desired normal forces — we call this the preload of a grasp. We denote the preload at contact i as p_i . Adding this term to (4.3) we obtain the following:

$$\begin{cases} c_{i,n} = -d_{i,n} + p_i & \text{if } d_{i,n} - p_i \leq 0 \\ c_{i,n} = 0 & \text{if } d_{i,n} - p_i > 0 \end{cases} \quad (4.7a)$$

$$\quad \quad \quad (4.7b)$$

Friction forces: We choose the Coulomb model to describe the friction forces at the contacts. For a stationary contact this model simply states that the frictional component of the contact force is bounded by the normal component scaled by the coefficient of friction μ_i . If a contact slides,

however, the *maximum dissipation principle* (MDP) [40] states that the friction force must oppose the relative motion at the contact. We can express the Coulomb friction law as follows:

$$\begin{cases} c_{i,t} \leq \mu_i c_{i,n} & \text{if } d_{i,t} = 0 & (4.8a) \\ c_{i,t} = \mu_i c_{i,n} & \text{if } d_{i,t} < 0 & (4.8b) \\ c_{i,t} = -\mu_i c_{i,n} & \text{if } d_{i,t} > 0 & (4.8c) \end{cases}$$

Similarly to the conditional constraints in (4.7) we will deal with this set of constraints by constructing multiple problems with different combinations of active constraints such that individual problems only consist of linear constraints.

4.3 Definition of stability

In Chapter 4.2 we introduced the mathematical constraints relating object motions and contact forces assuming a constant grasp geometry. Hence, they define the behavior of a grasp under application of an external disturbance assuming a constant grasp geometry. In this context we can now provide a more precise definition of stability.

As we are interested in the stability of a given grasp with respect to a specific external wrench applied to the grasped object, such a grasp geometry/ wrench pair defines an instance of the stability problem. The question of stability then becomes one of *solution existence*: A grasp is deemed stable if a solution exists to the set of constraints described in Chapter 4.2. More specifically, a grasp is deemed stable if a displacement exists such that contact wrenches arise that balance the wrench applied to the grasped object. As such, the motion can be interpreted as the (small) movement the bodies undergo under the applied loads before they reach a new equilibrium.

As the constraints are specific to the initial grasp geometry, non-existence of a solution only indicates instability of that exact geometry. It does not indicate if through changes in grasp geometry due to object motion the object will eventually settle in a new equilibrium. The initial grasp would be deemed unstable under our definition.

Note also that stability is explicitly defined with respect to a specific applied wrench as opposed to a more broad definition such as force closure or asymptotic stability in the control theoretic sense. This is an important distinction as a grasp can be stable with respect to a specific wrench even without satisfying force closure. This opens up our definition of stability and the following analysis to many other problems that may not be immediately appear related to grasping. A house of cards on a table in a gravitational field for instance may not intuitively resemble a grasp. The supporting surface certainly has no force closure over the contacting cards, yet a (well constructed) house of cards will be stable under the above definition.

We will leave open for now the question of what does and does not constitute a grasp and focus for the rest of this dissertation on mechanisms we believe most readers would immediately recognize as grasps with robotic hands. However, we expect the scope of our definition of stability and the following work to be much broader.

4.4 Solving for stability given contact states

The formulation we described in Chapter 4.2 introduces a major complication as equations (4.7) define two possible constraints and equations (4.8) define three possible constraints. Only one constraint of each set can be active a contact but we do not know which constraints hold a priori. We do not know if a contact detaches and if it does not if it slips in a negative sense, slips in a positive sense or rolls.

Note that which constraint is active is entirely determined by the relative motion at the corresponding contact. A contact may persist or detach, which determines the contact normal force. The friction force constraint is determined depending on if the contact slips in a positive sense, a negative or not at all. This means a contact must be in one of six states.

In order to describe a system with multiple contacts one must know the state of each contact. This introduces a combinatorial aspect to the problem due to the different possible combinations of contact states. We will investigate the number of possible combinations of these states in Chapter 4.5 and their enumeration in Chapter 4.6 but for now let us assume that we are given a valid

Persists / Detaches	Rolls / Slips
Persists	Rolls
Persists	Slips +
Persists	Slips -
Detaches	Rolls
Detaches	Slips +
Detaches	Slips -

Table 4.1: Enumeration of possible states for a single contact

combination of states such that we can construct the appropriate constraints and solve for equilibrium.

Note that every constraint possibility in equations (4.7)&(4.8) consists of a pair of an inequality and an equality. Thus we can construct a linear system of equations from the equality components of all the constraints also including the equations of equilibrium equation (4.1). Equation (4.2) is a simple linear mapping such that all \mathbf{d} can be expressed in terms of \mathbf{r} .

$$\mathbf{A} \begin{bmatrix} \mathbf{c} \\ \mathbf{r} \end{bmatrix} = \begin{bmatrix} \mathbf{G} & 0 \\ \mathbf{A}_1 & \mathbf{A}_2 \end{bmatrix} \begin{bmatrix} \mathbf{c} \\ \mathbf{r} \end{bmatrix} = \begin{bmatrix} -\mathbf{w} \\ \mathbf{p} \end{bmatrix} \quad (4.9)$$

Matrix \mathbf{A}_1 and \mathbf{A}_2 collect the equality constraints from (4.7)&(4.8) that correspond to the set of contact states we are given. \mathbf{p} contains the preloads p_i for the contacts and constraints where they are applicable and zeros elsewhere. For grasps without a preload it contains all zeros. As we have $2m + 3$ equations for an equal number of constraints matrix \mathbf{A} is square. Thus, there are two cases:

1. if \mathbf{A} is invertible solve the linear system (4.9). The solution is unique and if it satisfies the applicable inequality constraints in equations (4.7)&(4.8) then it is indeed a valid solution to the system.
2. if \mathbf{A} is singular solve a linear program with equality constraints (4.9) subject to the applicable inequality constraints in equations (4.7)&(4.8). If the linear program is feasible then the computed solution is valid.

If through either approach no valid solution is found then the set of contact states given cannot result in equilibrium. This gives us an algorithm that is exponential in the number of contacts as one could naively enumerate all 6^m possible contact states, construct the corresponding system of equations for each and solve the resulting linear problem as described above. There is, however, a method to reduce the number of combinations that must be checked for a solution as only some combinations are valid under rigid body constraints.

4.5 Number of possible contact states

In order to analyze the possible contact state combinations it is opportune to consider the case of contacts detaching and the different slipping conditions separately. Thus let us define two partitions: First we partition the contacts into those detaching and those, which persist. We define vector $U_k \in \{0, 1\}^m$. The i -th element of U_k is labeled u_i^k and indicates if contact i detaches.

$$\begin{cases} u_i^k = 1 & \implies \text{contact persists,} & d_{i,n} - p_i \leq 0, c_{i,n} = -d_{i,n} + p_i & (4.10a) \\ u_i^k = 0 & \implies \text{contact detaches,} & d_{i,n} - p_i > 0, c_{i,n} = 0 & (4.10b) \end{cases}$$

We now define the second partition of contacts this time into three sets: those slipping in a positive sense, those slipping in a negative sense and those that remain relatively at rest. We define vector $S_k \in \{-1, 0, 1\}^m$. The i -th element of S_k is labeled s_i^k and indicates the slip state of contact i .

$$\begin{cases} s_i^k = 0 & \implies \text{contact rolls,} & d_{i,t} = 0, c_{i,t} \leq \mu_i c_{i,n} & (4.11a) \\ s_i^k = 1 & \implies \text{contact slips in + sense,} & d_{i,t} > 0, c_{i,t} = -\mu_i c_{i,n} & (4.11b) \\ s_i^k = -1 & \implies \text{contact slips in - sense,} & d_{i,t} < 0, c_{i,t} = \mu_i c_{i,n} & (4.11c) \end{cases}$$

Finally \mathbb{U} is the set of all possible system contact detachment states. Thus $U_k \in \mathbb{U}$ for $k = 1..#\mathbb{U}$, where $\#\mathbb{U}$ is the cardinality of \mathbb{U} . Similarly \mathbb{S} is the set of all possible system contact

slip states. At first glance $\#(\mathbb{U}) = 2^m$ and $\#(\mathbb{S}) = 3^m$: since each contact can have two detachment states and three slip states, the total number of states for the system is exponential in the number of contacts.

However, it is known that the number of possible slip states for a planar rigid body in contact with other rigid bodies fixed in space is indeed quadratic in the number of contacts [45][46]. This perhaps surprising fact stems from the rigid body constraints that impose relations between the motions of all contacts on the same body. Trinkle et al. [39] point out that this also applies to a grasped object if the hand is immobile. In the following we shall prove this is indeed the case and show that the number of possible contact detachment states is also polynomial in the number of contacts, even for pre-stressed grasps. In Chapter 4.6 we describe an algorithm to enumerate all geometrically possible combinations of contact states.

Let us begin by noting that in the three-dimensional space of possible object motions $\mathbf{r} = [x, y, r]$, the constraints $d_{i,n} = (\mathbf{G}^T \mathbf{r})_{i,n} = 0$ and $d_{i,t} = (\mathbf{G}^T \mathbf{r})_{i,t} = 0$ define two-dimensional planes. We shall in the following only consider the planes generated by the tangential contact motion constraint as the processing they require is more involved. We will then describe the simplifications that can be made in processing the planes due to the normal contact motion constraints.

Consider a tangential motion constraint $(\mathbf{G}^T \mathbf{r})_{i,t} = 0$. Any object motion lying on this plane will result in zero relative tangential motion at this contact. Motion in the open halfspace where $(\mathbf{G}^T \mathbf{r})_{i,t} > 0$ will result in slip along the tangential axis in the positive direction, while motion in the complementary open halfspace $(\mathbf{G}^T \mathbf{r})_{i,t} < 0$ will result in slip in the negative direction. Combining the planes defined by each contact, we can construct an *arrangement* of planes. These planes segment the space of object motions into the following partitions:

- 3-dimensional *regions* where all contacts are slipping;
- 2-dimensional *facets* (region boundaries on a single plane) where one contact is rolling;
- 1-dimensional *lines* (intersections of multiple planes) where two contacts are rolling.

By construction, since all of our planes go through the origin, the only possible zero-dimensional

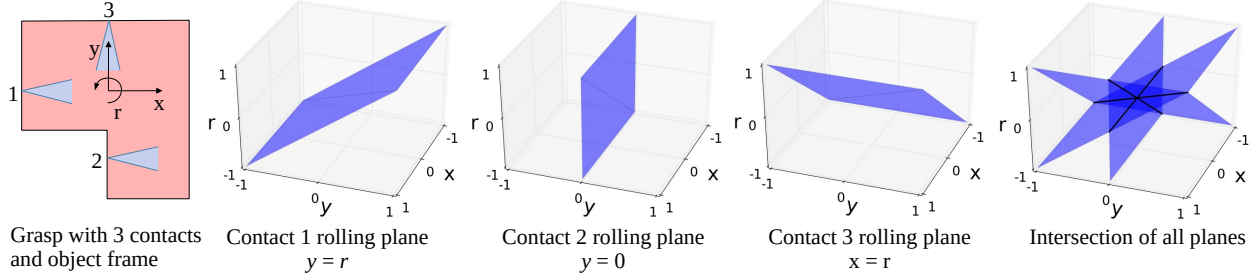


Figure 4.2: Arrangement of planes equivalent to contact roll-slip constraints. For the grasp shown on the left, each contact defines a plane in the three-dimensional space of possible object motions $\mathbf{r} = [x, y, r]$. For example, Contact 1 rolls if the translation component of \mathbf{r} along y is counteracted by an equal rotational component r . Similarly, Contact 2 rolls if the y component of \mathbf{r} is 0, and so on.

point intersection is the origin itself (see Fig. 4.2.) Such an arrangement of planes is said to be *central* [87]. For the benefit of generality, the partitions of a space created by an arrangement of hyperplanes are usually described in terms of the dimensionality of the partition: A k -dimensional partition is known as a "k-face" of the arrangement. Thus, we will refer to the *regions*, *facets*, *lines* and *points* as the 3-faces, 2-faces, 1-faces and 0-faces of the arrangement.

Given an arrangement of planes as described above, it follows that any system slip state S_k that is consistent with a possible object motion must correspond to either a 3-face, 2-face, 1-face and 0-face of this plane arrangement. Finding the maximum number of 3-faces given m planes in a central arrangement is equivalent to finding the maximum number of two-dimensional regions on a sphere cut with m great circles, which is known to be $O(m^2)$ [88]. However, the 3-faces do not define all the combinations of slip states we care about. We must also consider the cases where at least one contact rolls, namely the 2-faces, 1-faces and 0-faces defined as above.

Let $f_k^{(d)}(n)$ be the number of k -faces of an arrangement of n hyperplanes in d dimensional space. Zaslavski's formula [89] provides the following upper bound:

$$f_k^{(d)}(n) \leq \binom{n}{d-k} \sum_{i=0}^k \binom{n-d+k}{i} \quad (4.12)$$

In our case, the total number of slip states we are interested in is equal to $\sum_{k=0}^3 f_k^{(3)}(m)$ and hence bounded from above by a polynomial in m . This is, however, an upper bound that will

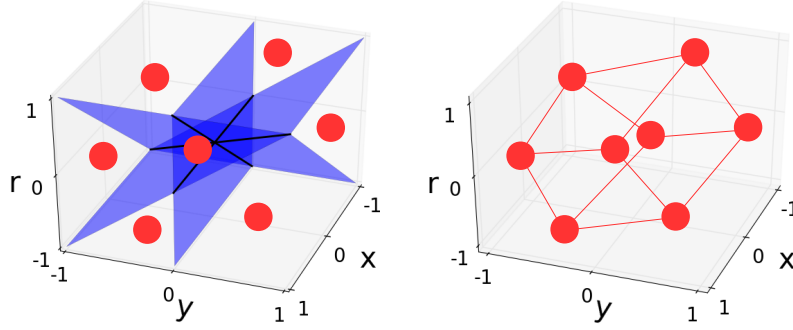


Figure 4.3: Dual polyhedron for the arrangement of planes. Each 3-face of the arrangement of planes (red dot) corresponds to a vertex of the polyhedron (for clarity, only 7 regions are marked in the left figure). Vertices are connected if the corresponding 3-faces share a 2-face.

not be attained in our case, as we show next. Let us construct the dual convex polyhedron to our arrangement of planes, which will be instrumental in enumerating all possible slip states. Each 3-face of the plane arrangement corresponds to a vertex of the polyhedron, and each two dimensional boundary (2-face) between 3-faces corresponds to an edge connecting the vertices corresponding to the neighboring 3-faces (see Fig. 4.3.) We can ensure this polyhedron is convex by selecting, as the representative vertex for each region, a point where the 3-face intersects the unit sphere. We note that the 1-faces of our plane arrangement correspond to the faces of the dual polyhedron. The dual polyhedron thus also fully describes our possible slip states.

Like any convex polyhedron, the dual we have constructed can be represented by a 3-connected planar graph. From this result, we can bound the number of slip states even more closely than with Zaslavski's formula: Any maximal planar graph with V vertices has at most $3V - 6$ edges and $2V - 4$ faces and hence the number of edges and faces of our polyhedron are linearly bounded by the number of its vertices. Since we already know the number of vertices to be $O(m^2)$, so are the number of edges and faces. Thus, the number of slip states we must consider is quadratic in the number of contacts.

For the number of detachment states the argument must be adapted if the grasp is pre-stressed, as the planes — due to the normal contact motion constraints — do not pass through the origin. The arrangement of planes is no longer *central*. Thus, we cannot construct a dual polyhedron and the above result does not hold. However, for the normal motion constraints we are only concerned with

the 3-dimensional regions and none of the lower dimensional elements of the partition. Zaslavski's formula still applies and provides an upper bound for the number of contact detachment states that is cubic in the number of contacts even in the case of preloaded grasps.

4.6 Contact state enumeration

We can now present a complete procedure for enumerating all possible detachment states U_k and slip states S_k of an m -contact system that are consistent with rigid body object motion. Again, we will only describe the process for the slip states as the procedure for the detachment states is a simplification (only the first step is required).

Step 1. We begin by enumerating all the slip states S in \mathbb{S} corresponding to 3-faces in our plane arrangement. We achieve this using Algorithm 1. Recall that all such $S \in \{-1, 1\}^m$.

The algorithm operates by initializing \mathbb{S} with just a single empty slip state $\{\}$, which corresponds to a 3-face that includes all of \mathbb{R}^3 . We then one by one introduce the planes defined by the contact slip expressions. Whenever we introduce a new plane we iterate through all slip states in \mathbb{S} . At the beginning of the iteration we remove slip state S_k from \mathbb{S} and check if its corresponding 3-face intersects with the halfspaces defined by the new plane.

The existence of this intersection can be efficiently tested for by a linear program: Use the elements in S_k and the corresponding planes to construct the linear inequalities that define its corresponding 3-face. Then add an additional inequality constraint for the halfspace either above or below the new plane. The feasibility of such a linear program tells us if a point exists that lies in both the original 3-face and the halfspace defined by the new plane. Thus, a 3-face and a halfspace intersect if the corresponding linear program is feasible. We then add a new 3-face for each halfspace with which S_k intersects. The new 3-faces are the same as S_k but we append a 1 or -1 to indicate if it lies above or below the newly added plane.

We note that for any state S obtained by this algorithm, all contacts are slipping, in either the positive or negative direction ($s_i^k = \pm 1$ for all i .) We have not yet considered rolling contacts.

Algorithm 1

```
Initialize  $\mathbb{S}$  with empty state  $S_0 = \{\}$ 
for  $i = 1..m$  do
  for  $k = 1..\#(S)$  do
    Remove  $S_k$  from  $\mathbb{S}$ 
    if 3-face  $S_k$  intersects halfspace above plane  $P_i$  then
      Create 3-face  $S_{k+} = \{S_k, 1\}$ 
      Add  $S_{k+}$  to  $\mathbb{S}$ 
    end if
    if 3-face  $S_k$  intersects halfspace below plane  $P_i$  then
      Create 3-face  $S_{k-} = \{S_k, -1\}$ 
      Add  $S_{k-}$  to  $\mathbb{S}$ 
    end if
  end for
end for
return  $\mathbb{S}$ 
```

Step 2. Now we create the slip states corresponding to 2-faces in the plane arrangements (one rolling contact). As mentioned before, these correspond to edges of the dual polyhedron, so we begin this step by constructing the dual polyhedron. We already have its vertices: each state S created at the previous step defines a 3-face of the plane arrangement, and thus corresponds to a vertex of the dual polyhedron. Then, for every two states S_k, S_l in \mathbb{S} that differ by a single s_i , we add the edge between them to the dual polyhedron (note that thus our polyhedron is also a partial cube where edges connect any two vertices with Hamming distance equal to 1 [90]). Furthermore, we also create an additional state S_{kl} corresponding to the facet between S_k and S_l . This will be identical to both S_k and S_l , with the difference that $s_i = 0$ (the entry corresponding to the plane that this 2-face lies in is set to 0).

Step 3. Next, we must compute the slip states corresponding to 1-faces in our plane arrangement (two rolling contacts), which correspond to the faces of the dual polyhedron. We obtain the faces of our dual polyhedron by computing the Minimum Cycle Basis (MCB) of the undirected graph defined by its edges (computed at the previous step). This gives us $F - 1$ of the faces of our polyhedron; to see why consider that the number of cycles in the minimum cycle basis is given by $E - V + 1$ [91]. Recall the Euler-Poincaré characteristic $\chi = V - E + F$ relating the number

of vertices, edges and faces of a manifold. For a convex polyhedron $\chi = 2$, and from this we can derive the number of faces of our dual polyhedron to be equal to $E - V + 2$. The last face is obtained as the symmetric sum of all the cycles in the MCB (defined as in [91]). Once we have the cycles corresponding to the faces of the dual polyhedron, we convert them into slip states as follows. For each cycle, starting from the slip state S_k corresponding to any of the vertices in the cycle, we set $s_i = 0$ for any plane i that is traversed by an edge in the cycle.

Step 4. Finally, we must add the single 0-face of the plane arrangement by adding a slip state $\{0\}^m$ to \mathbb{S} .

The total number of slip states S we obtain is thus 1 greater than the number of 3-faces, 2-faces and 1-faces of the plane arrangement, which is the same as the number of vertices, edges and faces in its dual polyhedron. We have already shown that this is polynomial (quadratic) in the number of planes (contacts). We also show that the enumeration algorithm above has polynomial runtime. We note that Step 1 has two nested loops, with one iterating over planes and the other one over existing states. The number of states at the end of this step is bounded by m^2 , thus the running time of this Step is $O(m^3)$. Step 2 must check every state against every other one, with $O(m^2)$ states, thus its running time is $O(m^4)$. Finally, the dominant part of Step 3 is the computation of the MCB. We have used an implementation with $O(E^3 + VE^2 \log V)$ running time, where V and E are the number of vertices and edges of the dual polyhedron. Since both E and V are polynomial in m , the running time of the MCB algorithm is as well. Thus our complete enumeration method has polynomial runtime in the number of contacts m .

Also note that the computation of contact detachment states is much simpler as we only require the 3-faces of the arrangement of planes defined by the normal contact motion constraints. Thus, only the first step of the above procedure is required. In order to obtain the total set of possible combinations of contact states we must combine the two sets \mathbb{U} and \mathbb{S} such that for every combination of persisting contacts we superimpose the set of all combinations of contact slip states. Note, that the slip state information for a detached contact does not hold any value and hence in practice Algorithm 1 could be modified to consider both the sets of planes due to normal and tan-

Algorithm 2

```
Build  $\mathbb{T} = \mathbb{U} \times \mathbb{S}$ , the set of all possible contact states
for  $k = 1.. \#(\mathbb{T})$  do
    Given  $T_k$ , solve system (4.9)
    if solution found then
        return grasp stable
    end if
end for
return grasp unstable
```

gential motion constraints simultaneously only recording the state combinations that are actually useful. Of course even without this optimization the total number of contact state combinations to be considered remains polynomial in the number of contacts.

4.7 Complete stability determination procedure

We can now formalize our complete algorithm using the components outlined so far (Algorithm 2). We first build the total set of possible contact states $\mathbb{T} = \mathbb{U} \times \mathbb{S}$. Then, for every $T_k \in \mathbb{T}$, we check for a solution to the system as described in Chapter 4.4. If one exists, we deem the grasp stable. If, after enumerating all possible T_k , we do not find one that admits a solution, we deem the grasp unstable. We make two important observations regarding Algorithm 2. First, its running time is polynomial in the number m of contacts. This follows from the results obtained so far: We know that $\#(\mathbb{T})$ is polynomial in m , as is the process for building it. For each T_k , we then solve at most a linear program with $2m + 3$ unknowns, which also has a polynomial runtime, which completes this result.

Second, Algorithm 2 guarantees that, if no solution is found, none exists that satisfies the constraints of our system. \mathbb{T} provably contains all the contact states consistent with rigid body motion; for each of these, equilibrium and contact conditions form a linear program for which we can provably find all solutions (if they exist). So, under the assumed formulation (virtual springs used to determine contact normal forces, and frictional constraints including the maximum dissipation principle), if a solution exists to the equilibrium problem, we must find it.

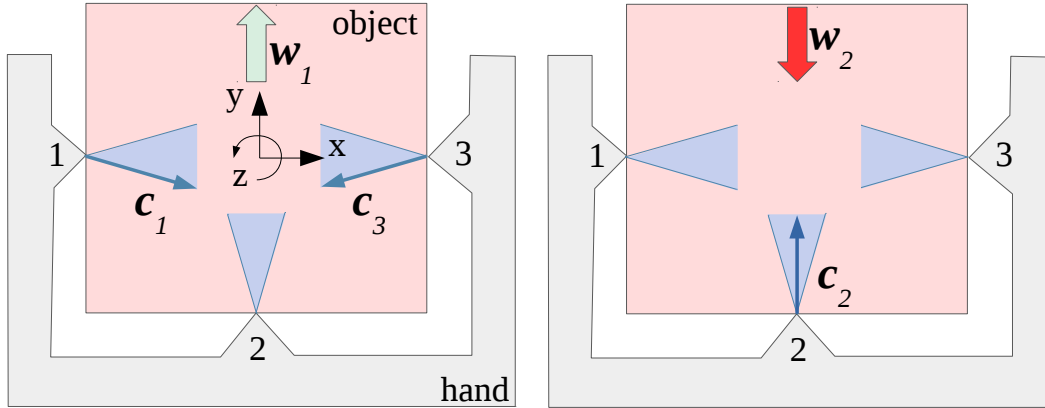


Figure 4.4: A grasping scenario where a rigid hand establishes multiple frictional contacts (numbered 1-3) with a target object. External disturbance w_1 (left, pushing the object up) can be resisted by contact forces c_1 and c_3 , but only if contacts 1 and 3 have been actively pre-loaded with enough normal force to generate the corresponding friction forces. In contrast, disturbance w_2 (right, pushing the object down), regardless of its magnitude, will always be passively resisted by contact force c_2 .

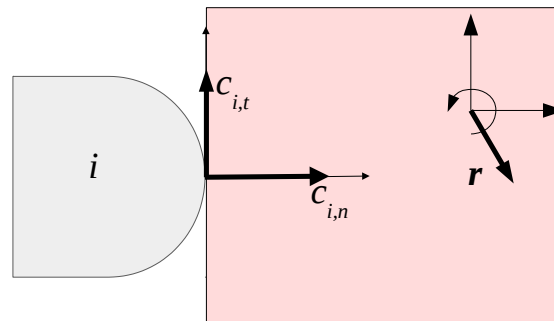


Figure 4.5: Illustration of the contact coordinate frame. r denotes object motion expressed in the object coordinate frame.

4.8 Applications to planar grasp stability analysis

In this section we will demonstrate that our framework predicts the correct force distributions and makes an accurate prediction on grasp stability. We will utilize the grasp shown in Fig. 4.4 because the correct force distribution and stability of the grasp is easily understood intuitively. Specifically, we would like to discriminate which applied wrenches will be balanced purely passively, and where an active preload of the grasp is required. We assume the friction coefficient is 0.5 across all contacts such that $\mu_i = 0.5$, $i = 0..m$.

Recall that there exist contact forces in the interior of the friction cones that balance both

wrenches shown in Fig. 4.4. Perhaps the most commonly used approach to grasp stability analysis is the Grasp Wrench Space method [21]. Indeed, when we consider the slice through the GWS visualized in Fig. 4.6(c) we can see that there exist contact forces that balance arbitrary forces in the plane. However, we argue that while w_2 will always be reacted passively, no matter the preload, in order to react w_1 we require the grasp to have been sufficiently preloaded. The GWS method correctly indicates the existence of equilibrium contact forces but does not predict if they may arise, and hence does not capture the necessity of a preload. Thus, in this context force closure is not a reliable indicator of stability.

Now let us apply our framework to this problem: Using our algorithm, we can test the resistance of this grasp to forces in the plane. We do this by discretizing the direction of application of force to the object and finding the maximum resistible force in each direction using a binary search. Figs. 4.6(a) & 4.6(b) show the region of resistible forces for a grasp without and with a preload respectively. As our algorithm takes into account passive effects it correctly predicts that, in both cases, forces with non-positive component in the y-axis and arbitrary magnitude can be withstood. Indeed, without preloading the grasp for any applied force $w = (0, w_y, 0)$, $w_y \leq 0$ our framework predicts contact forces $(0, 0)$ at contacts 1 and 3, and contact force $(-w_y, 0)$ at contact 2 (see Table 4.2). Furthermore, it captures the necessity of a preload in order to resist forces with positive component in the y-direction: For $w_y > 0$ our algorithm finds no solution, and hence the grasp must be unstable to this disturbance, unless an appropriate preload is applied.

We can compare our results to those obtained with compliance based approaches [34][36][23][37][38], which are commonly used to predict contact forces that arise in grasps due to disturbances. We can now use this grasp (Fig. 4.4) and our algorithm to show that even with the improvements to a linear compliance suggested by Prattichizzo et al. [38] resulting stability estimates are overly conservative. Their approach allows each contact to be in one of three states: rolling, slipping or detached. A slipping contact may not apply any frictional forces, while a detached contact may not apply any force at all. If we try every possible combination of states and modify the compliance of the grasp accordingly, this alleviates some of the problems of the purely linear

\boldsymbol{w}	P	Stable	\boldsymbol{c}_1	\boldsymbol{c}_2	\boldsymbol{c}_3	\boldsymbol{r}
(0, 0, 0)	0	Yes	(0, 0)	(0, 0)	(0, 0)	(0, 0, 0)
(0, 0, 0)	1	Yes	(1, -0.5)	(1, 0)	(1, 0.5)	(0, 0, 0)
(0, -1, 0)	0	Yes	(0, 0)	(1, 0)	(0, 0)	(0, -1, 0)
(0, -2, 0)	0	Yes	(0, 0)	(2, 0)	(0, 0)	(0, -2, 0)
(0, 1, 0)	0	No	—	—	—	—
(0, 1, 0)	1	Yes	(1, -0.5)	(0, 0)	(1, 0.5)	(0, 1, 0)
(0, 1, 1, 0)	1	No	—	—	—	—

Table 4.2: Contact forces $\boldsymbol{c}_i = (c_{i,n}, c_{i,t})$ and (virtual) object motion $\boldsymbol{r} = (x, y, r)$ for the grasp in Fig. 4.4 and a range of applied wrenches $\boldsymbol{w} = (w_x, w_y, w_z)$. The preload P is such that the normal force at each contact is equal to either 0 or 1 before any wrench is applied. The object motion and applied wrenches are expressed in the coordinate frame shown in Fig. 4.4 and contact forces are expressed in frames as shown in Fig. 4.5.

m	2	3	4	5	6	7	8	9
#(\$)	10	26	50	82	122	170	226	290
time(s)	0.006	0.02	0.09	0.42	1.5	4.8	13.8	35.7

Table 4.3: Number of slip states #(\$) and computation time for grasps with m randomly generated contacts.

compliance approach: If we consider contacts 1 & 3 to be slipping, our grasp in Fig. 4.4 may now withstand arbitrary forces, where $w_y \leq 0$.

This approach, however, does not allow us to arrive at the correct result in cases where $w_y \geq 0$. Consider the preloaded grasp before the application of an external wrench (Table 4.2.) The contact forces on both contacts 1 & 3 must lie on the friction cone edge in order to balance the preload applied by contact 2. If we now apply an external wrench $\boldsymbol{w} = (0, 1, 0)$, there exists no combination of rolling, slipping and detached contacts (and corresponding modifications of the linear compliance) that results in legal contact forces. Our algorithm, however, predicts a stable grasp (Table 4.2), showing how important friction is for grasp stability and why a correct treatment of friction is fundamental to stability analysis. Furthermore, we have arrived at this result in polynomial time — we did not have to consider exponentially many slip states, as in [38].

From a computational effort perspective, a summary of the performance of our algorithm for enumeration of slip states can be found in Table 4.3. All computation was performed on a commodity computer with a 2.80GHz Inter Core i7 processor.

4.9 Discussion

In this Chapter we have described an algorithm that can test the stability of a rigid planar grasp when a given disturbance wrench is applied to the grasped object. We propose modeling the contact normal forces through constitutive relations while maintaining accurate friction constraints. In order to apply this model we must distinguish between rolling, slipping and detaching contacts. We have shown that the number of combinations of contact states that are possible under rigid body motions is quadratic in the number of contacts and provide a polynomial time algorithm to enumerate all such combinations.

As has been noted in Chapter 4.5 the insight that the number of contact slip state combinations between two rigid bodies in contact is quadratic in the number of contacts is not new [45][46]. However, we have shown that this remains valid when introducing compliance at the contact normals, as is required to efficiently test for stability. Our novel algorithm for the polynomial-time enumeration of contact state combinations also enables the analysis of grasps that are preloaded before the application of an external wrench.

A limitation of the work presented above is that we defined a grasp preload in terms of the contact normal forces present before the application of an external wrench to the object. In practice, preloads are achieved by setting actuator commands. Thus, defining preloads in terms of joint torques for instance is of perhaps greater practical use as it would allow us to use our framework as a tool in computing appropriate actuator commands for a given task.

The required treatment of the kinematics of the hand means we must take into account not only the motion of the grasped object but also of the links making up the hand. Our algorithm can be extended to such multi-body systems, which would allow us to study the stability of multiple objects or objects grasped by hands with multiple links and torques applied at the joints. The constraints that describe such systems involve the motion of multiple objects and thus more motion variables than the three dimensional object motion we consider in the above treatment. Therefore the planes describing the constraints become higher dimensional hyperplanes. However, much of

the theory in Chapter 4.5, specifically Zaslavski's formula remains valid for such arrangements of hyperplanes:

For a given number of objects the number of contact state combinations remain polynomial in the number of contacts. However, the number of contact state combinations is exponential in the number of bodies. The enumeration of the faces of the arrangement that correspond to sets of contact conditions is more involved but arrangement of hyperplanes are well studied in the field of computational geometry and efficient algorithms are available for the solution of such problems [92].

The exponential growth of the number of possible contact state combinations with the number of bodies involved is a well known problem in the rigid body dynamics community. In fact, many researchers have independently shown that the underlying complementarity problems are NP-hard (see Chapter 2.2.) A further complication of these complementarity approaches is that, in order to determine stability, one has to show that *every* solution to the dynamics equations is stable. Due to the possibility of multiple solutions to the complementarity problem with different contact state combinations this means that unfortunately the only way to ensure stability is to check all possible combinations.

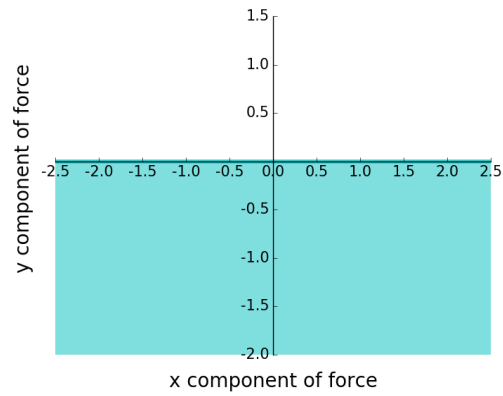
An approach to multi rigid body problems that instead uses our normal force compliance model would suffer from the same worst-case exponential complexity due to an exponential number of contact state combinations. However, in our model finding a single solution is sufficient to conclude grasp stability and thus the computational burden is reversed: You only have to check all combinations to be able to conclude that a grasp is *not* stable by checking that none of them have a solution.

Finally, we want to discuss the perhaps most significant limitation in that this work is only applicable to planar grasps. Unfortunately the key insight that allowed us to formulate an efficient solution to passive stability problems does not directly translate to spacial grasps: In 3D the directions a contact can slip in are no longer discrete and finite. A contact can slide in an infinite number of directions and hence we cannot break the treatment of sliding contacts into separate piecewise

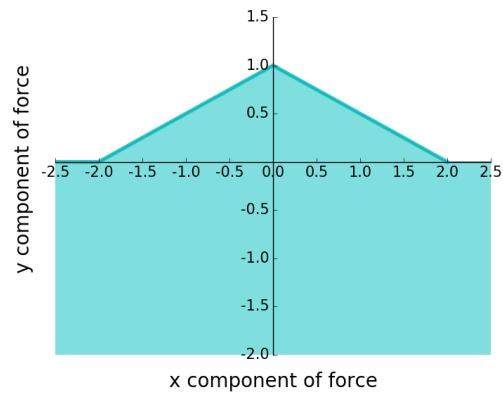
linear problems as we did above.

However, we were pleased to see that Huang et al. [93] adopted an approach based on arrangements of planes and developed an algorithm for the enumeration of slip states in three dimensions. They approach the problem of infinite sliding directions by discretizing the tangent plane into sectors of equal angles. Thus, sliding states are defined in terms of which sector contains the tangent velocity.

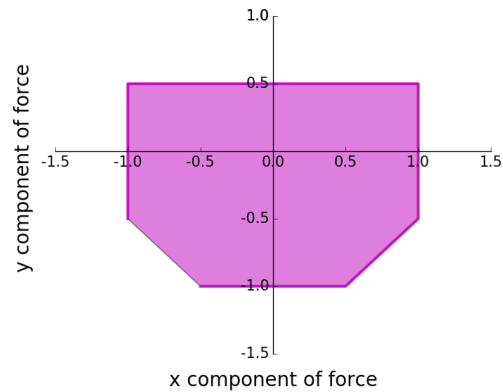
Despite these limitations, our treatment of the special planar case has proven to be a valuable first step towards modeling the passive characteristics of general grasps, which we will investigate in the following chapters.



(a) Resistible forces with no preload (our algorithm)



(b) Resistible forces with a preload such that the normal force at each contact is 1 (our algorithm)



(c) Slice through the three dimensional GWS for zero applied torque

Figure 4.6: Grasp stability representations for the grasp in Fig. 4.4. Our algorithm (a)(b) captures passive resistance to applied forces of arbitrary magnitude in directions, that allow for balancing contact forces to arise passively in response to the disturbance. The GWS representation (c) shows the space of applied forces the grasp can resist with contact forces that satisfy only friction constraints. We are using the L1 norm GWS, meaning the normal components of the contact forces sum to 1.

Chapter 5: Grasp Stability Analysis in Three Dimensions

5.1 Introduction

In Chapter 3 we described the importance of modeling passive effects for robotic manipulation and began our investigation with the planar case in Chapter 4. Of course most robotic grasps are not planar: The fingers and grasped objects do not in general inhabit the same plane. Furthermore, even grasps that may look to be planar at first (such as the grasp in Fig. 3.1) require modeling of all three spacial dimensions in the presence of out-of-plane forces or moments.

Thus, in order to further our understanding of the passive effects at play in the grasps commonly encountered in practice we must extend our work from Chapter 4 to spacial grasps. Unfortunately, our treatment of planar grasps does not easily generalize. In order to enforce the maximum dissipation principle (friction opposes motion) our framework relied on the fact that in the plane a contact can only slide in one of two directions. In three dimensions contacts can slide in an infinite number of directions and thus we cannot enumerate a finite number of contact states as we did in Chapter 4.

This means that enforcing the principle of maximum dissipation is more involved in three dimensions. However, as we will see an accurate treatment of the friction constraints including the maximum dissipation principle is of paramount importance for the modeling of passive effects. Simply dropping the maximum dissipation principle allows for unphysical solutions and thus we cannot determine stability. This may be somewhat surprising as we are only trying to solve for the contact wrenches of stable grasps where hence all motions are minuscule. We will present a physically motivated method for alleviating the consequences of dropping the MDP such that only physically realistic solutions are obtained.

Even though our formulation for planar grasps does not directly generalize to three dimensions,

the insights gained in the previous chapter will prove to be useful also in the three dimensional case. Specifically, we already know that we can use a compliance model to capture passive effects.

In order to develop a grasp model that is truly general and applicable to the vast majority of robotic hands currently in use we also choose to take into account effects previously omitted in Chapter 4. We will no longer assume the hand to be a rigid fixture but instead take into account the kinematics of the hand as well as the commanded actuator torques. This allows us to showcase the use of our framework as a practical tool.

5.2 Grasp model

The model we choose to describe a grasp in three dimensions is similar to the planar model introduced in Section 4.2 and we will make the same assumptions that initially the bodies are at rest and all motions (in this context displacements) are small such that the grasp geometry is constant.

We consider a hand making m contacts with a grasped object where we again use the *Point Contact with Friction* model to describe the contact forces. We will again denote normal and tangential components of contact specific vectors with subscripts n and t respectively. However, in three dimensions the tangential component of such a vector is no longer a scalar but a vector itself: At a contact i the contact force $\mathbf{c}_i \in \mathbb{R}^3$ has normal and tangential components $c_{i,n} \in \mathbb{R}$ and $\mathbf{c}_{i,t} \in \mathbb{R}^2$ respectively.

Equilibrium: In three dimensions the grasp map matrix also has different dimension ($\mathbf{G} \in \mathbb{R}^{6 \times 3m}$). One addition to the grasp model is that we will also consider the kinematics of the hand and must therefore also take into account not only object but also hand equilibrium. For a hand with l joints the transpose of the hand Jacobian $\mathbf{J} \in \mathbb{R}^{3m \times l}$ maps contact forces to joint torques $\boldsymbol{\tau} \in \mathbb{R}^l$.

$$\mathbf{G}\mathbf{c} + \mathbf{w} = 0 \quad (5.1)$$

$$\mathbf{J}^T\mathbf{c} + \boldsymbol{\tau} = 0 \quad (5.2)$$

These equilibrium equations can predict the resultant wrench on the object and the joint torques that arise in response to given contact forces, but, since neither \mathbf{G} nor \mathbf{J}^T are typically invertible in practice, it has no predictive capabilities in the opposite directions: we cannot use it to predict the contact response to known external wrenches, or joint torques. It thus fails to capture effects where contact forces are transmitted (either amongst the joints or between the joints and the external environment) through the object itself.

We could use one of the many methods discussed in Section 2.1 to find a set of contact wrenches \mathbf{c}_{eq} that balance a given applied wrench and are achievable with the kinematic and actuation capabilities of the hand. However, in the vast majority of cases in applied robotics, this simple method has major shortcomings. It requires that we know \mathbf{w} exactly at any point in time, which is unrealistic in all but the most controlled environments. Furthermore, most robotic hands are position controlled and hence lack the torque regulating capabilities necessary to accurately command the actuators for real time grasp control.

The approach actually used in the overwhelming majority of robotic grasping tasks is to command a given set of joint torques $\boldsymbol{\tau}^c$ and let the fingers jam around the object. We keep torque commands constant throughout the task (i.e. we take no further action) and rely on appropriate equilibrium contact forces \mathbf{c} and equilibrium torques $\boldsymbol{\tau}^{eq}$ to arise through *passive reactions*. This simple strategy is effective for hands powered by highly geared motors due to the non-backdrivable nature of the actuators: At any joint j the equilibrium torque τ_j^{eq} can exceed the commanded value τ_j^c in a passive response to torques τ_k^c , $k \neq j$ or the applied wrench \mathbf{w} . An intuitive example of this phenomenon might be an object being pressed against a finger by an external wrench. If the wrench is large enough to overwhelm the commanded joint torques then any additional torques at the finger joints are provided passively by the gearbox such that the finger remains fixed.

Much the same as in Chapter 4 we must introduce the notion of compliance to our grasp model in order to resolve the structural indeterminacy. Therefore the motion of the bodies making up the grasp become part of the solution we are seeking. This is much the same as was previously presented in Section 4.2. We denote object motion as $\mathbf{r} \in \mathbb{R}^6$, however now the joints of the hand

and therefore the hand links may also exhibit motion denoted by a change in joint angles $\mathbf{q} \in \mathbb{R}^l$.

We have already seen in Section 4.2 how contact motion due to the object moving allowed us to capture the unilateral contact behavior. However, we must now argue about *relative* motion at the contacts $\mathbf{d} \in \mathbb{R}^{3m}$, as both the object and the contacting link may move. Recall that in the context of our grasp model by motion we mean the displacements of the bodies involved and this relation is only valid for small displacements.

$$\mathbf{G}^T \mathbf{r} - \mathbf{J} \mathbf{q} = \mathbf{d} \quad (5.3)$$

Again, as we assume a constant grasp geometry matrices \mathbf{G} and \mathbf{J} are also constant. We can now reason about the contact forces and joint torques in terms of the motion of the object and joints.

Normal forces. In Chapter 4.2 we discussed a compliance formulation of the unilateral contact constraint. We will use the same constitutive equations for the contact normal forces obtained by placing virtual linear springs of unit stiffness along the contact normals.

$$\begin{cases} c_{i,n} = -d_{i,n} & \text{if } d_{i,n} \leq 0 \\ c_{i,n} = 0 & \text{if } d_{i,n} > 0 \end{cases} \quad (5.4a)$$

$$\begin{cases} c_{i,n} = -d_{i,n} & \text{if } d_{i,n} \leq 0 \\ c_{i,n} = 0 & \text{if } d_{i,n} > 0 \end{cases} \quad (5.4b)$$

In Chapter 4.2 we also included a normal force term for *preloaded* grasps. We can ignore this term here as we are now also explicitly modeling the hand kinematics. This allows us to define a preload in terms of joint torques instead of normal forces, which is how preloads are applied in practice. These preload joint torques then propagate through the links making up the hand as well as the object according to the equilibrium equations (5.1) & (5.2) and thus create the preload contact forces present before the application of any external forces.

Friction forces: Again, we choose the Coulomb model to describe the friction forces. The first part of the Coulomb model provides an upper bound to the magnitude of the friction force given

the normal force and the friction coefficient μ_i . As we are investigating the static equilibrium of a grasp we consider all friction coefficients to be those of static friction. This defines a cone \mathcal{F}_i at each contact.

$$\mathcal{F}_i(\mu_i, c_{i,n}) = \{\mathbf{c}_{i,t} : \|\mathbf{c}_{i,t}\| \leq \mu_i c_{i,n}\} \quad (5.5)$$

The second part of the Coulomb model concerns the *Maximum Dissipation Principle* [40]. Now we will show how the MPD results in friction forces that oppose the relative motion at the contact. The MDP states that given a relative contact motion the friction force at that contact must maximize the dissipation where the friction force is bounded by (5.5).

$$\mathbf{c}_{i,t} \in \arg \min_{\mathbf{c}_{i,t} \in \mathcal{F}_i} \mathbf{c}_{i,t}^T \cdot \mathbf{d}_{i,t} \quad (5.6)$$

Joint torques: Finally, we model the joints as nonbackdrivable, in order to capture the behavior of robotic hands driven by highly geared motors. This means that a joint j may only exhibit motion in the direction that its commanded torque is driving it in. As we know the commanded joint torques we can define motion in such a direction as positive.

$$q_j \geq 0 \quad (5.7)$$

A joint with zero commanded torque may not move, as any torque arising from external factors will be absorbed by the gearing.

The joint torque may exceed the commanded level, but only if this arises passively. This means that a joint that is being passively loaded beyond the commanded torque levels must be locked in place and may not move. A moving joint must apply the torque it was commanded to. Thus, we

must also distinguish between two types of joints.

$$\begin{cases} \tau_j \geq \tau_j^c & \text{if } q_j = 0 \\ \tau_j = \tau_j^c & \text{if } q_j > 0 \end{cases} \quad (5.8a)$$

$$\begin{cases} \tau_j = \tau_j^c & \text{if } q_j > 0 \end{cases} \quad (5.8b)$$

So far this joint model has assumed a the kinematics of a fully actuated direct drive robotic hand, where an actuator command equates to an individual joint torque command. However, a more general formulation allows modeling hand kinematics, where the joint torques can be expressed as linear combinations of actuator forces. This includes underactuated designs with fewer actuators than degrees of freedom such as, for example, a tendon driven hand with fewer tendons than joints. This implies, that a tendon — and hence an actuator — can directly apply torques to multiple joints by means of a mechanical transmission.

We thus define matrix \mathbf{R} , which maps from forces or torques at the actuators \mathbf{f} to joint torques $\boldsymbol{\tau}$. Note, that its transpose maps from joint motion to the motion of the mechanical force transmission at the actuator, which we assume to be nonbackdrivable. Inequality constraints on a vector are to be understood in a piecewise fashion.

$$\mathbf{R}\mathbf{f} = \boldsymbol{\tau} \quad (5.9)$$

$$\mathbf{R}^T \mathbf{q} \geq 0 \quad (5.10)$$

Hence, at an actuator l we may see a force f_l that exceeds the commanded value f_l^c — and again, this can only occur passively. This means, that an actuator force can only exceed the commanded value, if there is an attempt to backdrive the actuator, and hence the mechanical transmis-

sion does not exhibit any motion.

$$\begin{cases} f_l \geq f_l^c & \text{if } (\mathbf{R}^T \mathbf{q})_l = 0 \end{cases} \quad (5.11a)$$

$$\begin{cases} f_l = f_l^c & \text{if } (\mathbf{R}^T \mathbf{q})_l \geq 0 \end{cases} \quad (5.11b)$$

This actuation model is a generalization of the previously introduced joint model and will reduce as such if the actuators control individual joint torques directly.

Complete problem: The system comprising (5.1) – (5.11) defines the static equilibrium formulation for an arrangement of bodies; some fixed, some free, some constrained by unilateral or bilateral constraints. Some bodies may be acted upon by actuators or externally applied wrenches. The formulation satisfies all the requirements for determining stability including passive effects due to nonbackdrivability and underactuation but is also applicable to many other problems with arrangements of bodies in frictional contact.

Definition of stability: In the following we will make use of the same definition previously introduced in Chapter 4.3: For a given grasp geometry, actuator torques and applied wrench a grasp is deemed to be stable if a solution to the above system of constraints exists. However, note that the above formulation is very general in nature, and can not only be used in such *existence problems* (e.g. given \mathbf{f}^c , determine if \mathbf{r} and \mathbf{c} exist that balance a given \mathbf{w}). With the addition of an objective we can also apply it in *optimization problems* (e.g. determine the optimal \mathbf{f}^c that satisfies the existence problem above).

Remaining agnostic to the exact query that is being solved we will refer to the *exact problem* as the following query: given a subset of \mathbf{f} , \mathbf{r} , \mathbf{c} or \mathbf{w} , determine the rest of these variables such that (5.1) – (5.11) are exactly satisfied (i.e. the grasp is stable).

5.3 Formulation as a Mixed Integer Program

5.3.1 Unilaterality

Let us take a closer look at the types of constraints that make up the exact problem. The equilibrium equations in (5.1) & (5.2) as well as the kinematics (5.3) & (5.9) are linear equality constraints and require no further attention. The unilaterality constraints in (5.4) & (5.11) consist of pairs of linear equalities and inequalities but exhibit a combinatorial nature: Only one of the constraints is active at a time, the choice of which is unknown a priori.

In Chapter 4 we dealt with constraints of this nature by separately evaluating the problems arising from each choice of constraint combinations. As we were only interested in the *existence problem*, each individual problem involved solving at most a linear program. Therefore this approach could be efficiently leveraged to solve problems involving such combinatorial constraints. As we want to develop a formulation that can also be applied to the more complex *optimization problems* we choose a Mixed Integer Programming (MIP) approach instead. Both the normal force and the joint model relationships (5.4) & (5.11) can be cast as pairs of convex constraints with binary decision variables in an MIP that can then be solved using algorithms such as branch and bound.

The perhaps simplest implementation of such constraints is the 'Big M method'. For instance we can reformulate (5.4) as four linear inequality constraints with the addition of a binary decision variable $y_i \in \{0, 1\}$ and two large constants $M_{i,1}$ and $M_{i,2}$, which give the method its name. The binary variable can be interpreted as the variable deciding if a contact rolls ($y_i = 1$) or breaks ($y_i = 0$).

$$c_{i,n} \geq 0 \quad (5.12)$$

$$c_{i,n} + d_{i,n} \geq 0 \quad (5.13)$$

$$c_{i,n} \leq M_{i,1} \cdot y_i \quad (5.14)$$

$$c_{i,n} + d_{i,n} \leq M_{i,2} \cdot (1 - y_i) \quad (5.15)$$

The two constants must be chosen to be larger than the largest expected value of the left hand side of their respective inequality constraint. However, choosing too large a value can lead to numerical issues. An example of such a numerical issue is 'trickle flow', in which a small violation of the integrality constraint can lead to a violation of the inequality. Numerical optimization tools must work within finite tolerances and thus small violations are unavoidable. Specifically in our example a y_i that is slightly larger than zero allows for nonzero contact normal force when multiplied with a large $M_{i,1}$ even at a breaking contact.

An alternative approach is to use indicator constraints, which avoids these issues. These constraints allow a Mixed Integer solvers to directly branch on the constraint choices or derive tight 'big M' values during preprocessing [94].

$$\begin{cases} y_i = 1 \\ y_i = 0 \end{cases} \quad \begin{matrix} \implies \\ \implies \end{matrix} \quad \begin{matrix} c_{i,n} = -d_{i,n}, \\ c_{i,n} = 0, \end{matrix} \quad \begin{matrix} d_{i,n} \leq 0 \\ d_{i,n} > 0 \end{matrix} \quad \begin{matrix} (5.16a) \\ (5.16b) \end{matrix}$$

A potential downside is that indicator constraints tend to have weaker relaxations and thus may lead to larger MIP optimization times. In practice we have found that this disadvantage is more than compensated for by their ease of use as well as numerical stability when compared to the big M method. Thus, going forward we will use indicator constraints in order to deal with conditional constraints.

Of course we can also use indicator constraints to model the unilaterality of nonbackdrivable

actuator constraints (5.11) by introducing binary variable $z_l \in \{0, 1\}$, which indicates if the actuator is free to move ($z_l = 0$) or being overpowered by external forces ($z_l = 1$).

$$\begin{cases} z_l = 1 \\ z_l = 0 \end{cases} \quad \begin{matrix} \implies \\ \implies \end{matrix} \quad \begin{matrix} f_l \geq f_l^c, \\ f_l = f_l^c, \end{matrix} \quad \begin{matrix} (\mathbf{R}^T \mathbf{q})_l = 0 \\ (\mathbf{R}^T \mathbf{q})_l > 0 \end{matrix} \quad \begin{matrix} (5.17a) \\ (5.17b) \end{matrix}$$

5.3.2 Friction

The Coulomb friction law in (5.5) & (5.6) provides more complexity due to its non-convexity. This is readily apparent as the bilinear form in (5.6) is not positive definite [95]. It has been pointed out that solving for $\mathbf{c}_{i,t}$ given $\mathbf{d}_{i,t}$ or vice versa is a convex problem and can be done efficiently [58]. Solving for both simultaneously is much harder — in fact the global optimization of non-convex quadratic programs is in general NP-hard.

For our purposes it will be useful to reformulate the Coulomb friction constraints. Note, that in the case of isotropic friction dissipation is maximized if the friction force is anti-parallel to the relative sliding motion and lies on the boundary of the cone \mathcal{F}_i . Thus, we can also directly express the friction force in terms of the normal force and the relative sliding motion. We must distinguish between two cases:

- At a rolling contact that does not exhibit relative motion in a tangential direction (sliding) the friction force is constrained such that the contact force lies within the cone \mathcal{F}_i
- If a contact does exhibit sliding, the friction force must oppose the relative direction of motion, and the total contact force must lie on the friction cone edge.

$$\begin{cases} \|\mathbf{c}_{i,t}\| \leq \mu_i c_{i,n} & \text{if } \|\mathbf{d}_{i,t}\| = 0 \\ \mathbf{c}_{i,t} = -\mu_i c_{i,n} \frac{\mathbf{d}_{i,t}}{\|\mathbf{d}_{i,t}\|} & \text{otherwise} \end{cases} \quad \begin{matrix} (5.18a) \\ (5.18b) \end{matrix}$$

Note, that while the formulation in (5.18) requires the distinction between sliding contacts and those remaining at rest the original formulation (5.5) & (5.6) holds in both cases.

This reformulation introduces also a discontinuity as the relation between $\mathbf{c}_{i,t}$ and $\mathbf{d}_{i,t}$ is discontinuous at $\|\mathbf{d}_{i,t}\| = 0$. We could approach this discontinuity in a similar fashion as we did above to distinguish between rolling and breaking contacts by using indicator constraints. However this does not resolve the non-convexity as (5.18b) is still non-convex.

Unfortunately the methods we developed in Section 4 cannot be directly applied to three dimensions *even with prior knowledge of which contacts slip and which do not*. While in two dimensions, a contact can only roll or slide in one of two directions (and there are hence 3 slip states per contact), in three dimensions there are infinitely many directions a contact can slip in and we cannot further break down the sliding case. These characteristics of the Coulomb model presents much difficulty in the modeling of contacts with Coulomb friction and many approaches have been proposed to approximate the friction law. We reviewed a selection of such efforts in Chapter 2.2.

As all motion in our framework is purely 'virtual' and any real motion is expected to be minuscule one may be tempted to simply consider all contacts to be stationary and cut away the discontinuity and non-convexity introduced by the MDP. Thus we would simply ignore the maximum dissipation principle (5.6) and with it (5.18b). The remaining quadratic inequality constraint (5.18a) is convex. In fact, it has been shown that (5.5) can be cast as a *linear matrix inequality* (LMI) [30].

Unfortunately, this approach does not work as we will now illustrate. The rigid, passively loaded fingers allow an optimization formulation with unconstrained object movement to 'wedge' the object between contacts creating large contact forces. This allows the grasp to withstand very large applied wrenches by performing 'unnatural' virtual displacements that satisfy all our constraints and lead to equilibrium, but violate the principle of conservation of energy: the energy stored in the virtual springs and the energy dissipated due to friction are greater than the work done by the externally applied wrench and the actuators. In the example shown in Fig. 5.1 the applied force does no work while energy is being stored in the springs and being dissipated due to

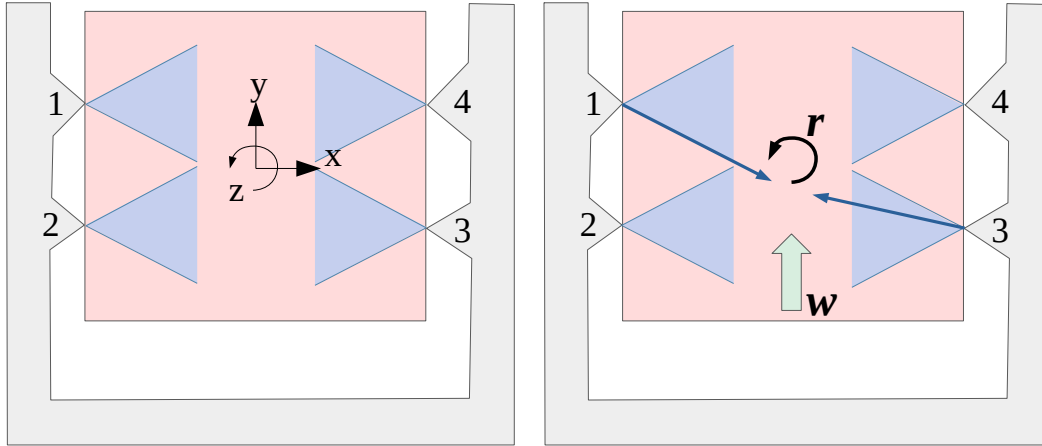


Figure 5.1: Unconstrained friction forces (except for friction cone constraint). Left: undisturbed system with no contact forces (also showing the object reference frame). Right: reaction to force \mathbf{w} applied to the object. A rotation \mathbf{r} loads the contacts such that contact forces (blue arrows) can resist the applied wrench (green arrow), even in the absence of a preload.

friction at contacts 1 and 3.

From the principle of virtual work it follows that a solution that satisfies both equilibrium and the maximum dissipation principle also satisfies conservation of energy. Hence, in order to enforce conservation of energy and obtain physically meaningful results we must enforce the MDP or find a reasonable approximation.

5.4 Iterative solution approach

Now that we have discussed the consequences of simply dropping the MDP we describe a physically motivated method to obtain accurate results. The method described in this section does not offer a guarantee of convergence. In Chapter 6 we will describe a method that is guaranteed to converge to the exact solution.

Recall that we model some compliance of the grasp in order to be able to capture passive effects. Thus, we think of a stable grasp as one that moves from one equilibrium state to another when an external wrench is applied to the grasped object. The changes in contact forces necessary to balance the applied wrench arise through the motions of the object and hand links. These motions are minuscule for the stiff hands we consider here and therefore we can ignore dynamic

effects and argue from a purely quasistatic viewpoint.

Forces applied to an object tend to move that object in the direction of the applied force. This is why the unphysical motion in Fig. 5.1 seems intuitively unnatural — the object moves in a direction orthogonal to the force applied to it. Of course the complex effects due to grasp geometry as well as a non-convex friction law mean that in general a grasped object will not move exactly along the direction of the force applied to it. While these effects are difficult to model we can devise an iterative scheme to approximate them.

In this scheme we will take small steps (in terms of object motion) such that the object may only move in the direction of the net resultant wrench applied to it. While we cannot enforce the maximum dissipation principle and its consequence — friction opposes motion — we can offer an approximation that is physically well motivated. We will introduce an objective term to the optimization that, at every step of the iteration, will minimize the magnitude of the net resultant wrench on the object. The reasoning is that such forces, when projected to the objects reference frame, oppose the net resultant wrench to their best ability. As motion is only allowed in the direction of this net resultant wrench, the contact forces computed thus oppose this motion to their best ability. Taking steps that are sufficiently small ensures that the complex geometric and friction effects of the grasp are accurately captured.

We implement this scheme by removing the object equilibrium constraint (5.1) and including an objective in the optimization formulation such as to minimize the net resultant wrench \mathbf{w}^k (the net sum of the applied wrench and contact forces) acting on the object at step k .

$$\text{minimize: } \|\mathbf{w}^k\| = \|\mathbf{w} + \mathbf{G}^T \mathbf{c}^k\| \quad (5.19)$$

We also constrain the object movement such that motion is only allowed in the direction of the unbalanced wrench acting on the object remaining from the previous step. We limit the step size by a parameter γ for numerical stability and accuracy:

Algorithm 3 Inner loop of the iterative solution scheme: Minimize the resultant wrench, where object motion is only allowed in the direction of the current net resultant wrench.

Input: f^c — commanded actuator forces, w — applied wrench, r^{k-1} — previous object displacement, w^{k-1} — previous net wrench

Output: c^k — contact forces, r^k — next step object displacement, w^k — next step net wrench

procedure MOVEMENT CONSTRAINED EP(f^c, w, r^{k-1}, w^{k-1})

minimize: $\|w^k\|$ ▷ net wrench

subject to:

 Eqs. (5.1) , (5.2) & (5.9) ▷ object and hand equilibrium

 Eqs. (5.3) & (5.16) ▷ normal force unilaterality and constitutive relation

 Eq. (5.17) ▷ actuator unilaterality

 Eq. (5.18a) ▷ friction cone

 Eq. (5.20) ▷ object movement

return c^k, r^k, w^k

end procedure

$$r^k = r^{k-1} + s w^{k-1}, \quad 0 \leq s \leq \gamma \quad (5.20)$$

After each iteration, we check for convergence by comparing the incremental improvement to a threshold ϵ . If the objective has converged to a sufficiently small net wrench (we chose $10^{-3}N$), we deem the grasp to be stable; otherwise, if the objective converges to a larger value, we deem the grasp unstable. Note that we must use the objective in the optimization formulation in this approach, which means we are constrained to the solution of *existence problems*. In this case the problem we are solving is this: *Given f^c , determine if c will arise that balances applied wrench w* . Thus, we formulate a *movement constrained existence problem* as outlined in Algorithm 3 to be solved iteratively as outlined in Algorithm 4 allowing us to make a determination as to the stability of the grasp. The computation time of this process is directly related to the number of iterations required until convergence.

However, such an iterative approach is not guaranteed to converge, or to converge to the physically meaningful state of the system. Thus, while this approach is simple to implement and provides a good estimate of grasp stability we can make no guarantees of solutions obtained: The solution we find is not guaranteed to be a good approximation of a solution to the *exact problem*

Algorithm 4 Outer loop of the iterative solution scheme: Repeatedly solve the "Movement Constrained EP". Update the current object motion and net resultant wrench at every step.

Input: f^c — commanded actuator forces, w — applied wrench

Output: c — contact forces, w_{res} — net resultant

procedure ITERATIVE EP(f^c, w)

$r^0 = 0$

$w^0 = w$

loop

$(c^k, r^k, w^k) = \text{Movement Constrained EP}(f^c, w, r^{k-1}, w^{k-1})$ ▷ Algorithm 3

if $\|w^{k-1} - w^k\| < \epsilon$ **then** ▷ Check if system has converged

break

end if

end loop

return c^{final}, w^{final}

end procedure

as defined in Chapter 5.2. Furthermore, if algorithm 4 does not return a valid and stable solution we do not know if such a solution may not exist. Nonetheless, this iterative approach has proved useful in analyzing the passive behavior of grasps as we will show in Chapter 5.5.

5.5 Application to grasp analysis in three dimensions

We will illustrate the application of the iterative solution approach discussed in Chapter 5.4 on example grasps with the Barrett hand and an underactuated tendon-driven gripper. We pointed out that a limitation of the iterative approach is that we may only solve *existence* type problems as the objective is required in the formulation and is not available for us to optimize a quantity of our choosing. Recall, however, that the question of 'will a given grasp with given joint commands resist a specific applied force' is such an existence problem and hence we can investigate the range of forces applied to the object our example grasps can resist.

To facilitate visualization we will confine the forces applied to the object to the a plane. As our framework can only answer 'spot checks' — that is determine stability for a specific applied force — we discretize this plane by direction vectors with a spacing of 1° between them. We then determine the maximum force applied to the object the grasp can withstand for each of these directions. We do this by performing a binary search converging on the maximum magnitude of

the force before the grasp becomes unstable.

We model the Barrett hand as having all nonbackdrivable joints. Our qualitative experience indicates that the finger flexion joints never backdrive, while the spread angle joint backdrives under high load. For simplicity we also do not use the breakaway feature of the hand; our real instance of the hand also does not exhibit this feature. We model the joints as rigidly coupled for motion, and assume that all the torque supplied by each finger motor is applied to the proximal joint.

We show force data collected by replicating the grasp on a real hand and testing resistance to external disturbances. To measure the maximum force that a grasp can resist in a certain direction, we manually apply a load to the grasped object using a Spectra wire in series with a load cell (Futek, FSH00097). In order to apply a pure force, the wire is connected such that the load direction passes through the center of mass of the object. We increase the load until the object starts moving, and take the largest magnitude recorded by the load cell as the largest magnitude of the disturbance the grasp can resist in the given direction.

Barrett hand: Let us first consider the grasp in Fig. 5.2, which is similar to the grasp introduced in Section 3.1 to serve as an example for the importance of the passive resistance capabilities that nonbackdrivable joints provide. We now have the necessary tools to analyze such grasps. Considering only forces in the grasp plane this grasp effectively becomes a 2D problem: simple enough to be understood intuitively, but still complex enough to give rise to interesting interplay between the joints and contacts.

Consider first the problem of resisting an external force applied to the object center of mass and oriented along the y -axis. This simple case illustrates the difference between active and passive resistance. Resistance against a force oriented along the positive y -axis requires active torque applied at the joints in order to load the contacts and generate friction. The force can be resisted only up to the limit provided by the preload, along with the friction coefficient. If the force is applied along the negative y -axis, resistance happens passively, provided through the contacts on the proximal link. Furthermore, resistance to such a force does not require any kind of preload,

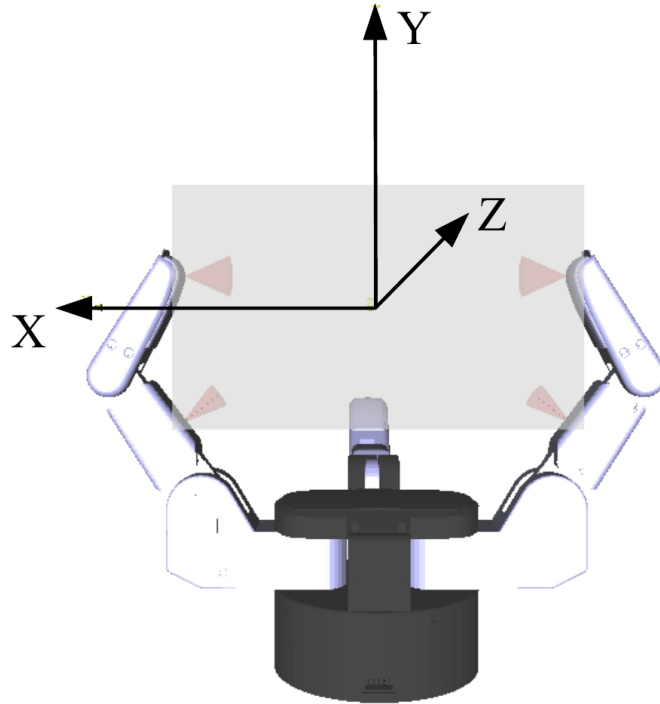


Figure 5.2: Grasp example 1. Note that this is the same grasp we used in Chapter 3.1 to illustrate the consequences of passive reactions.

and is infinite in magnitude (up to the breaking limit of the hand mechanism, which does not fall within our scope here).

For an external force applied along the x -axis, the problem is symmetric between the positive and negative directions. Again, the grasp can provide passive resistance, through a combination of forces on the proximal and distal links. For the more general case of forces applied in the xy -plane, we again see a combination of active and passive resistance effects. Intuitively, any force with a negative y component will be fully resisted passively. However, forces with a positive y component and non-zero x component can require both active and passive responses. Fig. 5.3 shows the forces that can be resisted in the xy -plane, both predicted by our framework and observed by experiment.

For both real and predicted data, we normalize the force values by dividing by the magnitude of the maximum resistible force along the positive direction of the y -axis (note thus that both predicted and experimental lines cross the y -axis at $y = 1.0$). The plots should therefore be used to compare trends rather than absolute values. We use this normalization to account for the fact

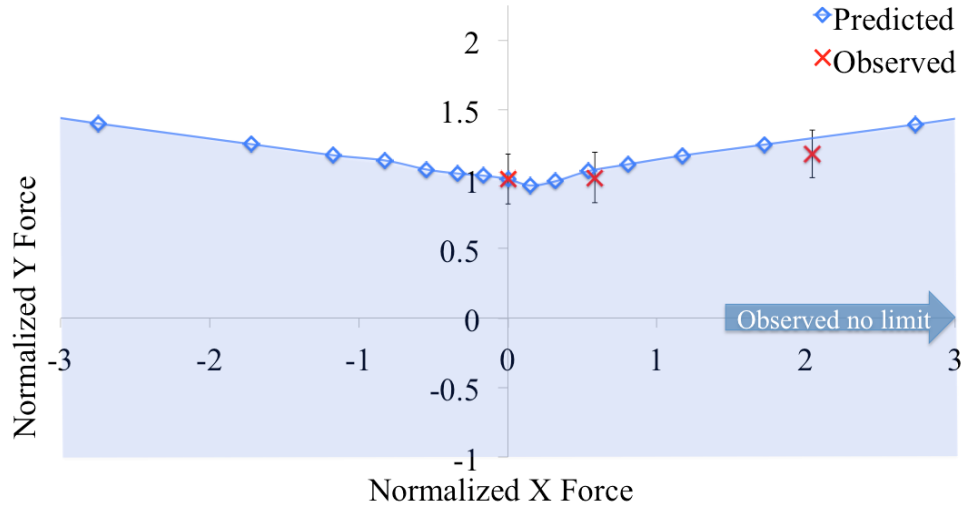


Figure 5.3: Normalized forces in the xy -plane that can be resisted by the grasp in Fig. 5.2: observed by experiment (mean \pm one standard deviation) and predicted by our framework. For both real and predicted data, we normalize the force values by dividing by the magnitude of the maximum resistible force along the positive direction of the y -axis (note thus that both predicted and experimental lines cross the y -axis at $y = 1.0$). In all directions falling below the blue line, the prediction framework hit the upper limit of the binary search (arbitrarily set to 10^3 N). Hence we deem forces in the shaded area resistible. In the direction denoted by 'Observed no limit', the grasp was not disturbed even when reaching the physical limit of the experimental setup.

that the absolute torque levels that the hand can produce, and which are needed by our formulation in order to predict absolute force levels, can only be estimated and no accurate data is available from the manufacturer. The difficulty in obtaining accurate assessments of generated motor torque generally limits the assessments we can make based on absolute force values. However, if one knows the real magnitude of the maximum resistible external force along any direction, in which this magnitude is finite, one could infer from these figures the real maximum resistible wrenches in the other directions.

Moving outside of the grasp plane, Fig. 5.4 shows predicted and measured resistance to forces in the xz -plane. Again, we notice that some forces can be resisted up to arbitrary magnitudes thanks to passive effects, while others are limited by the actively applied preload.

As was mentioned previously, a common method for grasp creation is to choose a set of actuator commands to preload the grasp before applying any external wrench. These preloads are then maintained throughout the task trusting in passive effects to stabilize the grasp. One advantage

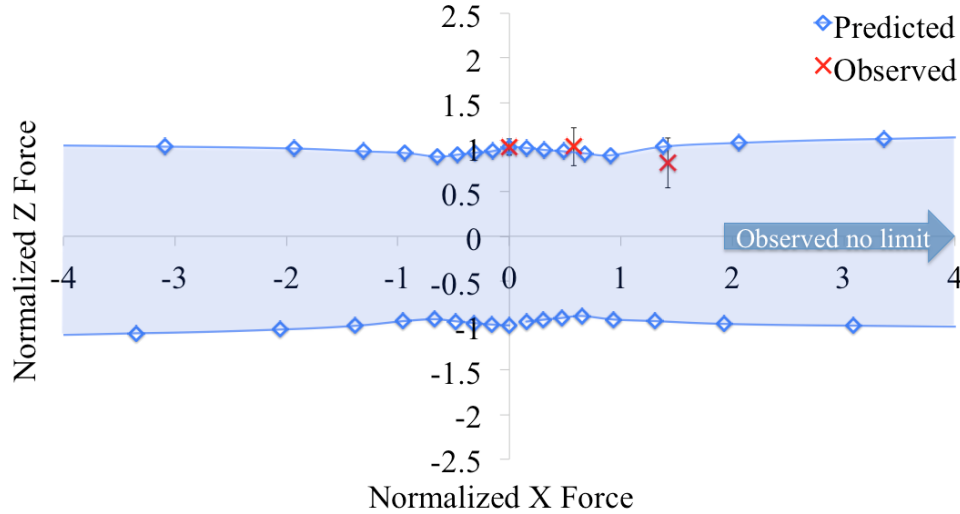


Figure 5.4: Normalized forces in the xz -plane that can be resisted by the grasp in Fig. 5.2: predicted by our framework, and observed by experiment. In all directions falling between the blue lines (shaded), the prediction framework hit the upper limit of the binary search (arbitrarily set to 10^3 N). In the direction denoted by 'Observed no limit', the grasp was not disturbed even when reaching the physical limit of the experimental setup.

of studying the effect of applied joint torques on grasp stability is that it allows us to observe differences in stability due to different ways of preloading the same grasp. For example, in the case of the Barrett hand, choosing at which finger(s) to apply preload torque can change the outcome of the grasp, even though there is no change in the distribution of contacts. We illustrate this approach on the case shown in Fig. 5.5. Using our framework we can compute regions of resistible wrenches for two different preloads (see Fig. 5.6).

We compare the ability of the grasp to resist a disturbance applied along the x -axis in the positive direction if either finger 1 or finger 2 apply a preload torque to the grasp. Our formulation predicts that by preloading finger 1 the grasp can resist a disturbance that is 2.48 times larger in magnitude than if preloading finger 2. Experimental data (detailed in Table 5.5) indicates a ratio for the same disturbance direction of 2.23. The variance in measurements again illustrates the difficulty of verifying such simulation results with experimental data. Nevertheless, experiments confirmed that preloading finger 1 is significantly better for this case.

This result can be explained by the fact that, somewhat counter-intuitively, preloading finger 1 leads to larger contact forces than preloading finger 2, even if the same torque is applied by each

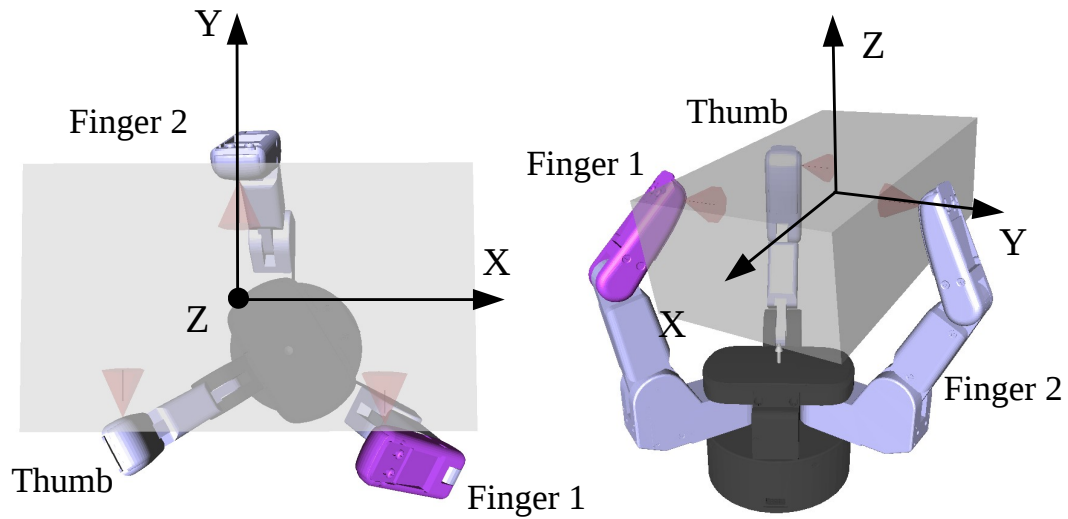


Figure 5.5: Top and side views for grasp example 2 also indicating finger labels. Note that the spread angle degree of freedom of the Barrett hand changes the angle between finger 1 and finger 2; the thumb is only actuated in the flexion direction.

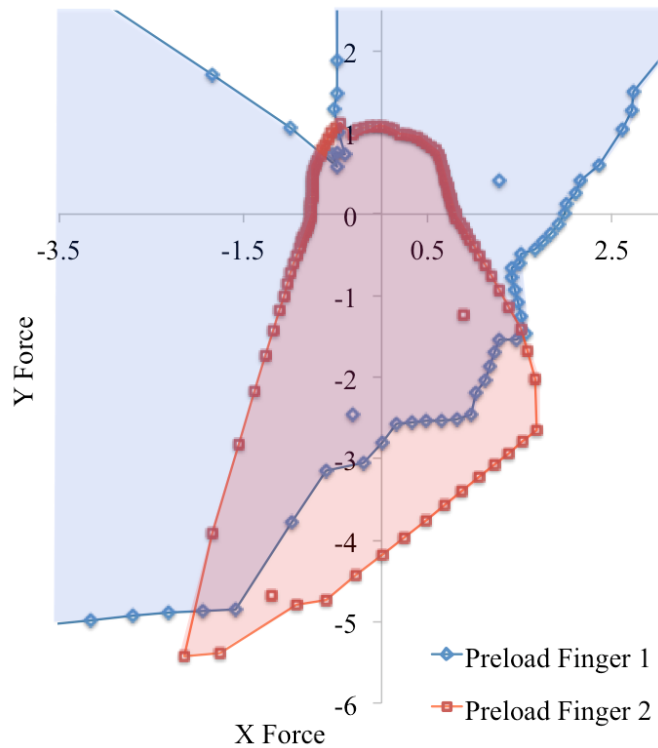


Figure 5.6: Forces in an xy -plane that can be resisted by the grasp in Fig. 5.5 (shaded) as predicted by our framework, depending on which finger is preloaded. Note the four outlier results and that they have not been included in the determination of the regions of resistible forces. The forces are normalized and hence dimensionless.

	Measured resistance				Predicted	
	Values(N)	Avg.(N)	St. Dev.	Ratio	Value	Ratio
F1 load	12.2, 10.8, 7.5, 7.9, 9.3	9.6	1.9	2.23	1.98	2.48
F2 load	3.7, 4.1, 5.0	4.3	0.7		0.80	

Table 5.1: Predicted and measured resistance to force applied along the positive x -axis in the grasp problem in Fig. 5.5. Each row shows the results obtained if the preload is applied exclusively by finger 1 or finger 2 respectively. Experimental measurements were repeated 5 times for finger 1 (to account for the higher variance) and 3 times for finger 2. Predicted values are non dimensional, and hence the ratio between the two preload cases is shown.

motor. Due to the orientation of finger 1, the contact force on finger 1 has a smaller moment arm around the finger flexion axes than is the case for finger 2. Thus, if the same flexion torque is applied in turn at each finger, the contact forces created by finger 1 will be higher. In turn, due to passive reaction, this will lead to higher contact forces on finger 2, even if finger 1 is the one being actively loaded. Finally, these results hold if the spread degree of freedom is rigid and does not backdrive; in fact, preloading finger 1 leads to a much larger passive (reaction) torque on the spread degree of freedom than when preloading finger 2.

Referring to Fig. 5.6, we note that actively preloading finger 1 results in greater resistance only in some directions. There is much structure to the prediction made by our framework that could be exploited to make better decisions when preloading a grasp with some knowledge of the expected external wrenches.

Underactuated hand: We now apply our framework to a grasp with a two-fingered, tendon-driven underactuated gripper (see Fig. 5.7). The gripper has four degrees of freedom, but only two actuators driving a proximal and a distal tendon. The proximal tendon has a moment arm of 5mm around the proximal joints. The distal tendon has moment arms of 1.6mm and 5mm around the proximal and distal joints respectively. The actuators are non backdrivable and hence the tendons not only transmit actuation forces, they also provide kinematic constraints to the motion of the gripper’s links.

As the tendons split and lead into both fingers, we assume that they are connected to the actu-

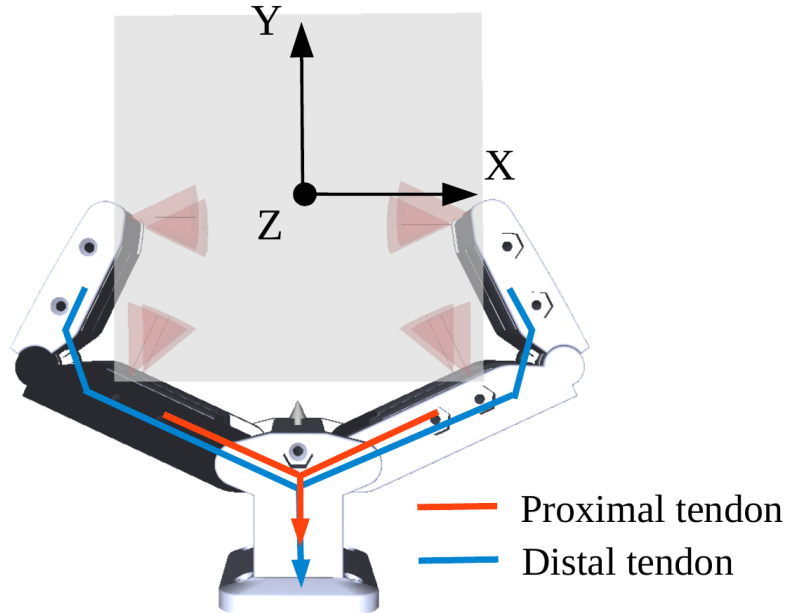


Figure 5.7: Grasp example 3. Note that in terms of contact positions, this grasp is very similar to that in Fig. 5.2. However, the kinematic differences cause these two grasps to behave very differently.

ator by a differential. This introduces compliance to the grasp: if one proximal joint closes by a certain amount, this will allow the other proximal joint to open by a corresponding amount. This compliance means that the underactuated grasp in Fig. 5.7 will behave fundamentally different than the very similar grasp in Fig. 5.2. To see this, consider the region of resistible wrenches in the xy -plane (Figs. 5.3 & 5.8). In both cases the object is gripped by two opposing fingers, however, while in the case of the Barrett hand the grasp could withstand arbitrarily large forces pushing the object directly against a finger, our framework predicts only limited resistance to such forces in the case of the underactuated hand.

We used our framework to apply two different sets of preload actuator commands f^c and analyzed the resistance of the resulting grasp to an externally applied wrench. We chose to apply a torque around the x -axis and considered two preload cases: applying an active load on the proximal tendon only ($f^c = [1, 0]^T$), leaving the distal tendon to be loaded passively as well as the reverse — applying an active load on the distal tendon only ($f^c = [0, 1]^T$), leaving the proximal tendon to be loaded passively. For equal actuator force, our framework predicts, that a preload created by

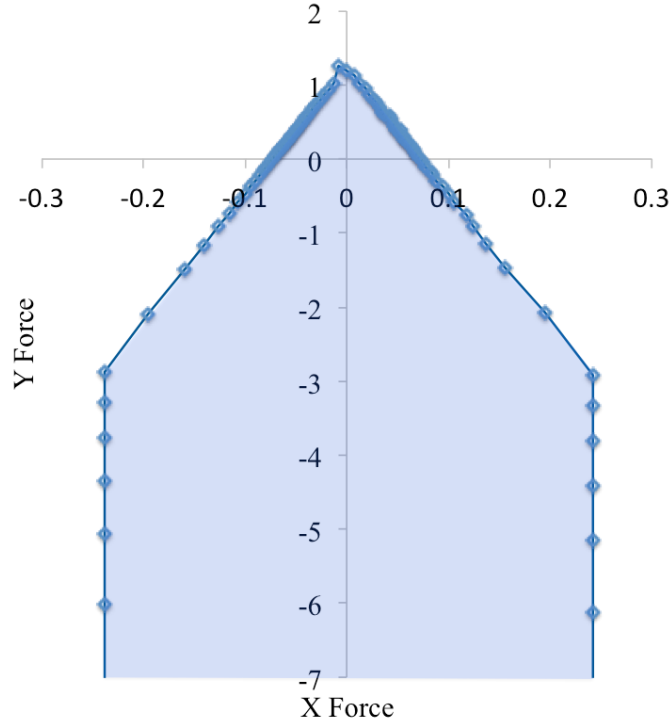


Figure 5.8: Forces in an xy -plane that can be resisted by the grasp in Fig. 5.7 (shaded) as predicted by our framework. The forces are normalized and hence dimensionless. Note the difference in scale on the x - and y -axes.

only actively loading the distal tendon leads to almost twice as much resistance to torques applied in the direction of the x -axis than only actively loading the proximal tendon.

Experimental verification of this prediction proved to be difficult, as results had high variance and application of a pure torque to the object along an axis that penetrates the distal links of the gripper was complicated. However, we mounted the gripper such that the grasp plane was in the horizontal and placed weights on the top end of the box object. We found the resistance to these applied wrenches indeed to be much higher when actively loading the distal tendon as opposed to the proximal.

The reason for this discrepancy in resistance to this wrench becomes apparent when looking at the contact forces arising from the different preload commands (see Fig. 5.9.) When only actively loading the proximal tendon (Fig. 5.9(a)) the preload contact forces are concentrated at the distal contacts(!). In fact, the contacts on the proximal links break entirely. These contacts, however,

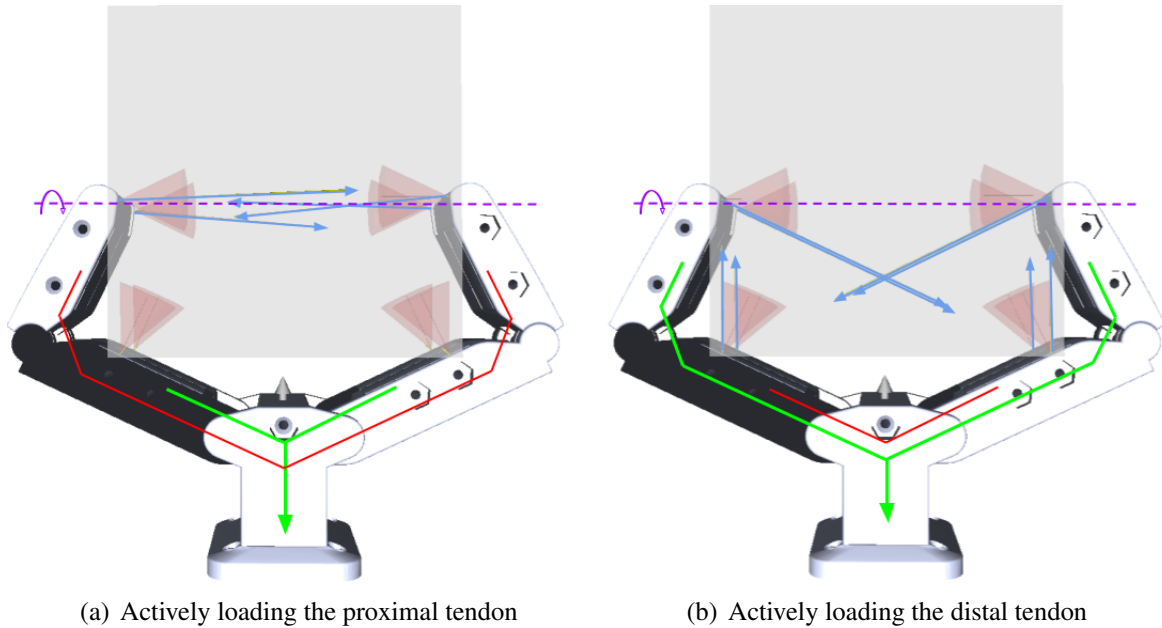


Figure 5.9: Different preload contact forces arising from different preload actuator commands (blue arrows) — the tendon shown in green is being actively loaded by the actuator. As a result the red tendon is loaded passively. The violet line denotes the torque applied to the grasped object. Note that the forces shown are those that arise purely as a result of the preload actuator commands and hence *before* the application of any external wrench to the object.

have the largest moment arm with respect to the torque applied to the object and are hence crucial for the ability of the grasp to resist such torques.

When instead only actively loading the distal tendon (Fig. 5.9(b)) contact forces arise on all four links. The contact forces at the proximal links particularly allow the grasp to resist torques around the horizontal object axis. Our framework has captured the passive effects present in this underactuated hand and helped us to understand how to best make use of the actuators available.

5.6 Discussion

In this Chapter we have developed a grasp model and the corresponding algorithms to determine the passive stability of spatial robotic grasps. We showed the importance of the maximum dissipation principle for the determination of passive reaction effects. We did so by showing how ignoring the maximum dissipation principle allows for unphysical solutions such that stability cannot be determined. We proposed a physically motivated iterative scheme that allows us to

approximate the law of conservation of energy and hence the maximum dissipation principle.

The resulting algorithm enabled us to determine the passive stability of spacial grasps for both a fully actuated as well as an underactuated hand. We showed that our framework correctly captures passive phenomena and demonstrated a practical application of our algorithm as a tool for choosing appropriate preload actuator commands. We compared the predictions made by our framework to data collected from real robotic grasps and found that while empirical grasp stability analysis is difficult, our framework appears to agree well with the observed behaviors.

However, our current real underactuated hand only allows experimental validation of a subset of our analysis results. We would like to design a hand that we can use to further validate our framework and study the effects of underactuation on grasp stability. For instance, our framework predicts that wrench resistance is highly dependent on the torque ratios at the joints due to the kinematics of the force transmission. We would like to experiment with a variety of underactuated hands, with varying kinematic and actuation models, to investigate these effects and demonstrate the effectiveness of our framework as a design tool.

An important limitation of our algorithm is that we had to use the objective in the optimization formulation in order to approximate the maximum dissipation principle. This means that we could only solve problems of the *existence* type and perform a spot check if a grasp with given actuator commands could resist a specific disturbance. As the objective is not available we cannot use it to do more practical analysis such as finding optimal actuator commands.

A further limitation is that in a subset of cases, the solver reports maximum resistible wrenches of very different magnitude along some directions relative to neighboring directions. For example, in the second example grasp from the previous section (Fig. 5.5), when computing resistance to disturbances sampled from the xy -plane (Fig. 5.6), we obtain two outliers for each preload case that do not follow the trend of the surrounding points. These outliers are quite rare and tend to fall within the area deemed to contain resistible wrenches (shaded). These effects will require further investigation.

A promising avenue to pursue in terms of alleviating these outliers might be to take into account

the effect of uncertainties (e.g. in exact contact location) on our model. We believe exploring the sensitivity of the model to such uncertainties may yield many valuable insights and make our framework even more relevant to practical robotic grasping.

The most significant limitation of our algorithm stems from its iterative nature. While our iterative approach allows us to approximate the maximum dissipation principle, such an iterative approach is not guaranteed to converge, or to converge to the physically meaningful state of the system. As such, our approach offers an approximation without any formal guarantees. In practice, however, our algorithm produces physically plausible results that could be confirmed by empirical validation.

Chapter 6: Grasp Stability Analysis with the Maximum Dissipation

Principle

6.1 Introduction

In this Chapter we will make use of the same grasp model as described in Chapter 5.2. This model, particularly what we have called the *complete problem*, is very general and captures all of the characteristics of robotic grasps we are interested in. It accounts for both object and hand equilibrium, the unilaterality of both contacts and nonbackdrivable actuators as well as the Coulomb friction law including the Maximum Dissipation Principle (MDP).

We showed how the majority of this grasp model can be cast as a Mixed Integer Program in Chapter 5.3.1. The only component that eluded our formulation was the maximum dissipation aspect of the Coulomb friction law. In Chapter 5.3.2 we demonstrated the importance of the MDP for the determination of passive resistance in robotic grasps. We showed that simply omitting the MDP allows for unphysical solutions to the grasp model formulation making a determination of stability impossible. However, we also discussed the difficulty in accurately modeling the MDP due to its non-convexity.

In Chapter 5.4 we proposed a physically motivated iterative scheme that aims to approximate the MDP. However, this approach does not explicitly include the MDP and is therefore unlikely to converge to a solution that actually satisfies the MDP to high accuracy. In fact, our previous approach provides no formal guarantee of convergence. Furthermore, we had to use the objective of the MIP optimization formulation in order to approximate the MDP, which meant that the objective was not available for more involved analysis. This is unfortunate, as many queries of practical importance can be posed as optimization problems. In fact, much of the grasp force analysis literature discussed in Chapter 2.1 seeks to find contact wrenches or actuator torques that are optimal

with respect to some objective.

In this chapter we will develop a Mixed Integer formulation that explicitly models the MDP. To this end we propose a relaxation of the friction model such that we can solve the system as an MIP. Through successive and hierarchical tightening of the relaxation we can efficiently find solutions that satisfy all constraints — including the MDP — to arbitrary accuracy. A very useful property of tightening approaches is that they allow for strong guarantees: if, at any stage of refinement our model fails to find a solution, we can guarantee that no solution exists to the exact problem. This allows for early exit from computation in cases where equilibrium cannot exist. Furthermore, tightening approaches can greatly reduce the size of the optimization problem that has to be solved in order to find a solution. We use these properties to develop a grasp model that, to the best of our knowledge, is the first that can handle three-dimensional frictional constraints that include the MDP, up to arbitrary accuracy (and thus approaching the solution to the exact problem) where solutions can be solved for in a computationally efficient fashion. Our model allows us to produce solutions on commodity computers fast enough for practical applicability.

Our formulation furthermore frees up the objective for any query posed as an optimization. Depending on the choice of variables and optimization objective, our model can be used for a wide range of queries. We illustrate its applicability to grasp stability analysis by answering multiple queries on a number of example grasps. The queries we show here include those already introduced in 5.5: Given applied joint torques, will the grasp be stable in the presence of a specified external disturbance, assuming passive resistance effects? Additionally, the formulation developed in this chapter allows for queries such as the following: Given applied joint torques, what is the largest disturbance that can be passively resisted in a given direction? Given a disturbance, what are the optimal joint torques that a grasp can apply for stability?

Finally, we develop a method to account for uncertainties in the grasp modeled. Specifically, we can guarantee robustness to uncertainties in contact normal direction. We use this algorithm to analyze the passive stability of spacial grasps similar to those we investigated in Chapter 5.5. We also extend our analysis to the optimization of actuator torques and demonstrate the practical

applicability of our algorithm. We believe these are all useful tools in the context of grasp analysis.

6.2 A formulation using McCormick envelopes

As mentioned above we will make use of the same grasp model as described in Chapter 5.2 but will deviate in our treatment of the friction constraints in order to explicitly model the MDP in (5.6). Of course one could cast the MDP in its original minimization formulation which is of course non-convex as the bilinear form in (5.6) is not positive definite [95]. However, one could attempt to solve the exact problem (5.1) – (5.11) using a global optimization approach based on a convex relaxation of the bilinear forms using McCormick envelopes [96], which relies on upper and lower bounds on the variables involved in the bilinear forms. In order to illustrate such an approach let us consider an example of a bilinear form $w(x, y)$ in two dimensions.

$$w(x, y) = x \cdot y \tag{6.1}$$

Given upper and lower bounds such that $x^L \leq x \leq x^U$ and $y^L \leq y \leq y^U$ we replace the xy term with variable w and introduce the following linear inequality constraints:

$$w \leq x^U y + x y^L - x^U y^L \tag{6.2}$$

$$w \leq x y^U + x^L y - x^L y^U \tag{6.3}$$

$$w \geq x^L y + x y^L - x^L y^L \tag{6.4}$$

$$w \geq x^U y + x y^U - x^U y^U \tag{6.5}$$

A graphical interpretation of this convex relaxation to the bilinear form is shown in Fig. 6.1(a). The linear inequalities we introduced provide convex underestimators and overestimators also known as a McCormick envelope. Of course a solution to this relaxed problem will not in general be a solution to the exact problem. It will, however, provide a lower bound for the objective value.

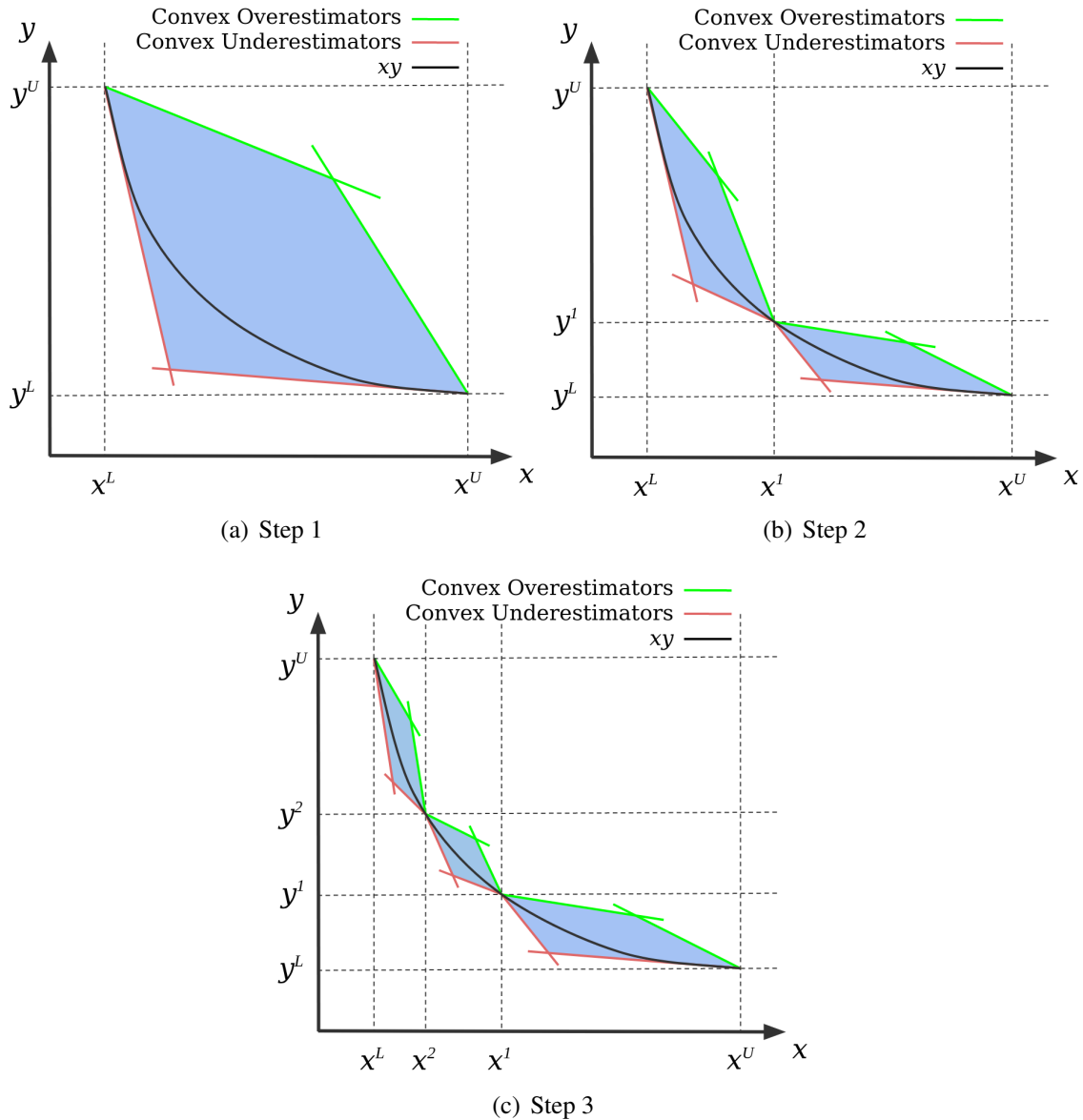


Figure 6.1: McCormick envelopes for the bilinear form $w(x, y) = x \cdot y$.

Tightening the relaxation will result in a lower bound closer to the exact solution. Hence, tight relaxations are imperative for obtaining accurate results.

A common method to obtain such a tight relaxation is its successive hierarchical tightening. We search for a solution in a coarse relaxation and then refine just the envelope containing it (see Fig. 6.1). Algorithms such as Spatial Branch-and-Bound (sBB) [97] can be used to efficiently refine and prune parts of the solution space and find global minima of such non-convex optimization problems. Implementations include the α BB algorithm [98] or the BARON [99] software for

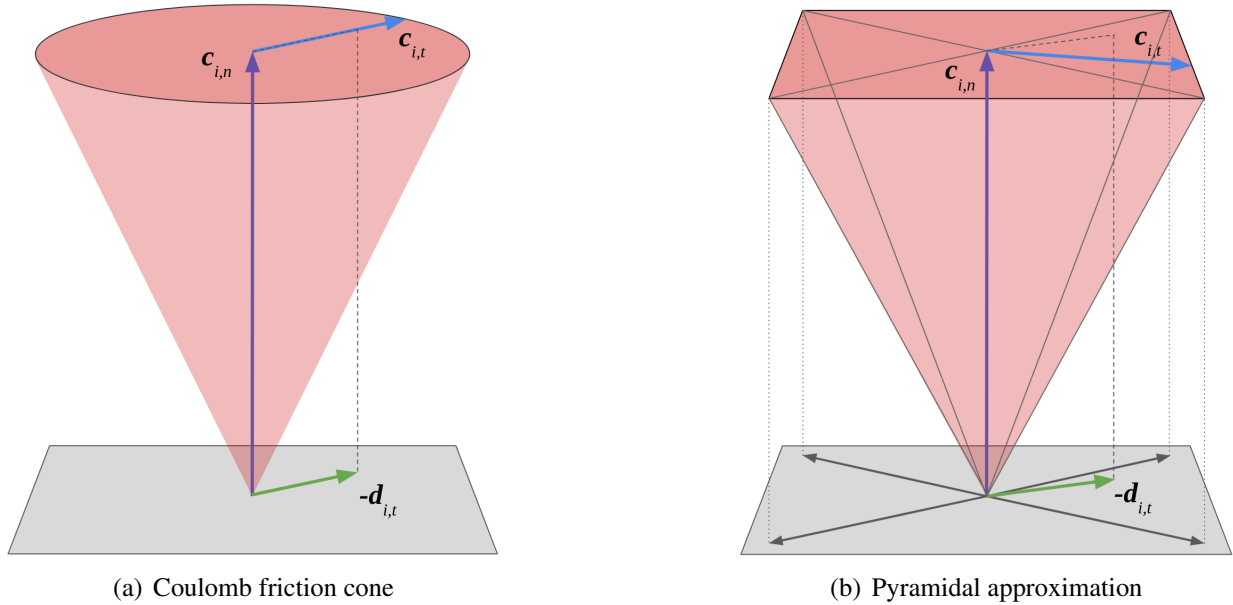


Figure 6.2: Illustration of the exact Coulomb friction cone and a pyramidal approximation with $k = 4$. The black arrows positively span the contact tangent plane and make up the matrix of basis vectors \mathbf{D}_i .

global optimization.

Of course this approach generalizes to bilinear forms in higher dimensions such as that encountered in the maximum dissipation principle (5.6). However, it requires knowledge of upper and lower bounds for the variables involved in the bilinear form. In the grasping problems we are trying to solve such bounds are not explicit in the model and are difficult to estimate.

6.3 Convex relaxation of the Coulomb friction law

Taking inspiration from these convex relaxation techniques we make use of the particular structure of friction cones to derive a relaxation that does not require variable bounds. This is useful since in the grasping problem there are no explicit bounds on contact forces and particularly motions and they are therefore difficult to predetermine. Furthermore, in our approach we formulate the MDP as a non-convex constraint, which we relax instead of the optimization objective. This allows us to use the objective to solve for interesting grasp characteristics such as the optimum actuator commands.

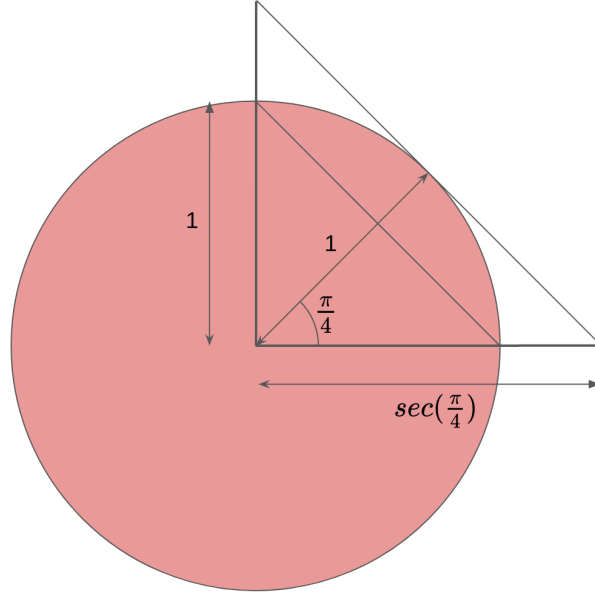


Figure 6.3: Slice through the friction cone showing two possible lengths of friction edges for a discretization with $k = 4$. The shorter friction edge length leads to a discretized cone fully inscribed by the circular cone, while the longer friction edge length leads to a discretized cone that itself fully contains the circular cone.

We start from the common linearized friction model [100] which replaces the circular friction cone at contact i with its discretization as a polygonal cone $\hat{\mathcal{F}}_i$ (see Fig. 6.2.) Matrix $\mathbf{D}_i \in \mathbb{R}^{2 \times k}$ contains as its columns a set of k vectors that positively span the contact tangential plane and thus the space of possible friction forces. Frictional forces can now be expressed as positive linear combinations of these so called *friction edges* with weights $\boldsymbol{\beta}_i \in \mathbb{R}_{\geq 0}^k$. Vector $\mathbf{e} = [1, 1, \dots, 1]^T \in \mathbb{R}^k$ sums the weights $\boldsymbol{\beta}_i$. Inequality constraints on a vector are to be understood in a piecewise fashion.

$$\mathbf{c}_{i,t} = \mathbf{D}_i \boldsymbol{\beta}_i \in \hat{\mathcal{F}}_i \quad (6.6)$$

$$\hat{\mathcal{F}}_i(\mu_i, c_{i,n}) = \{\mathbf{D}_i \boldsymbol{\beta}_i : \boldsymbol{\beta} \geq 0, \mathbf{e}^T \boldsymbol{\beta} \leq \mu_i c_{i,n}\} \quad (6.7)$$

Traditionally, the basis vectors in \mathbf{D}_i are unit vectors. Thus, the discretized friction cone is completely inscribed by the exact circular cone (see Fig. 6.3.) This leads to an approximation

to the possible friction forces that is conservative in the context of grasp stability. In our case, however, in order to derive a valid convex relaxation we require the relaxed discretized friction cone to contain the exact cone. This is important in order to guarantee that we can find a solution to the relaxed problem if one exists to the exact problem. Thus, we instead choose basis vectors of length f for Matrix \mathbf{D}_i .

$$f = \sec\left(\frac{\pi}{k}\right) \quad (6.8)$$

Let us now also express relative tangential contact motion as a weighted combination of the same friction edges, with weights $\alpha_i \in \mathbb{R}_{\geq 0}^k$. For reasons that will soon become apparent, we actually choose to express the opposite of the tangential motion:

$$\mathbf{D}_i \alpha_i = -\mathbf{d}_{i,t}, \quad \alpha_i \geq 0 \quad (6.9)$$

If the friction edges in \mathbf{D}_i are arranged in an ordered fashion such that neighboring friction edges in the tangent plane are also neighbors in \mathbf{D}_i we can constrain friction to (approximately) oppose motion by requiring that the *friction force lie in the same sector of the linearized friction cone as the negative of the tangential contact motion*. Without loss of the above properties, we require that all but two components of β_i must be zero and that non-zero components are either consecutive or lie at the first and last positions of vector β_i . This can be achieved by constraining β_i with a special ordered set $\mathbf{z}_i \in \mathbb{R}_{\geq 0}^{k+1}$ of type 2 (SOS2) [101], which has one more component than β_i itself.

$$\beta_{i,1} \leq z_{i,1} + z_{i,k+1}, \quad \beta_{i,2} \leq z_{i,2}, \quad \dots, \quad \beta_{i,k} \leq z_{i,k}, \quad \mathbf{z} \in \text{SOS2} \quad (6.10)$$

A special ordered set of type 2 is a set of ordered non-negative numbers of which at most two can be non-zero. If two numbers in the SOS2 are non-negative they must be consecutive in their ordering. This type of constraint can be formulated in the framework of mixed integer problems and therefore is admissible to problems to be solved by MIP solvers. We now similarly constrain

the weights α that determine relative motion with the same SOS2 as in (6.10).

$$\alpha_{i,1} \leq z_{i,1} + z_{i,k+1}, \alpha_{i,2} \leq z_{i,2}, \dots, \alpha_{i,k} \leq z_{i,k} \quad (6.11)$$

Note that these constraints hold for both sliding as well as rolling contacts. If a contact is rolling then all components of α_i must be zero. Thus, any two consecutive components of z_i may be non-zero and since β_i are the weights of the basis vectors in D_i the friction force may point in any direction in the tangent plane. If the contact slides then some components of α_i must be nonzero. As both α_i and β_i are constrained by z_i and only two consecutive components of z_i may be nonzero, this means the friction force must lie in the same sector of the friction pyramid as the negative of the relative tangential contact motion, but may not necessarily be collinear (see Fig. 6.2(b).)

Finally, we can constrain the magnitude of the friction force in addition to its direction. In the exact Coulomb model the friction magnitude must be maximized at sliding contacts, while for stationary contacts it only has an upper bound. In our relaxation this means that at rolling contacts the friction force may lie anywhere within the discretized cone containing the exact circular cone. At a sliding contact we require that the *friction force lies within the discretized cone containing the circular cone, but outside the smaller discretized cone that is itself contained by the exact cone.* See Fig. 6.4 for an illustration of this relaxation. Note, that in either case the relaxation contains the solution set of the exact Coulomb friction model.

Defining vector $\mathbf{f} = [f, f, \dots, f]^T \in \mathbb{R}^k$ containing the lengths of the friction edges (6.8) making up the friction cone approximation we can express this constraint as follows:

$$\begin{cases} \mathbf{e}^T \beta_i \leq \mu_i c_{i,n}, & \text{if } \mathbf{e}^T \alpha_i = 0 \\ \mathbf{e}^T \beta_i \leq \mu_i c_{i,n}, \mathbf{f}^T \beta_i \geq \mu_i c_{i,n}, & \text{otherwise} \end{cases} \quad (6.12a)$$

$$\quad \quad \quad (6.12b)$$

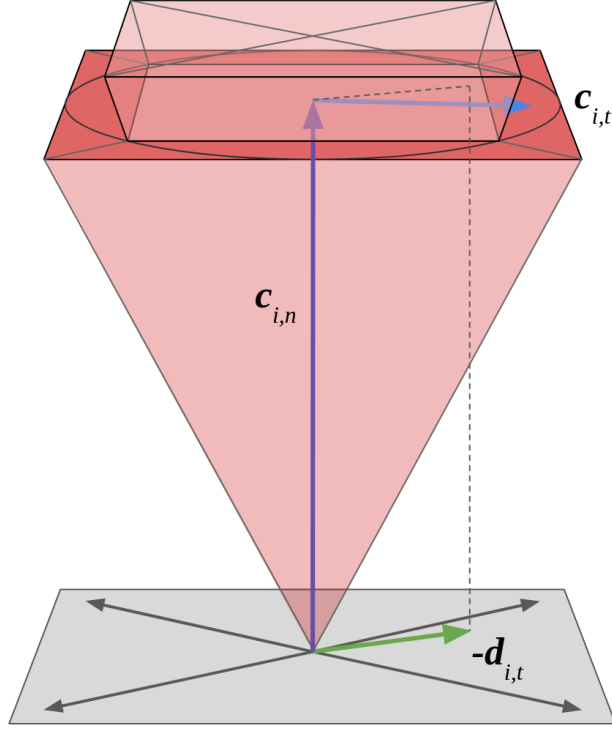


Figure 6.4: Complete convex relaxation of the circular friction cone. At a rolling contact the contact force may lie anywhere within the larger discretized cone. At a sliding contact the friction force must lie in the same sector as $-\mathbf{d}_{i,t}$. Furthermore the contact force must remain inside the larger, but outside the smaller discretized cone.

Constraint (6.12) can also be included in an MIP as an indicator constraint using a binary decision variable $w_i \in \{0, 1\}$.

$$\begin{cases} w_i = 0 \implies & \mathbf{e}^T \boldsymbol{\beta}_i \leq \mu_i c_{i,n}, \quad \mathbf{e}^T \boldsymbol{\alpha}_i = 0 & (6.13a) \\ w_i = 1 \implies & \mathbf{e}^T \boldsymbol{\beta}_i \leq \mu_i c_{i,n}, \quad \mathbf{f}^T \boldsymbol{\beta}_i \geq \mu_i c_{i,n} & (6.13b) \end{cases}$$

We now have a complete model of friction. For a finite value of k , this model is approximate. However, in the limit as $k \rightarrow \infty$ the indicator constraints (6.13) are equivalent to the Coulomb friction model in (5.5) & (5.6).

6.4 Successive hierarchical refinement

We can solve the complete system described by constraints (5.1)-(5.4), (5.7)-(5.11) and the new piecewise convex relaxation of Coulomb friction (6.13) as an MIP with algorithms such as branch and bound. In order to improve our approximation, we could choose a high number of edges k for the discretized friction cones. In practice, however, that approach is not feasible as the time taken to solve an MIP is sensitive to the number of integer variables in the problem. As SOS2 constraints are implemented using binary variables a highly refined friction cone approximation quickly becomes computationally intractable. This is the trade-off traditionally encountered with discretization methods: coarse discretizations provide only rough approximations of the exact constraints, while high resolutions discretizations are computationally intractable.

Our approach is based on the key insight that one can obtain an equally accurate solution by solving a problem with a coarse friction cone approximation, and *successively refining the linearized friction constraints only in the region where friction forces arise*. Our approach thus proceeds as follows:

- We solve our problem using a coarse approximation of the friction cone (few friction edges). From the solution, we identify the sector of the linearized cone (the area between two edges) where both the friction force and the negative relative motion lie.
- To obtain a tighter bound, we add new friction edges that refine *only the sector identified above*. We then repeat the procedure with the new, selectively refined version of the friction cone.

Consider a rough approximation with four friction edges (Fig. 6.5(b).) If we allow rolling friction to reside inside the areas shaded in either shade of red, while sliding friction must lie within the dark red border, the space of allowable solutions to the exact problem is contained inside our linear and piecewise convex approximation. Assume that, at this level of refinement, there is a solution to an equilibrium problem, with a friction force residing inside the upper right sector. We refine this

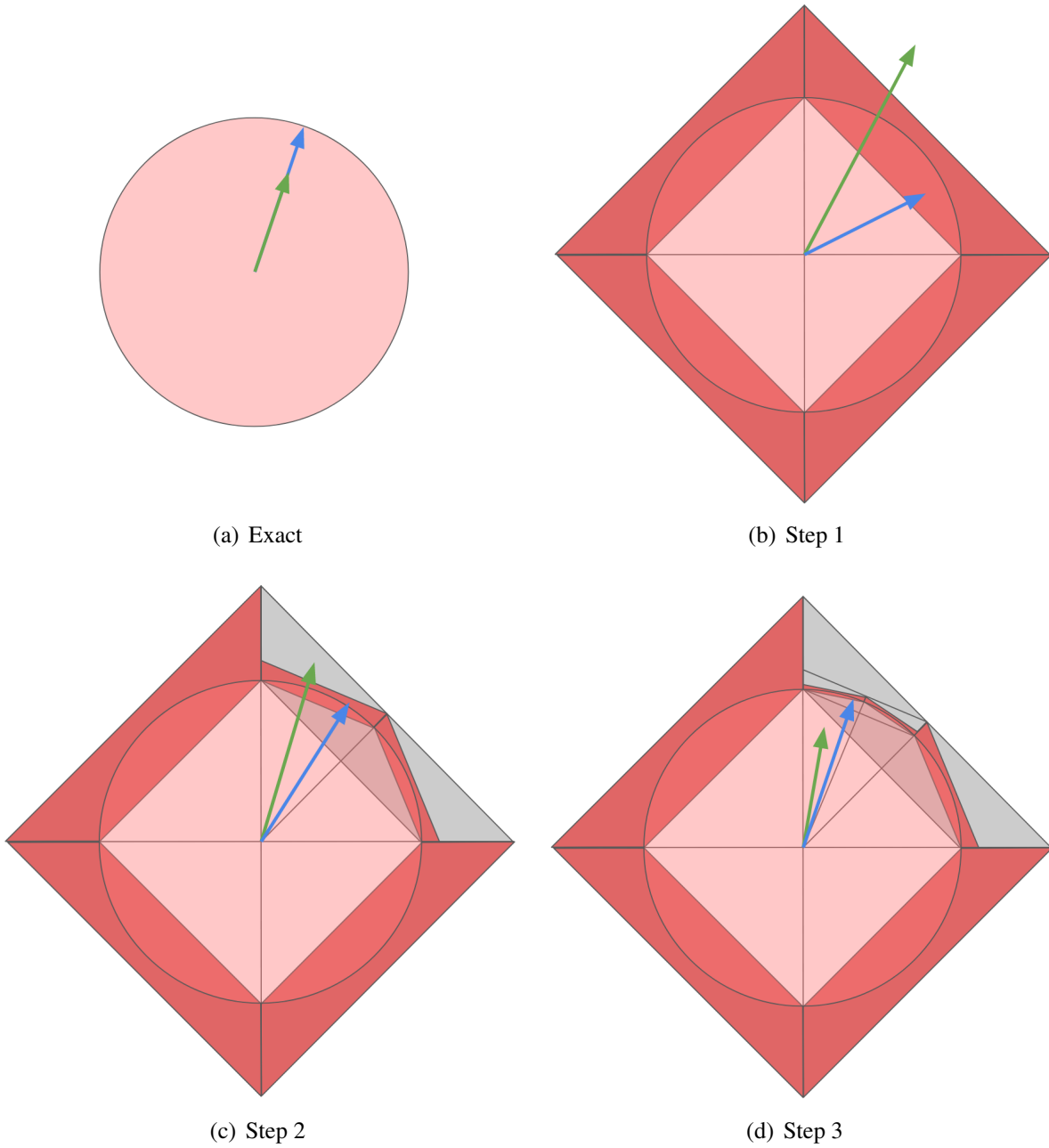


Figure 6.5: A slice through the exact circular friction cone as well as a piecewise convex relaxation. Shown are the first three steps of our algorithm refining the friction law relaxation successively and locally. The dark red regions are the space of feasible friction forces at a sliding contact. At a rolling contact the light red regions are added to the feasible friction force space. The green and blue arrows are $\mathbf{d}_{i,t} = \mathbf{D}_i \boldsymbol{\alpha}_i$ and $\mathbf{c}_{i,t} = \mathbf{D}_i \boldsymbol{\beta}_i$ respectively, which drive refinement of their local friction cone sector. In gray we show the relaxation from previous steps to show how a coarse relaxation contains the entire solution space of all successively tighter relaxations.

sector, taking care that the space of allowable solutions to the exact problem is contained inside within this new refinement refinement (see Fig. 6.5(c).) We continue this procedure (Fig. 6.5(d) etc.) until one of two things happen: we either reach a level of refinement where no solution exists, or we refine down to the point where the active sector is as small as we want it to be, bringing us arbitrarily close to the solution to the exact problem.

Note that the friction cone in the coarse approximation of Fig. 6.5(b) differs in a subtle way from that in Figs. 6.3 & 6.4: The edges of the larger discretized cone containing the exact solution space are no longer tangent to the exact solution space. Instead, the discretized friction cone is slightly enlarged. This was done to maintain a crucial characteristic of convex relaxations in optimization problems: The minimum found in a coarse convex relaxation should provide a lower bound for the minimum found in a more refined and thus tighter relaxation. This requires that the solution space at of a coarse relaxation completely contains the solution space of a tighter more refined relaxation.

Thus, only at the final level of refinement can the edge of the discretized friction cone lie tangent to the exact circular cone (Fig. 6.5(d).) In consequence, the discretized cone at a coarser level (Fig. 6.5(c)) must be offset from the exact cone in order for the relaxation to contain the two finer relaxations. The same argument means that the relaxation in Fig. 6.5(b) must be offset from the circular cone in order for it to contain the relaxations in Fig. 6.5(c) in their entirety.

Thus, we must make a slight modification to the friction edge lengths computed in (6.8). Let us pick the initial basis vectors in \mathbf{D}_i such that the angle γ between all pairs of successive vectors is equal. We pick an initial angle $\gamma = \pi/2$. We refine our polyhedral friction cone by bisecting sectors defined by the non-zero components of α_i and define the angle at which to stop refinement as $\gamma/2^q$. We now find the required length l_1 of these initial friction edges such that the initial solution set contains the solution sets at all further refinement levels.

$$l_1 = \prod_{r=1}^{q+1} \sec\left(\frac{\gamma}{2^r}\right) \quad (6.14)$$

Thus, we modify the friction edges in \mathbf{D}_i accordingly. We define vector \mathbf{f}_i to contain the lengths

of the friction edges making up the friction cone approximation in an order corresponding to the order of the weights β_i . Constraints (6.13) are modified accordingly.

$$\begin{cases} w_i = 0 \implies & \mathbf{e}^T \boldsymbol{\beta}_i \leq \mu_i c_{i,n}, \quad \mathbf{e}^T \boldsymbol{\alpha}_i = 0 & (6.15a) \\ w_i = 1 \implies & \mathbf{e}^T \boldsymbol{\beta}_i \leq \mu_i c_{i,n}, \quad \mathbf{f}_i^T \boldsymbol{\beta}_i \geq \mu_i c_{i,n} & (6.15b) \end{cases}$$

We are now ready to solve the initial coarse relaxation problem defined by (5.1)-(5.4), (5.7)-(5.11) and (6.15). We find the two active friction edges d_1 and d_2 and create three new edges that point in the direction of d_1 , $d_1 + d_2$ and d_2 and have magnitude l_2 . For this and all following refinements we have

$$l_p = \prod_{r=p}^{q+1} \sec\left(\frac{\gamma}{2^r}\right) \quad (6.16)$$

where p is the level of refinement of the sectors to be created. We insert the new friction edges between d_1 and d_2 in matrix \mathbf{D}_i and their lengths in \mathbf{f}_i . Finally we remove any redundant friction edges (edges that are identical or edges that lie between any such edges). Solving this new problem we can continue refining the friction discretization until the angle of the active sectors at all contacts reach an angle of $\gamma/2^q$. We do not further refine any sector that has already reached this threshold. The overall method is shown in Algorithm 5.

Note that this convex relaxation does not rely on explicit bounds on the problem variables as would be the case were we using McCormick envelopes. Instead, we use the bounds implicit in the friction cone constraint (5.5) in our relaxation. This is also a further advantage of our approach as the relaxation has an easily understood physical interpretation.

Recall that one of the defining characteristics of our convex relaxation is that we have chosen our friction edges so that, at any level of refinement, *the solution set to the approximate problem contains the solution set of the exact problem*. This means that if, at any point during the refinement, no solution can be found that satisfies the convex relaxations, we can guarantee that no solution can exist to the exact version of the problem either. This guarantee immediately fol-

Algorithm 5 Grasp analysis through successive relaxation

procedure RELAXATION REFINEMENT**Input:** O — objective function C — additional constraints γ — initial refinement level (angle between friction edges) q — maximum refinement level desiredInitialize \mathbf{D} with basis vectors of length l_1 as defined in (6.14)**do**Minimize O subject to (5.1)-(5.4), (5.7)-(5.11), (6.15) and C .**if** no solution exists **then****return** no feasible solution**end if**refinement_needed \leftarrow False**for** each contact i **do**Find active edges in \mathbf{D}_i $\delta_i \leftarrow$ angle between active edges**if** $\delta_i > \gamma/2^q$ **then** $p \leftarrow \log_2(\gamma/\delta_i) + 2$ Add new edges to \mathbf{D}_i of length l_p according to (6.16)Remove redundant edges from \mathbf{D}_i refinement_needed \leftarrow True**end if****end for****while** refinement_needed**return** solution**end procedure**

lows from the properties that the solution set at any refinement level includes the solution set at the next level, and that, in the limit, our discretization approaches the exact constraints. (Note that alternative approaches that work with discretized friction constraints, such as the LCP formulations discussed in Chapter 2.2, do not exhibit this property.) In practice, this means that, when no solution exists to the exact equilibrium problem, our algorithm can determine that very quickly, only solving relatively coarse refinement levels.

The second advantage this scheme provides is that when a solution does exist, we can typically refine it to high accuracy (a very close approximation to the solution of the exact problem) using relatively few friction edges. This is not theoretically guaranteed: in the worst case, our approach could require all sectors to be fully refined before finding an adequate solution at the desired

resolution, and may hence perform worse than using a fully refined friction discretization to begin with. However, we have never found that to be the case. Typically, only a small region of the discretization must be refined as the contact forces are also constrained by equilibrium relations (5.1) & (5.2) and will generally point in similar directions at all levels of refinement, leading to a very localized and targeted tightening of the relaxation. Thus, this algorithm is efficient enough to analyze complex grasps on a consumer PC to levels of refinement that are otherwise unachievable.

6.5 Robustness to geometrical uncertainties

In the above we outlined a grasp model that allows us to analyze the grasp stability given perfect information about the geometry of the grasp. We assume we know exactly the contact position and orientation. In practice however we often encounter uncertainties, which can greatly affect the stability of a grasp. Even when using tactile sensors in order to locate contacts made between the hand and the object the contact normals (and hence orientation) are often difficult to obtain accurately. Therefore we would like to make our framework robust to discrepancies up to a certain magnitude. We introduce the method we use for this here, and illustrate its importance in the following section.

Let us suppose we have an upper bound on our uncertainty in the contact normal η . Thus, the actual contact normal lies in a space of possible contact normals that deviate by at most angle η from the nominal contact normal n . In order for a grasp to be robust to deviations defined by this space we would like it to be robust in the worst-case. The worst-case contact normal \hat{n} is one that is at an angle η to the nominal contact normal and such that its projection into the tangent plane points in the same direction as the relative tangential contact motion. In our space of contact normals such a normal would be the most effective at unloading the contact and hence destabilizing the grasp (see Fig. 6.6.) The relative contact motion in the direction of the worst-case normal would then be given by

$$d_{i,\hat{n}} = d_{i,n} \cos(\eta) - \|\mathbf{d}_{i,t}\| \sin(\eta) \quad (6.17)$$

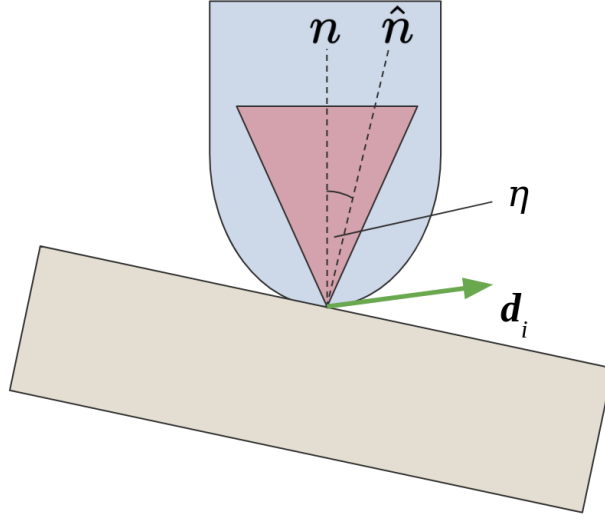


Figure 6.6: Illustration of a worst-case normal within uncertainty η given relative contact motion \mathbf{d}_i : The real normal \hat{n} deviates from the nominal normal n in such a way as to minimize the contact normal force.

However, we need to find a linear approximation for $\|\mathbf{d}_{i,t}\|$ as including it exactly would introduce a non-convex quadratic equality constraint. Fortunately we can use the amplitudes of the friction edges α . The summation of the product of all contact motion amplitudes and the length of the corresponding friction edges gives us an estimate of the magnitude of the relative tangential contact motion.

$$\|\mathbf{d}_{i,t}\| \approx \sum_{s=1}^k f_{i,s} \alpha_{i,s} = \sum_{s=1}^k l_p \alpha_{i,s} \quad (6.18)$$

Here p is the level of refinement of the active sector (i.e. the sector corresponding to the nonzero components of α_i .) The problem with this formulation is that due to the triangle inequality this overestimates the relative tangential contact motion. This effect diminishes at finer resolutions as friction edges become closer to parallel, but the destabilizing effect is potentially larger at coarser resolution. However, recall that our refinement method requires that the solution set at coarser levels includes the solution set at finer levels. We thus require the destabilizing effect to be weaker at coarse resolutions and become stronger approaching its exact value as $p \rightarrow \infty$.

Note that (6.18) is exact for contact motion parallel to any friction edge but for any tangential

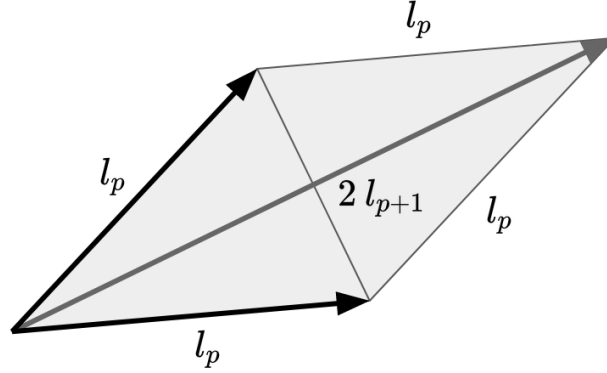


Figure 6.7: The vector addition of two adjacent friction edges of length l_p is a vector of length $2l_{p+1}$.

motion that lies between two edges it overestimates the magnitude of the relative sliding motion. The overestimation is most pronounced if the sliding motion exactly bisects the two adjacent friction edges. Thus, in order to prevent overestimation of sliding motion while retaining the tightest possible relaxation we must modify (6.18) such that it instead is exact for motions bisecting any two adjacent friction edges and underestimates sliding motion everywhere else.

Let us first find out by how much (6.18) overestimates tangential motion in the worst case. Recall that $f_{i,s} = l_p$ can be calculated using the refinement level p of the corresponding friction edges and (6.16). Consider two generic adjacent friction edges of length l_p . Fig. 6.7 illustrates that the worst-case overestimation occurs for vectors bisecting the two friction edges. Furthermore, due to the geometry of the relaxation described in Fig. 6.5 and (6.16) we know that the vector addition of two adjacent friction edges is a vector of length $2l_{p+1}$. Thus, the factor by which (6.18) overestimates tangential motion that bisects any two friction edges of length l_p is

$$\frac{l_p}{l_{p+1}} \quad (6.19)$$

We can now divide (6.18) by this factor such that we obtain an approximation of the tangential motion magnitude that underestimates everywhere except at the midpoint between two edges where it is exact.

$$\|\mathbf{d}_{i,t}\| \approx \sum_{s=1}^k l_{p+1} \alpha_{i,s} \quad (6.20)$$

As $p \rightarrow \infty$ this estimation becomes exact. We can now plug this back into (6.17) for a linear approximation of the worst-case relative normal contact motion.

$$d_{i,\hat{n}} = d_{i,n} \cos(\eta) - \sin(\eta) \sum_{s=1}^k l_{p+1} \alpha_{i,s} \quad (6.21)$$

We now replace the normal relative contact motion in (5.4) with $d_{i,\hat{n}}$ in order to obtain solutions that are robust to uncertainties in contact normal up to an angular discrepancy of η .

6.6 Application to grasp analysis in three dimensions

6.6.1 Existence problems

The range of queries we can answer with the approach described in Chapter 6.4 is less limited than that of the iterative approach discussed in Chapter 5. However, existence problems are still the most simple queries to solve and are a good starting point before moving on to more complex queries.

Let us solve for the stability of the grasp shown in Fig. 6.8 when we apply a force of 1N to the object in the positive y -direction *without preloading the joints at all*. To answer this query, we use Algorithm 5 as follows:

$$\text{objective: none} \quad (6.22)$$

$$\text{additional constraints: } \mathbf{w} = [0, 1, 0, 0, 0, 0]^T \quad (6.23)$$

$$\boldsymbol{\tau}^c = \mathbf{0} \quad (6.24)$$

Note that, in the absence of an optimization objective, we are simply asking if a solution exists that satisfies all the constraints of the problem, equivalent to determining values for all the un-

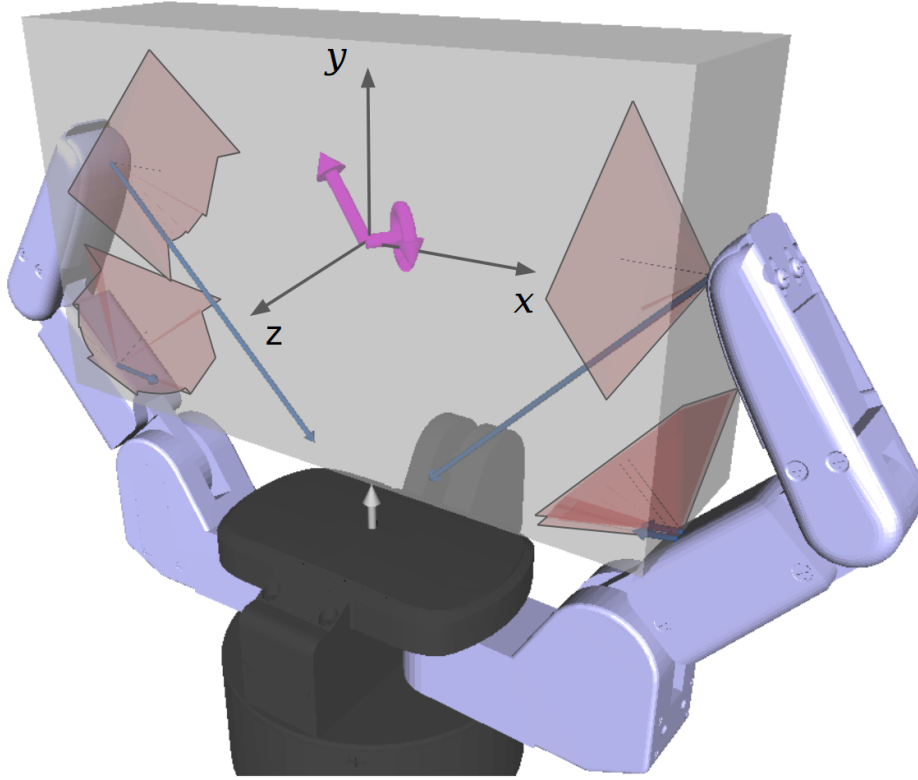


Figure 6.8: Equilibrium contact forces (blue arrows) that are predicted to arise by our framework when a force of 2.2N is applied to the object in the y -direction. The proximal joints have both been preloaded with 0.1Nm. Note the refinement of the pyramidal friction cone approximation. Only a minority of sectors have been refined. Sectors that are not of interest in this specific grasp problem remain in a less refined state and thus only contribute little to the complexity of the overall problem. The sectors containing the equilibrium contact forces are $< 1^\circ$ small. The maroon arrows denote the direction of predicted object motion.

knowns (contact forces, virtual motions, etc.) such that the grasp is stabilized. Using Gurobi [94] as a solver for the constituent MIPs, Algorithm 5 finds no feasible solution to this problem (i.e. it predicts the grasp is unstable in the presence of the given disturbance.) This is the expected result: the grasp may not resist a force of 1N in the y -direction without any preloading, as it is intuitively clear that the object will slide out.

Let us now consider the case where we apply a preload torque of 0.1 Nm at the proximal joints. Due to the simplicity of the grasp we can analytically determine the expected maximum force in the y -direction the grasp can withstand: a ~ 90 mm contact moment arm and a friction coefficient of 1.0 results in a maximum total friction force applied to the object of ~ 2.2 N. Using

a similar formulation as before (no objective, $\tau^c = 0.1\text{Nm}$ at the proximal joints), we indeed find that Algorithm 1 accepts a solution (i.e. predicts stability, see Fig. 6.8) for a disturbance of 2.2N in the y -direction ($\mathbf{w} = [0, 2.2, 0, 0, 0, 0]^T$), but finds no solution for a disturbance of 2.5N in the same direction ($\mathbf{w} = [0, 2.5, 0, 0, 0, 0]^T$).

6.6.2 Space of resistible disturbances

The option to add an objective allows us to formulate more interesting queries. Algorithm 5 provides us with a simple method of characterizing the space of possible disturbances on the object a grasp can withstand through purely passive reaction. We can directly determine the exact *maximum disturbance* applied to the grasped object in a given direction that a grasp may resist purely passively. To this end we might prescribe a preload τ^m for the actuators to be kept constant, and a direction \mathbf{d} along which to apply a disturbance to the object. To compute the largest magnitude disturbance the grasp can withstand in that direction, we use Algorithm 5 as follows:

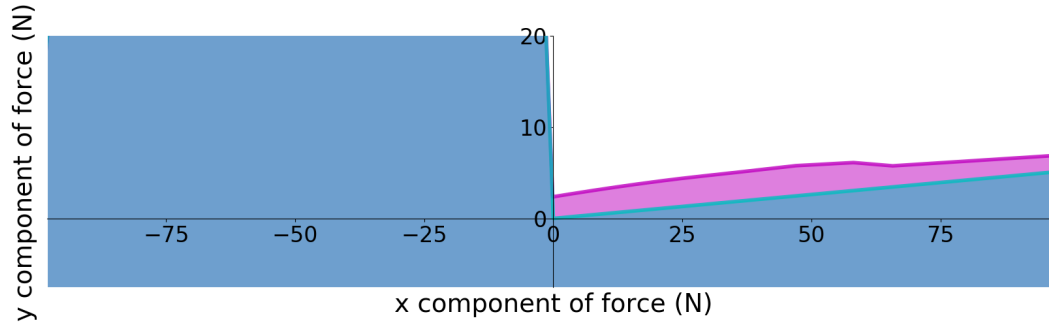
$$\text{objective: } \text{maximize } s \tag{6.25}$$

$$\text{additional constraints: } \mathbf{w} = s\mathbf{d} \tag{6.26}$$

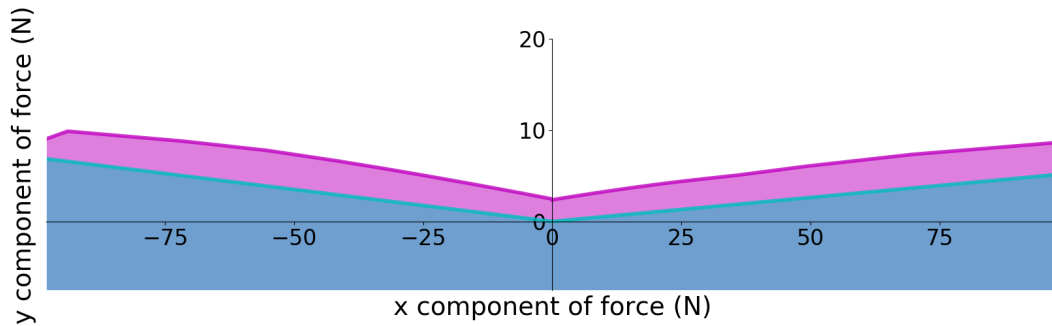
$$\tau^c = \tau^m \tag{6.27}$$

We already analytically estimated the resistance of our example grasp to disturbances in the positive y -direction to be $\sim 2.2\text{N}$. The maximum resistible force predicted by our framework is 2.33N and thus very similar. The 6% difference is well within the uncertainty introduced by estimating the exact geometry of the grasp.

In order to further investigate the stability of the grasp and also the capabilities of our framework let us consider the maximum resistible disturbances in multiple directions. We discretize the grasp plane by direction vectors with a spacing of 1° between them. We then determine the maximum force applied to the object the grasp can withstand for each of these direction. The results



(a) No contact normal uncertainty



(b) Robust to contact normal uncertainties

Figure 6.9: Resistible forces in the grasp plane of the grasp in Fig. 6.8 as predicted by our model and algorithm. In blue are forces that can be resisted even without the application of preloading torques at the joints. When loading the two proximal joints with 0.1Nm the maroon area is added to the space of resistible forces.

are visualized in Fig. 6.9, where Fig. 6.9(a) plots results without considering robustness to contact normal uncertainty, while Fig. 6.9(b) assumes an uncertainty of 2.5° .

The results match our intuition that any downward force can be reacted without any loading of the fingers. Furthermore the model captures the need for finger loading in order to resist upward forces. It also shows an effect of passive finger loading for forces with nonzero x component: pushing sideways increases the amount of resistance to upwards forces.

The reason for the asymmetry of Fig. 6.9(a) however is not immediately obvious, as the grasp itself appears symmetric. In fact however, the two distal contacts are ever so slightly offset, causing the object to pivot about the left distal contact and wedging itself stuck if enough leftward force is applied. The grasp in Fig. 6.10 makes it clearer why this behavior occurs - here the contacts are visibly offset. Note, that this wedging behavior is very different from the wedging behavior

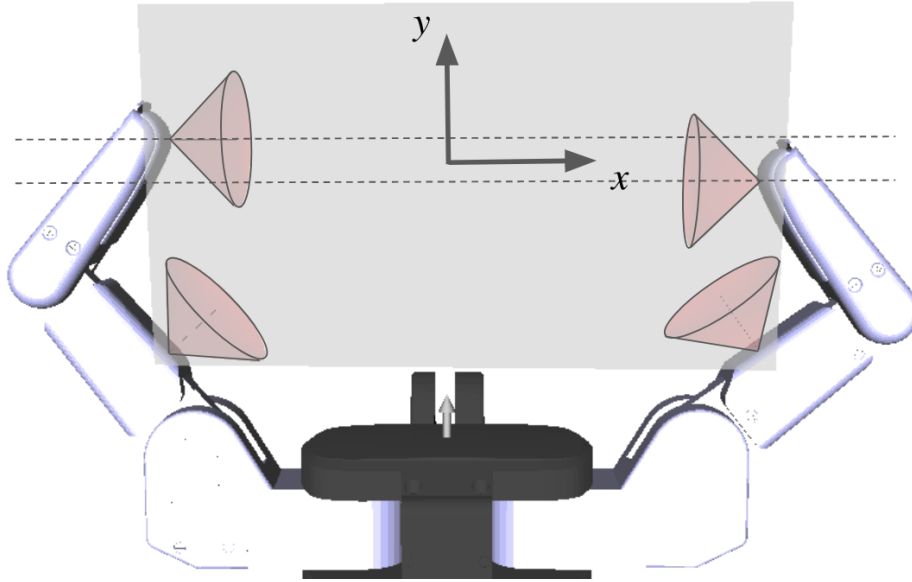


Figure 6.10: A grasp designed to highlight the 'wedging' effect. The two contacts on the distal link are offset with respect to each other allowing wedging to occur.

discussed in Chapter 5.3.2, which occurred when omitting the MDP. There, the wedging occurred no matter the applied wrench such that arbitrary wrenches could be resisted. Furthermore, the resulting contact forces did not satisfy energy conservation.

In contrast, in our framework only specific wrenches allow wedging to occur. These wrenches depend on the geometry of the grasp and are consistent with the rigid body statics of the grasp problem. The equilibrium contact forces predicted by our framework satisfy the MDP and hence energy conservation. However, as our method allows us to solve the rigid body problem very accurately, only a small offset is required for our model to predict wedging of the object; an offset that is easily within the accuracy of a typical triangular mesh. Note, that this behavior is fully consistent with the rigid body assumption (although we introduced compliance at the contacts we ignore changes in grasp geometry due to motion) and the predictions made by our framework are correct, albeit highly sensitive to the grasp geometry.

Of course in practice it is not advisable to rely on such volatile geometric effects. Therefore taking into account geometric uncertainties is of paramount importance for practical applications. Fig. 6.9(b) shows which forces can be robustly resisted when we consider the uncertainty in normal

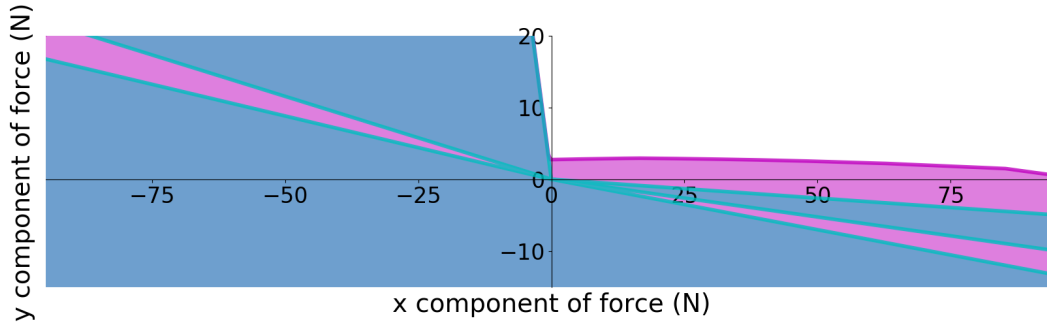


Figure 6.11: Forces in the xy -plane predicted resistible for the grasp in Fig. 6.10 using our model and algorithm. In blue are forces that can be resisted even without the application of preloading torques at the joints. When loading the two proximal joints with 0.1Nm the maroon area is added to the resistible forces. We also take into account a contact normal uncertainty of 2.5 degrees to make sure the grasp is robust to such discrepancies.

angle to be no larger than 2.5° (using the approach outlined in Chapter 6.5.) The resulting plot of resistible forces is approximately symmetric corresponding to the near-symmetry of the grasp. The indicated spaces of resistible forces both with and without a preload are consistent with our intuition and the empirical data presented in Chapter 5.5.

We showed how we can make the stability predictions less sensitive to the small scale geometric characteristics of the grasp and thus robust to uncertainties. At a larger scale, however, wedging effects can be robustly leveraged. In the grasp in Fig. 6.10 the contacts are significantly offset and the forces this grasp may resist robustly are shown in Fig. 6.11. Thus, if we know the range of disturbances likely to be encountered during a manipulation task our framework can be a valuable tool in picking an appropriate grasp.

One feature of Fig. 6.11 perhaps requires further elaboration: The gaps in the second and fourth quadrants of Fig. 6.11 where forces may only be resisted when a preload is applied but not otherwise. These gaps stand out because they appear thin and are surrounded by large areas where applied forces are resistible even without a preload. We thus investigated what effects cause these wedges in order to verify if these predictions are physically accurate:

The grasps shown in Figs. 6.8 and 6.10 were created such that all contacts are as close as possible to lying in a mutual plane. This is because three dimensional grasps can be very complex while two dimensional grasps often allow us to use our intuition to validate the predictions made by

our framework. However, we are using the open-source GraspIt! [13] package in our grasp analysis and a limitation of this package is that it is difficult to create grasps that are truly two dimensional in nature. Due to the meshing of the finger and object geometries as well as the intricacies of collision checking in GraspIt! the contacts always lie somewhat offset from the central plane.

In the specific case of the grasp in Fig. 6.10 the contacts do not quite lie within the xz -plane, in which the forces applied to the object lie. This means that two contacts are generally not sufficient in order to balance an applied force. Let us investigate the gap in the second quadrant of Fig. 6.11: When a force is applied along the $(-1, 0)$ direction the distal contact of the left finger acts as a fulcrum and the object rotates clockwise loading the contact on the proximal contact of the right finger. When a force is applied in the $(-1, 1)$ direction the left finger contact again acts like a fulcrum, however now the object rotates counter-clockwise loading the distal contact on the right finger.

Somewhere in between those two cases the applied force points almost directly at the fulcrum contact and instead of rotating the object is mostly pressed against the left finger breaking both contacts on the right finger. Thus, only two contacts remain and the grasp becomes unstable. In this particular case the object would rotate out of the grasp around the y -axis as the two remaining contacts on the left finger do not lie in the same plane as the applied force.

Let us now consider the grasp in Fig. 6.12. Note that this grasp comprises four contacts (one on each distal link plus one on a proximal link) which do not lie on the same plane, and thus has to be analyzed in a three-dimensional framework. We consider here an apparent task the robot grasping the flask may need to execute. In order to pour a liquid contained in the flask it is necessary to tip it. If we choose to use the robot wrist for this tipping motion then the force of gravity acting on the flask and its contents lies in the xy -plane. The grasp must thus be able to resist such forces in order to complete its task successfully. Furthermore, we have a choice of direction in which to turn the flask in order to pour its content. Creating a visualization (shown in Fig. 6.13) as before we can deduce the need for a preload, and that it is more robust to turn the flask counter-clockwise. Thus, once a grasp has been established our framework can help in making decisions as to how a task is

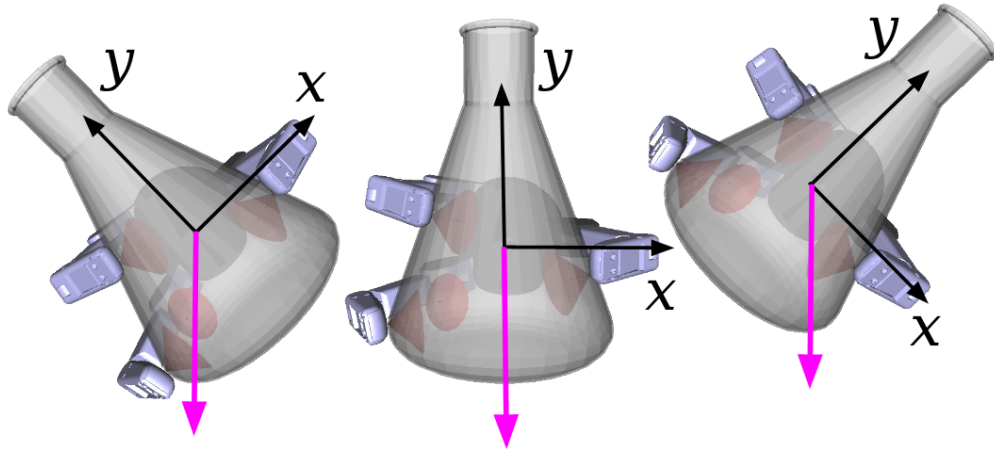


Figure 6.12: 3 dimensional grasp that highlights the necessity of a grasp to be able to withstand a range of forces applied to the object. During a pouring task gravity (pink) moves in the xy -plane.

to be executed.

6.6.3 Actuator command optimization

The passive stability of a grasp is not only determined by its geometry: the actuator commands are equally important. Consider for example the grasp in Fig. 6.14. The three contacts the hand makes with the object all lie approximately in the xz -plane. Contacts 1 and 2 lie approximately on the x -axis and oppose each other. Let us assume we create a grasp by commanding the proximal joints of fingers 1 and 2 to each apply 0.1Nm. Let us vary the torque commanded at the proximal joint of finger 3 and observe the difference in passive stability. Specifically, we will use our framework to investigate the maximum disturbance on the object the grasp can resist in two directions. Fig. 6.15 shows the resulting predictions from our algorithm.

First we are interested in forces along the positive z -axis. As expected, the resistance is largest if no motor torque is applied by finger 3. Any load by this finger only adds to the disturbance and does not help in resisting it. When the torque applied by finger 3 reaches 0.09 Nm, it has completely removed any resistance to z -direction forces. This can be easily verified: The coefficient of friction chosen for this example is 0.45 and the moment arms from joint to contact are identical for all three fingers. As there cannot be any out-of-plane forces, the normal forces at all contacts will

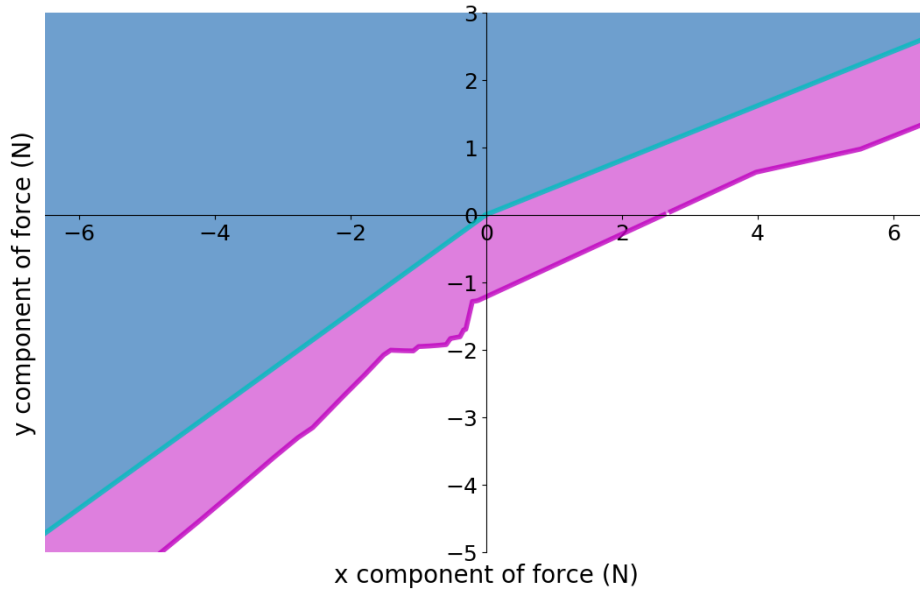


Figure 6.13: Forces in the xy -plane predicted resistible for the grasp in Fig. 6.12. In blue are forces that can be resisted even without preloading joint torques. When loading the proximal joints with 0.1Nm , the maroon area is added to the resistible forces. We use a contact normal uncertainty of 2.5 degrees.

be proportional to the applied joint torque. Thus, applying 0.09Nm at finger 3 claims all possible contact friction at both contacts 1 and 2: no further forces in that direction can be resisted.

Let us now consider passive resistance to torques applied to the object around the x -axis. If we do not load finger 3 the object is only held by contacts 1 and 2. As both these contacts lie on the x -axis they cannot apply any torque to the object in that direction. Thus, the grasp cannot resist any torques around the x -axis unless we also load finger 3. The third finger provides the contact necessary for resisting the torque on the object. The more we load finger 3, the larger the force at contact 3 and the larger the resistible torque. At some point however, as discussed above, the forces at finger 3 begin to overwhelm fingers 1 and 2 and the object slides out along the z axis even without any external disturbances.

This example shows the importance of preload and passive stability: for this grasp, loading finger 3 helps resistance against some disturbances, but hurts against others. The right amount of preload must thus be chosen based on the task. To the best of our knowledge, no existing grasp analysis method can make such predictions.

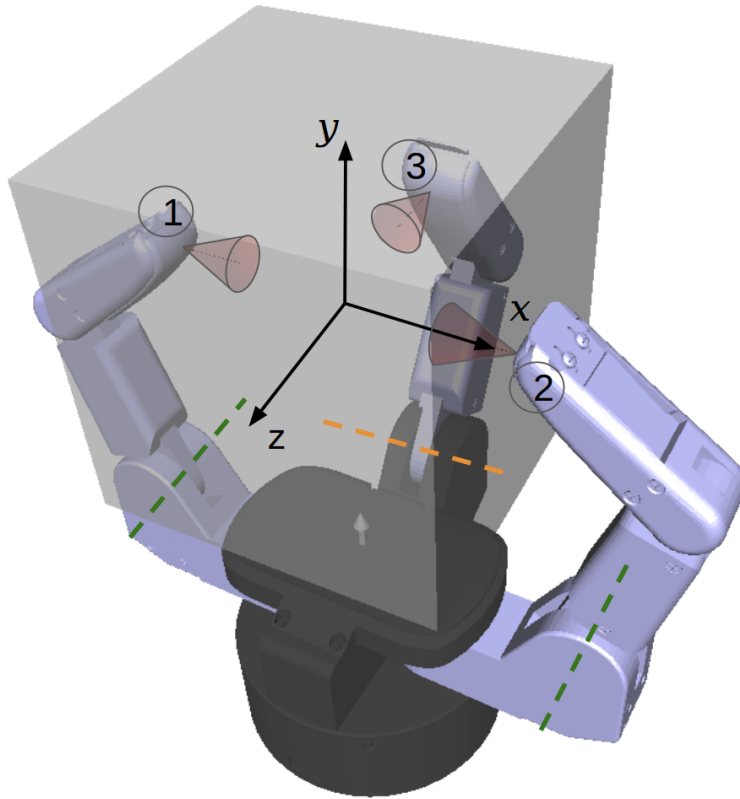


Figure 6.14: Example grasp to illustrate the importance of appropriately choosing grasp preloads. We assume a preload of 0.1Nm at the proximal joints of fingers 1 and 2 (axes marked as green dashed lines). We apply a range of preload torques at the proximal joint of finger 3 (axis marked as yellow dashed line) and evaluate passive stability.

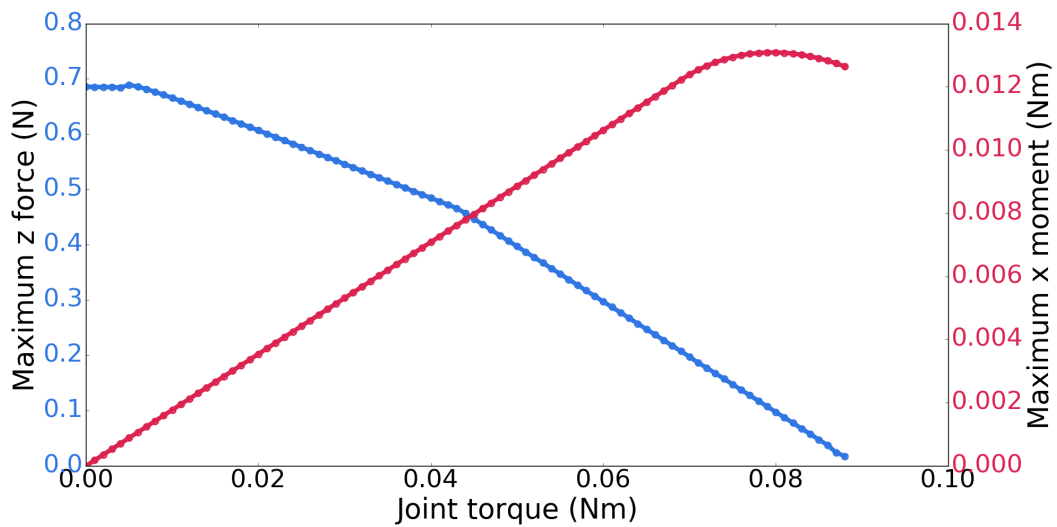


Figure 6.15: Force in the z -direction (blue) and moment in the x -direction (red) the grasp in Fig. 6.14 can resist for a range of preloads at finger 3.

Using our model, we can also find actuator commands that are optimal with respect to any specific objective we choose. For example we may want to minimize the maximum torque a single actuator must produce to resist a given wrench \mathbf{w}^m . We now use Algorithm 5 as follows:

$$\text{objective: } \text{minimize } \max_j \tau_j^c \quad (6.28)$$

$$\text{additional constraints: } \quad \mathbf{w} = \mathbf{w}^m \quad (6.29)$$

For the grasp in Fig. 6.12, we can compute the optimal actuator commands for a force of $\mathbf{w}^m = [0, -1.21743, 0, 0, 0, 0]^T$, the largest force in the negative y -direction that can be resisted when applying a preload of 0.1Nm at every proximal joint, according to our previous analysis. We find that the optimal torques at these joints are actually $\boldsymbol{\tau}^c = [0, 0.042, 0.073]^T$. This shows that a large amount of the naive preload (0.1Nm at every joint) is wasted in the sense that it does not increase disturbance resistance in this particular direction. In fact it appears that loading finger 1 was detrimental to grasp stability with respect to this disturbance.

In many practical applications it may be of interest to take into account physical limits such as the maximum torque an actuator can apply or a maximum permissible normal force in order to not break the grasped object. Such constraints can be expressed as linear inequalities and are straightforward to add to our model.

6.6.4 Computational performance

In Chapter 6.4 we state that an accurate solution to the grasp problem with discretized friction cones but without hierarchical refinement requires a very large number of friction edges. We further argue that solving such a problem becomes computationally intractable as a large number of friction edges results in a large number of binary variables in the MIP. To verify these hypotheses, we analyze the convergence of our algorithm with varying levels of refinement of the friction approximation. We use the grasp in Fig. 6.12 as an example, with the task of finding the largest force

in the negative x -direction that the grasp can withstand. We do so at varying levels of refinement, and record the predicted force magnitude and runtime.

We compare two approaches: The first method ("full resolution") directly uses a friction cone approximation that is at the desired level of accuracy in its entirety. The second method ("hierarchical refinement") always starts with a coarse approximation and refines it as described in Algorithm 5. Throughout all experiments, both methods (when able to finish) produced identical solutions, but the running times varied greatly. All recorded data can be found in Table 6.1.

We notice that, at high levels of refinement, full resolution becomes intractable, whereas hierarchical refinement finds a solution efficiently. The study of how the refinement level affects the returned solution is more complex. The exact value of the solution generally reaches a point where increasing the accuracy of the approximation (adding more friction edges) stops making a significant difference. In some cases, as in the case of the maximum wrench in the left side of Table 6.1, this happens for accuracy levels that only hierarchical refinement can reach. In others, as in the case of the maximum robust wrench (with 2.5° normal uncertainty) in the right side of Table 6.1, both methods are able to find good approximations of the final value. At the more shallow levels, full resolution will often outperform hierarchical refinement, but since we generally do not know which of these cases any specific query might fall into, only hierarchical resolution allows us to increase the accuracy without the risk of compute time exploding. These results show both that high accuracy is actually required in order to obtain meaningful results, and that solving such problems without hierarchical refinement is computationally intractable.

Another interesting finding is that the predicted maximum resistible force is exceedingly large when only four friction edges are used in the first step of the refinement process. This is because at this stage the MDP is only enforced such that the friction force and negative relative tangential contact motion lie within a 90° sector. This allows sufficient freedom to the solver to use the rigidity of the robot hand when backdriven along with unphysical object motions to create large contact forces - much like what was described in Chapter 5.3.2 where there are no constraints on the friction direction at all. This illustrates again the need for a high accuracy solution to the grasp

Equivalent number of friction edges	Without robustness scheme			With robustness scheme		
	Maximum wrench (N)	Time at full resolution (s)	Time with hierarchi- cal refinement (s)	Maximum wrench (N)	Time at full resolution (s)	Time with hierarchi- cal refinement (s)
4	>100	0.088	0.088	>100	0.11	0.11
8	7.07435	0.22	0.43	7.07435	0.24	0.46
16	6.34905	0.43	0.65	3.73377	0.45	1.02
32	3.71036	0.72	1.92	3.70539	0.97	1.33
64	3.70095	1.58	2.33	2.31479	1.83	3.09
128	3.69775	5.80	3.50	1.21805	5.12	10.9
256	3.69751	>600	4.87	1.21756	20.3	13.0
512	3.69681	-	4.34	1.21743	102	17.8
1024	3.07268	-	13.3	1.21740	394	22.9
2048	3.07267	-	15.0	1.21739	-	32.2

Table 6.1: Performance of the analysis of the grasp in Fig. 6.12. We compute the magnitude of the largest force that can be applied in the negative y -direction without destabilizing the grasp. We do this for varying levels of refinement expressed as the number of sectors the friction cone approximation contains. We record compute times for both an approach where all sectors are already of the desired size and our hierarchical refinement approach.

Grasp	Number of contacts	Stability check	Maximum disturbance		Optimal torques	
		Time (s)	Mean time (s)	Median time (s)	Mean time (s)	Median time (s)
(a)	3	0.246	0.797 ± 0.067	0.754	0.389 ± 0.063	0.343
(b)	3	0.234	0.785 ± 0.085	0.745	0.447 ± 0.074	0.408
(c)	3	0.294	0.893 ± 0.056	0.907	0.347 ± 0.017	0.345
(d)	3	0.259	0.664 ± 0.081	0.560	0.308 ± 0.036	0.281
(e)	4	1.07	10.0 ± 3.4	6.39	3.26 ± 0.50	3.83
(f)	4	15.7	36.7 ± 6.5	39.5	13.5 ± 4.8	9.58
(g)	4	2.78	33.8 ± 9.3	20.8	16.8 ± 5.3	12.3
(h)	4	8.02	23.7 ± 4.2	23.2	12.3 ± 3.3	8.10
(i)	4	1.66	14.4 ± 2.7	11.4	1.67 ± 0.12	1.60
(j)	5	6.06	150 ± 24	105	22.8 ± 5.8	19.0
(k)	6	51.0	398 ± 104	344	136 ± 54	80.6
(l)	6	27.5	488 ± 99	330	777 ± 288	626

Table 6.2: Runtime analysis of our method for the three tasks demonstrated in this paper performed on a consumer desktop computer for the grasps shown in Fig. 6.16. Where multiple trials were performed we report the mean ± standard error as well as the median runtimes.

stability problem including the MDP.

In order to investigate the practical applicability of our method, we tested the runtime of our algorithm on a range of grasps that could be encountered in a grasping task (see Fig. 6.16.) We generated these grasps on a range of differently shaped objects using a brute force grasp planner [102]. On each of these grasps we applied our framework to perform the three tasks demonstrated above: Checking for stability, finding the maximum resistible wrench in a given direction and computing the optimal actuator commands. In the second task the direction along which to find the maximum resistible disturbance can have an impact on the runtime of the algorithm. We hence repeated the solution process with ten different randomly generated directions to obtain more meaningful results. Similarly, the time it takes to optimize the actuator commands depends on the external wrench applied to the object and hence we also repeat these experiments with ten randomly sampled external wrenches. The results are recorded in Table 6.2. In order to guarantee accurate results we continued refinement until we reached a level equivalent to 2048 sectors in the friction approximation. Empirically we have found this level of refinement guarantees convergence for all grasps tested (although many converged sooner.)

We note that, as expected, the runtime of our algorithm grows with the number of contacts. For grasps with three contacts, all queries typically had sub-second runtime; up to and including five contacts we noticed a runtime typically between 1 and 30 seconds. Also as expected, stability checks (the most fundamental operation needed for a grasp) are faster than computations like maximum resistible disturbance or optimal joint torques. This suggests different applications of our framework for different scenarios: pruning a larger number of possible grasps using the faster stability analysis, then computing the optimal torques only on the most promising candidates. Even with six contacts, our method had a runtime on the order of minutes, suitable for example for fixturing analysis in a manufacturing line. Finally, we also note that, in the absence of our hierarchical refinement, it is altogether intractable to approach this level of accuracy for all except the simplest of grasps.

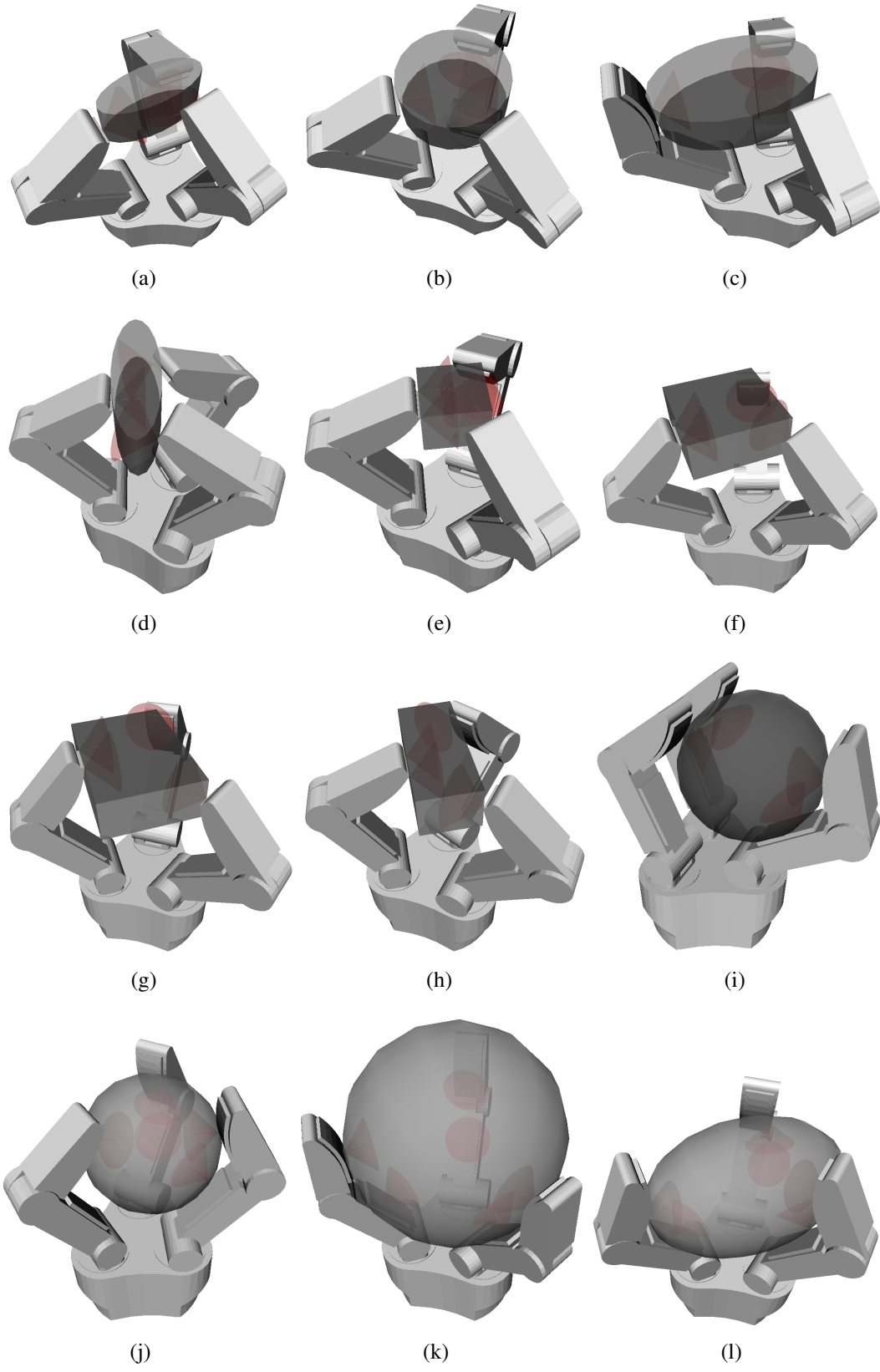


Figure 6.16: Algorithmically generated grasps to investigate the computational performance of our method.

6.7 Discussion

In this Chapter we described a grasp stability model that allows for efficient and accurate solution methods under realistic constraints. Noting that an exact formulation of Coulomb friction includes non-convex constraints (due to the Maximum Dissipation Principle), we discussed how convex relaxations along with successive hierarchical tightening can be used to solve non-convex optimization problems. We specifically discussed McCormick envelopes and pointed out their limitations.

Instead, we proposed a discretization method that allows the Coulomb friction law to be reformulated as a piecewise convex Mixed Integer Program solvable through branch and bound. However, such discretization methods traditionally involve a trade-off: coarse discretizations provide only rough approximations of the exact constraints, while high resolutions discretizations are computationally intractable. To address this problem, we introduce a hierarchical refinement method that progressively increases the resolution of the discretization only in the relevant areas, guided by the solution found at coarser levels.

Our local refinement method remains efficient up to high discretization resolution, and also similarly to traditional tightening methods for convex relaxations provides strong guarantees: if a solution cannot be found at a coarse approximation level, the underlying exact problem is guaranteed not to have a solution either. Combined, these two features make our method efficient for problems both with and without exact solutions. It is, to the best of our knowledge, the first time that grasp stability models incorporating Coulomb friction (along with the MDP) have been solved with such high discretization resolution.

Our model and algorithm accepts many types of queries: for example, we can analyze the space of wrenches applied to an object that a given grasp can withstand, or compute optimal joint commands given a specific object wrench. Thanks to the hierarchical refinement method, these can be solved efficiently (on the order of seconds per query) even with very high resolution approximations of the MDP.

Running our analysis method on a number of example grasps, we showed that our method predicts effects both intuitive (pressing directly against contacts is passively stable, but pulling the object away requires preload torques) and more subtle (an object wedging itself in a grasp in response to a disturbance for a given contact geometry.) In contrast, grasp stability models that do not consider the MDP produce unrealistic results, and fail to predict the dependence of disturbance resistance on applied preloads.

A limitation of our method is that, while it performs well in practice, its theoretical running time remains worst-case exponential in the level of discretization for friction constraints. Furthermore, for cases where a coarse discretization yields a sufficiently accurate solution, hierarchical refinement might be outperformed by an equivalent method with uniform resolution (although these cases are generally unknowable in advance, without actually solving up to high resolutions.)

From a practical perspective, we would like to explore additional applications of our approach. In the context of grasp analysis and planning the runtime of our algorithm is currently too large for online grasp planning with more than a few contact. Therefore, we see the main practical relevance of our method in enabling practitioners to understand and utilize passive effects in grasping and in providing labels for learning-based grasp planners. The model we introduced can allow multiple types of queries, and in this paper we have only presented some of the possible applications.

Our framework may also be applicable to problems encountered in the field of robotic locomotion, for instance to determine the balance of a legged robot on uneven terrain [103]. In fact, we believe that our model and algorithm is applicable to many other fields concerned with the stability of arrangements of rigid bodies with frictional contacts and other unilateral constraints such as pushing in clutter and robotic construction.

From a theoretical perspective there are many interesting problems remaining. Firstly, we took care that our convex relaxation satisfies the requirement that a coarse relaxation contains the solution space of all successively tighter relaxations. This characteristic is important for Branch and Bound algorithms that prune parts of the solutions space based on the fact that the minimum

found in such a coarse relaxation provides a lower bound to the minimum in any tighter relaxation. Instead of making use of this, we solve an entire Branch and Bound problem at every refinement step. This means that Branch and Bound is recomputing much of its search tree at every step. Instead, we could save the tree generated at one refinement step and use it to warmstart Branch and Bound at the next. This promises large improvements in performance and the relaxation we proposed in this chapter satisfies all the requirements for such an approach.

Furthermore, recent work by Huang et al. [93] built upon our own work discussed in Chapter 4 and developed an algorithm that can determine all possible combinations of contact slip states. The slip state of a contact is defined as the sector of a discretized tangential plane containing the relative tangential contact motion — much the same as in our work discussed above. They make use of the fact that not every combination of contact slip states is possible under rigid body motion constraints. Their algorithm could be a useful pre-processing tool that can prune large amounts of the Branch and Bound search tree based on these rigid body constraints.

Finally, we have thus far turned to commercial solvers for the solution of the Mixed Integer Programs that describe our grasp models. These solvers search for an exact solution through computationally expensive methods such as the Branch and Bound algorithm. Recently, however, there has been promising work on the development of more efficient, albeit approximate solution methods [104]. Reducing the computational demands of our algorithms would greatly affect their practical applicability and hence we will investigate these novel methods.

Chapter 7: Grasp Stability Analysis for Reinforcement Learning of in-hand manipulation

7.1 Introduction

In-hand manipulation (i.e. reorienting a grasped object with respect to the grasping hand) is a challenging task in robotics due to the problem’s large state-space and hard to model dynamics. While there are numerous analytical approaches making use of planning and optimization algorithms (some of which we mentioned in Chapter 2.3) they rely on the ability to derive analytic models of the kinematics and dynamics of the bodies involved as well as the contact phenomena. This results in many complications as small errors in the models can have dramatic effects. Accurately modeling friction forces by itself is a large area of study (see Chapter 2.2.) Furthermore, partial observability of the state — unknown geometries as well as uncertainty in the contact positions and forces due to occlusion for instance — make it impossible to compute complete models of the grasp.

In contrast, model-free reinforcement learning takes an end-to-end approach treating the grasp and its dynamics as a black box: The grasped object, hand kinematics and contact mechanics are assumed unknown. Reinforcement learning reasons probabilistically: Through stochastic exploration a policy is trained to learn which actions maximize rewards given the current partial observation of the state. It can therefore be applied to problems with partial observability such as most manipulation tasks. In consequence, however, such methods forgo any formal guarantee of success.

While model-free RL has shown great promise in high-dimensional manipulation tasks, its sample complexity remains problematic. Furthermore, policies applied to in-hand manipulation on real robots thus far all require some level of external support for the manipulated object.

This is either done through resting the object on a tabletop [78], on the up-turned palm of the hand [11][12][81], or fixing some of its degrees of freedom through external constraints [80].

It is our intuition that the notion of maintaining a robust quasi-statically stable grasp throughout a task greatly simplifies general in-hand manipulation. While humans leverage dynamic phenomena to great effect controlling them requires rich tactile feedback and great skill. Thus we will focus on manipulation skills that maintain quasi-static stability as we believe they are more easily attainable for robotic systems, albeit less powerful than general manipulation leveraging dynamic effects.

We also believe that efforts to maintain quasi-static stability throughout a manipulation task can improve the sample complexity of training RL policies for dexterous manipulation¹. Consider the process of collecting data in order to train a policy: whenever the grasp becomes unstable and the object is dropped the rest of the episode can no longer contribute to learning the task. While resetting the environment is trivial in simulation, on a real robot it requires a reset mechanism, which can be complicated to design.

In Chapter 3 we argued that robotic hands designed solely for grasping tasks (such as picking an object from clutter) have evolved in such a way as to trade off complexity for passive stability. Most researchers applying reinforcement learning are currently leveraging vision and motion capture instead of tactile sensing [11][12][80][81]. We believe the reason for this lies in the limited tactile sensing capabilities of the current generation of robotic hands and expect tactile sensing to begin playing a more prominent role as this technology evolves. In fact, members of our group are actively developing and building tactile sensors that will supply us with high fidelity contact position and force information over the majority of the finger surface [105].

As a new generation of highly sensorized multi-finger robotic hands is beginning to emerge the use of rich sensor data from tactile and proprioceptive sensors will become a viable alternative to purely vision based approaches to dexterous in-hand manipulation. Note that, while the global shape of the object may be unknown tactile sensors allow us to observe the local shape of the

¹Bicchi [15] defines dexterous manipulation as "the capability of the hand to manipulate objects so as to relocate them arbitrarily for the purposes of the task"

object. This new generation of robotic hands can also satisfy the assumption that is central to most of the grasp modeling literature we discussed in Chapter 2.1: Active control over contact forces through actuator commands. Thus we can determine the (local) stability of a grasp or actuator commands necessary for stability using classical grasp stability theory.

However, it appears the theoretical works have had little impact in the learning community so far. While we believe RL by itself to be able to train policies that maintain stable grasps throughout a reorientation task (we show this is the case in Chapter 7.2) it appears wasteful to spend training time in order to learn an aspect of the task for which we already have good analytical tools. Thus we argue there is merit to the idea of applying such model-based approaches to the smaller problem of maintaining quasi-static grasp stability (for which the necessary state variables are locally fully observable) while using model-free methods for the larger problem of global manipulation planning under partial observability.

In this chapter we present exploratory work. We will demonstrate that pure model-free reinforcement learning can be successfully applied to in-hand manipulation tasks in simulation. It was important to us to find a task on which pure reinforcement learning can generate satisfactory policies to ensure that RL is capable of solving the manipulation planning problem and to serve as a baseline for later comparison.

We will then elaborate on the intuition behind introducing analytic grasp modeling theory and propose a method that uses rich tactile feedback as well as such analytical hand models to modify RL actions such that grasp stability is maintained at all times. Work in this direction is ongoing, with no results to report at the time of this writing, but numerous experiments currently being undertaken. Finally, we will discuss some of the many open questions that remain.

7.2 In-hand manipulation with pure reinforcement learning

7.2.1 Experimental design

Let us first describe the experimental setup we chose in order to investigate robotic in-hand manipulation. We created a hand model in the MuJoCo physics simulator [106], which provides

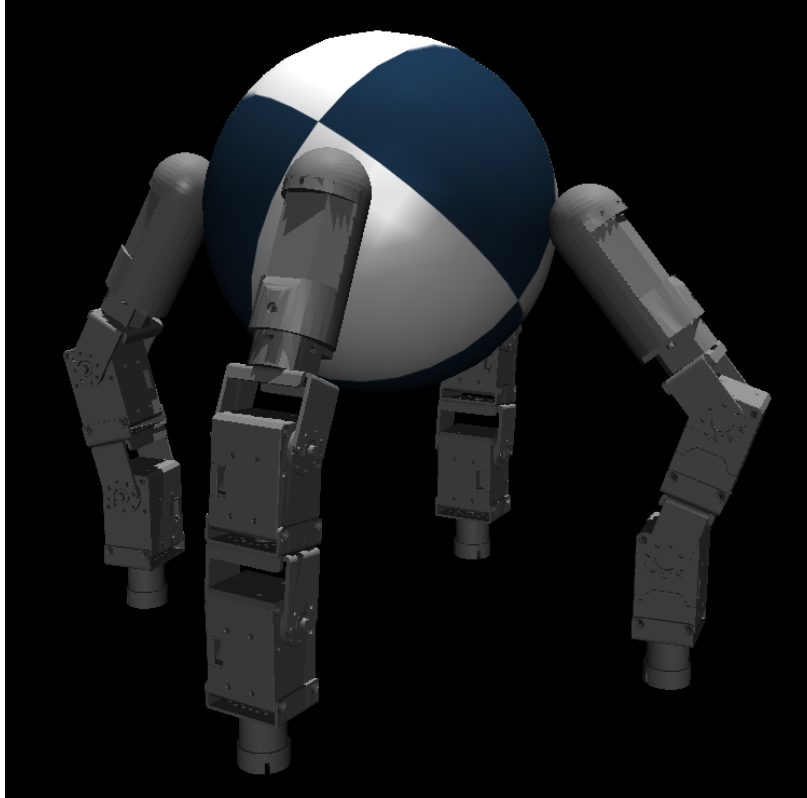


Figure 7.1: Simulation of the four fingered hand and spherical object in MuJoCo.

us both with a fast simulation of the grasp dynamics as well as a method of determining contact positions and forces. The hand we constructed has four identical fingers and 12 independent fully actuated degrees of freedom (see Fig. 7.1.) As we are currently also constructing a physical version of this hand we chose the physical parameters such as the finger skin stiffness and actuator gains to correspond to those of the physical hand design.

We chose to place a series elastic coupling between each joint and corresponding actuator as series elastic couplings of known stiffness along with encoders on both ends of the coupling provide a simple method of torque measurement. This also provides us with multiple choices with regards to the low-level control scheme of the hand. What we mean by this is choosing if the setpoint provided to the actuator controller is in terms of joint torques or joint positions for instance. While series elastic actuators with torque sensing capabilities would allow for the implementation of torque control or even more complex variants of impedance control there are convincing reasons to use position control instead.

Consider a grasp in equilibrium using a torque controlled hand. Any change to the actuator setpoint will disturb the equilibrium and lead to growing accelerations and thus an unstable grasp [14]. In control theoretic terms such a grasp is not in stable equilibrium as a small disturbance will cause the system to accelerate away from equilibrium. In contrast, a position controlled hand with compliant actuators allows for grasps that are in stable equilibrium: A small change in setpoint likely results in the system moving to a new equilibrium. We therefore chose position controlled actuators such that we can achieve grasps that are in stable equilibrium.

For the sake of simplicity we chose a spherical object of mass 0.1kg for these initial experiments. The local geometry of a sphere is uniform across its surface and thus we hope to mitigate some effects of partial observability. Using the Proximal Policy Optimization [79] algorithm we trained policies using as a reward the instantaneous rotational velocity of the sphere around the global vertical axis. We use a neural network with 4 hidden layers of 512 nodes each to encode the policy.

The observation consists of the joint positions, actuator setpoints, contact positions and contact normal forces. At every time step we sample an action from the policy $\mathbf{a} \in \mathbb{R}^{12}$ from which we calculate the actuator setpoint change $\Delta\mathbf{q} \in \mathbb{R}^{12}$. In order to limit the velocity of hand joints we define vector \mathbf{q}^{max} , which contains the maximum permissible setpoint change magnitude for each joint. A value of 0.05 radians appeared to work well with a policy frequency of 20Hz.

$$\Delta q_j = \max(-1, \min(1, a_j)) \cdot q_j^{max}, \quad \text{for all actuators } j \quad (7.1)$$

7.2.2 Results

We were able to successfully train policies to manipulate the sphere as desired. The emergent behaviors are periodic and can therefore be likened to a gait. This was expected as the reward function chosen encourages continued motion of the grasped object. More specifically, we see the hand pinching the sphere between two neighboring fingers and passing on to the next set of neighboring fingers in order to rotate it (see Figs. 7.3 & 7.4.) We show the training curve of such

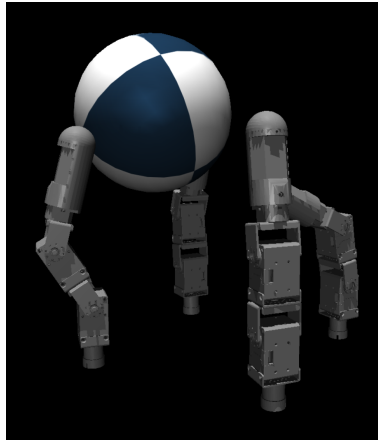


Figure 7.2: Training curve for a successful in-hand manipulation task. Shown on the horizontal axis is the number of policy updates. Each update consists of 96 episodes of 64 steps each.

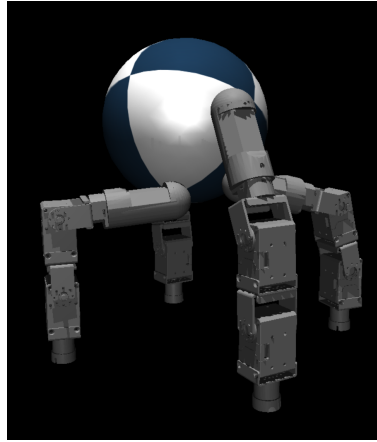
a successful experiment in Fig. 7.2. It is clear that the gait produced by the policy requires large movements of the sphere in the horizontal plane in order to achieve rotation around the vertical axis.

We found that the randomization of initial states during training is of profound importance. A good randomization that provides a distribution of stable grasps that is as varied as possible allows for training with shorter episode lengths, which in turn greatly improves sample complexity. This is not a surprising finding. The intuition behind this is that without initial state randomization the episode length would have to be at least as long as the period of the emergent behavior we are trying to synthesize in order to be able to learn a full period of the behavior. As we are trying to learn a continuous rotation task we are expecting the policy to learn to gait the fingers in such a periodic fashion. Initial state randomization means that the policy can learn smaller sections of this gait in shorter episodes.

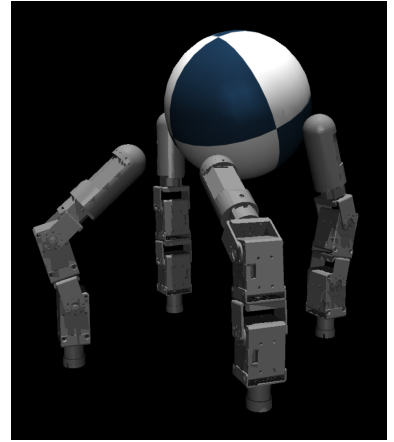
Furthermore, it appears that adding gravity in the simulation makes the task much more difficult. Much more effort had to be spent tuning hyperparameters in order to obtain behaviors that resemble periodic gaits. Different objects also appear to provide the task much difficulty. While learning policies to manipulate a cylinder aligned with the vertical axis was relatively successful, we could not train policies for more complex objects such as cubes.



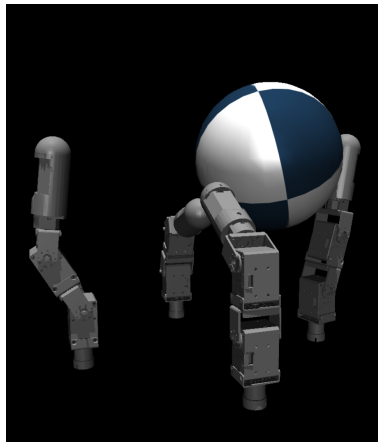
(a)



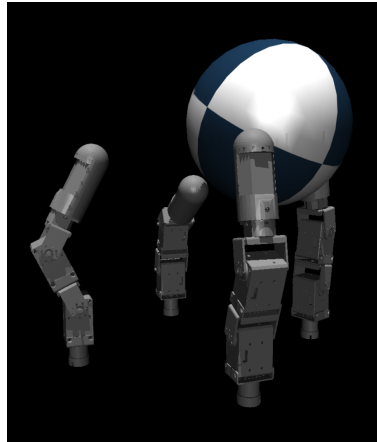
(b)



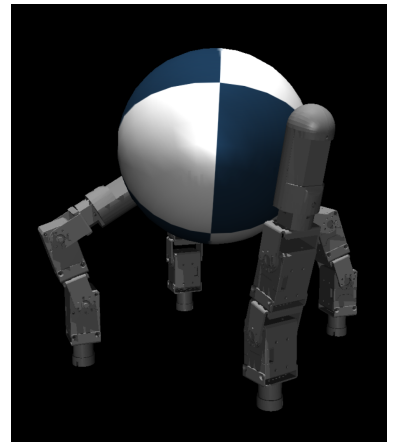
(c)



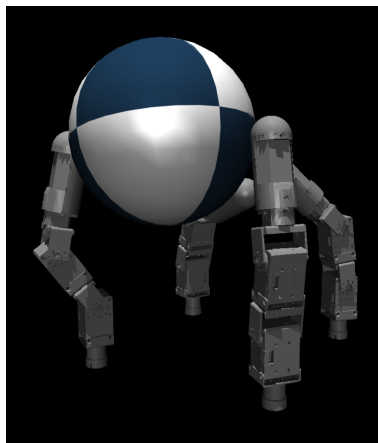
(d)



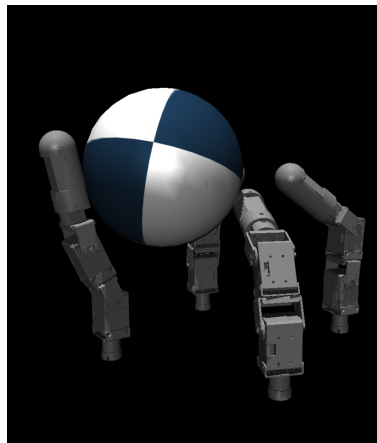
(e)



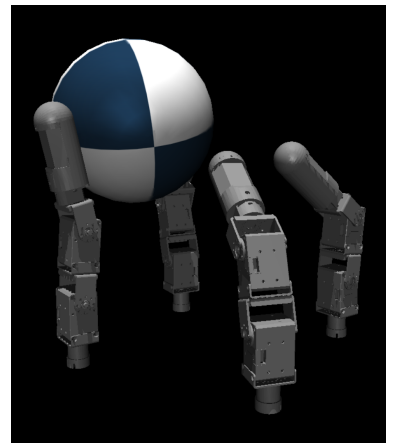
(f)



(g)



(h)



(i)

Figure 7.3: One complete period of the manipulation gait learned with pure reinforcement learning as seen from the side.

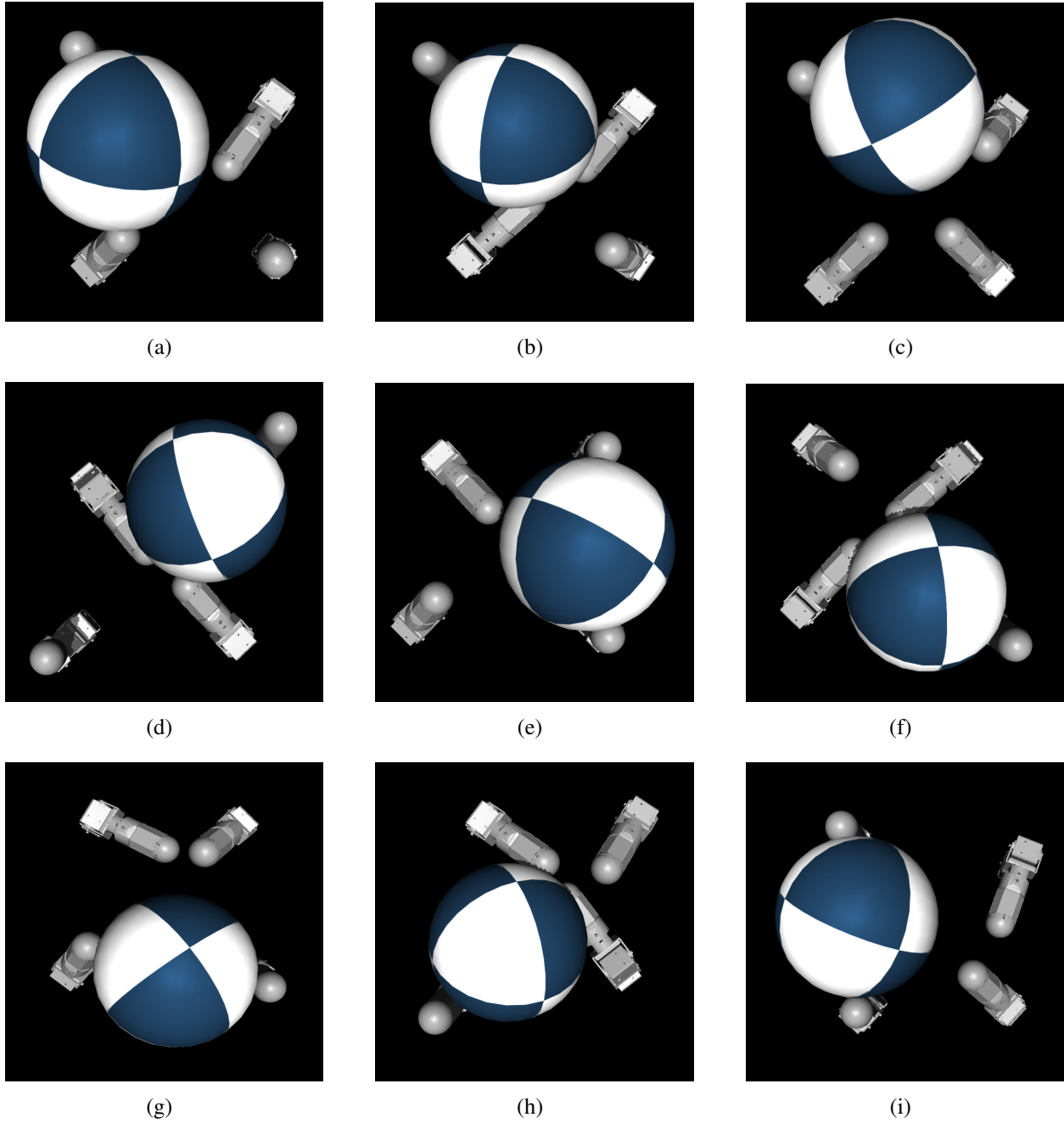


Figure 7.4: One complete period of the manipulation gait learned with pure reinforcement learning as seen from the top.

Being able to train adept policies for an in-hand manipulation task was an important stepping stone for us. Perhaps unsurprisingly, the above results show that reinforcement learning can be effectively leveraged to tackle the difficulties due to fact that the in-hand manipulation task is only partially observable. Fig. 7.2 however illustrates the sample complexity of such an approach.

While learning is fast at the beginning, it took over 2500 updates until learning appeared to plateau. These 2,500 updates correspond to 240,000 episodes, 15,360,000 steps or approximately 9 simulation days of experience. This process took approximately 9 hours of wall time on a commercial 11th generation server.

Note that the problem of rotating a sphere around a single axis is expected to be much simpler than the task of moving general objects in arbitrary directions. If it is possible to train policies to solve more general tasks using reinforcement learning alone the number of samples required is expected to be vastly greater than those we report above. Furthermore, while training times on this scale are acceptable in simulation, they are prohibitively large for training on real hardware. We believe that analytical grasp models can help us improve sample complexity or even allow us to learn policies for tasks for which pure reinforcement learning is insufficient. In the following we will illustrate the intuition behind this using a simplified problem.

7.3 Islands and Bridges: An equivalent problem?

Our central insight is that a defining characteristic of the state space of manipulation problems is that only a small subset of it corresponds to stable grasps. Defining the state space to consist of the object pose as well as the joint angles of the hand then a majority of the space does not correspond to grasps with valid contacts, much less a stable grasp. In fact, if the robotic hand and object are rigid, then the contact conditions define a lower-dimensional manifold in the full-dimensional state space [107].

A stochastic reinforcement learning algorithm operating in this space would not be able to successfully traverse this manifold as stepping of it is virtually guaranteed. In practice, of course, grasps are not perfectly rigid. Series elastic actuators as well as soft contact interfaces are a popular choice for exactly this reason: to provide some 'width' such that the lower-dimensional manifold defined by the contact conditions turns into a full-dimensional volume. A policy that changes the position setpoint of an actuator connected to its joint through a series elastic coupling has a greater chance of maintaining a valid contact state.

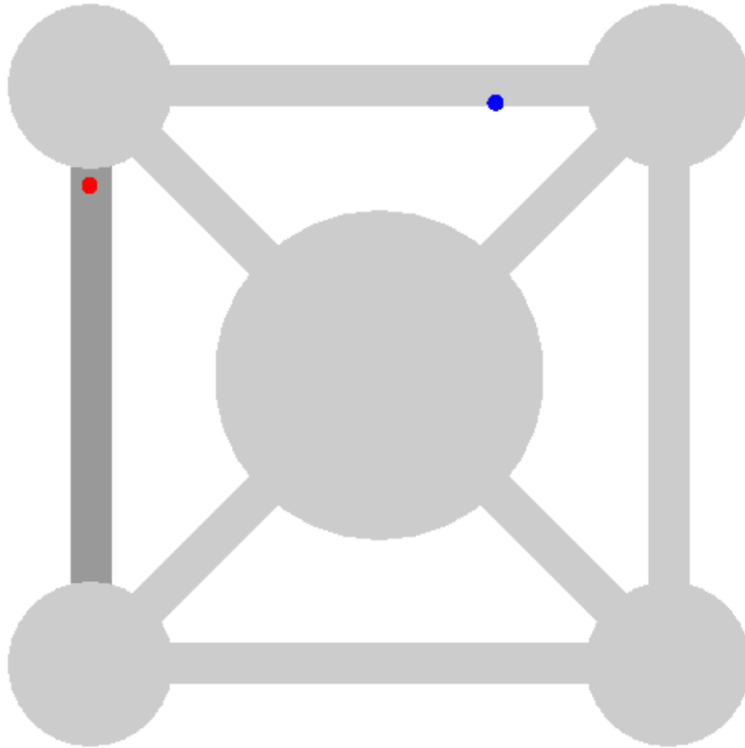


Figure 7.5: Illustration of the 'Islands and Bridges' problem. The red and blue dots corresponds to the current state and goal state respectively.

The fact remains, however, that the vast majority of the state space does not correspond to valid grasps and that the regions of stability are seldom far removed (in state space) from an unstable configuration. We like to think of such a region of stability as an 'island'. In order to continuously reorient a grasped object contacts must necessarily break to reestablish contact somewhere else [73]. When a contact is broken a grasp tends to become less stable — that is until a new contact is established somewhere else. We think of this process as crossing a 'bridge' — a region closer to instability that takes us to another, more stable region. An island can thus also be thought of as corresponding to one grasp geometry. When gaiting a finger we cross a 'bridge' to another grasp geometry.

We therefore believe that there are parallels between the in-hand manipulation problem and this problem which we call 'Islands and Bridges' (see Fig. 7.5.) For reasons of visualization we limit the problem to two dimensions such that the current state is denoted as a cartesian position

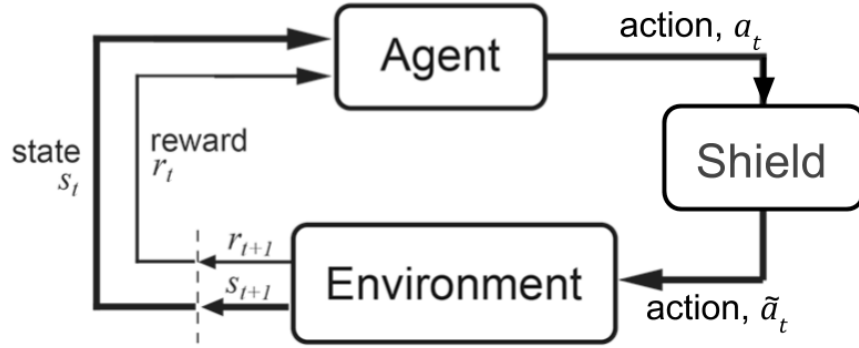


Figure 7.6: Shield RL

coordinate in this environment made up of distinct islands and bridges connecting them. Any state that lies on such an island or bridge corresponds to a stable grasp. A path from one point in this environment to another hence corresponds to an in-hand manipulation of the grasped object. Thus, the task of in-hand manipulation from one grasp state to another corresponds to finding such a path.

Fig. 7.5 also illustrates the difficulty of solving such a task with reinforcement learning: Any step off the thin bridges results in a failure (i.e. dropping the object.) In order to perform in-hand manipulation the policy must learn to navigate state space without ever entering these unstable regions. Therefore, it is our intuition that if we can confine the policy to the subset of the space which is useful, the task becomes easier to learn. We use this simplified problem to investigate the efficacy of methods that constrain the agent to the useful subset of the state space. We call a method that modifies agent actions such that the given constraints are satisfied a *shield*.

Let us formalize the notion of a shield. The method of shielding RL [108] is shown in Fig. 7.6. All actions sampled from the policy (deterministic or stochastic) are subject to the shield and, if necessary, are modified by the shield to ensure 'safety'. Let us denote the shield function as Ψ .

$$\tilde{a}^t = \Psi(a^t, s^t) \quad (7.2)$$

where a_t is the action sampled by the RL agent and \tilde{a}_t is the safe action given out by the shield function. It is infeasible to consider the safety of an action over all future time steps, hence we

perform a single-step lookahead for determining the safety of an action. We declare an action a safe action if the resulting state satisfies a set of *shield constraints* and thus define shield constraint function ζ .

$$\zeta(s^{t+1}) = \begin{cases} 1, & \text{if constraints satisfied} \\ 0, & \text{otherwise} \end{cases} \quad (7.3)$$

Thus, we must be able to predict the state s^{t+1} given s^t and a^t . In the case of our 'Islands and Bridges' problem this is trivial. Defining the state as the cartesian position in the environment $s^t = [x, y]^T$ and the action as a step in this cartesian space $a^t = [\delta x, \delta y]^T$ we can compute the predicted state as follows:

$$s^{t+1} = s^t + a^t \quad (7.4)$$

We can also define a distance function M that is defined as the closest distance of the current state to the edge of the safe region.

$$\zeta(s^{t+1}) = \begin{cases} 1, & \text{if } M(s^{t+1}) \geq 0 \\ 0, & \text{otherwise} \end{cases} \quad (7.5)$$

We can now define the shield function Ψ for the islands-and-bridges problem. A simple implementation would be to simply ignore any action if it results in a state outside of the safe region.

$$\tilde{a}^t = \Psi_{simple}(a^t, s^t) = \begin{cases} a^t, & \text{if } M(s^{t+1}) \geq 0 \\ [0, 0]^T, & \text{otherwise} \end{cases} \quad (7.6)$$

An issue with this formulation is that it does not work with deterministic policies. Simply ignoring an action and remaining in the same state means that the same action will be sampled again and rejected again for all future times. Thus, a more sophisticated shield might be to find the action that results in a state that satisfies ζ while maintaining the smallest deviation from the originally sampled action.

$$\tilde{a}^t = \Psi_{smart}(a^t, s^t) = \arg \min_{M(s^{t+1}) \geq 0} \|\tilde{a}^t - a^t\| \quad (7.7)$$

We implemented both of these shields and applied them to the task of navigating in the islands-and-bridges environment. Specifically, the task consists of navigating from a randomly sampled initial position to a randomly sampled goal position. We define two rewards r : A dense and a sparse reward that only rewards the agent if it is within a distance ϵ from the goal.

$$r_{dense}^t = -\|s^t - s_{goal}^t\| \quad (7.8)$$

$$r_{sparse}^t = \begin{cases} 1, & \text{if } \|s^t - s_{goal}^t\| \leq \epsilon \\ 0, & \text{otherwise} \end{cases} \quad (7.9)$$

If the agent steps outside of the safe region (failure) or reaches the goal region of radius ϵ (success) the episode is over and no more reward may be collected. We used PPO to train a stochastic policy without a shield, with the simple shield and with the smart shield as described above. After training the shield remains in place. We show the success rates for all three cases and both rewards throughout the training process in Fig. 7.7.

From these success rates it is evident that the shield provides large advantages during training of the PPO agent. While a sparse reward results in higher success rates for the unshielded case, it is still no match for the success rates achieved using either the simple or smart shields. It is also evident that the simple and smart shields perform similarly. However, only the smart shield allows for policies to be trained that guarantee success. Perhaps surprisingly it appears relatively large

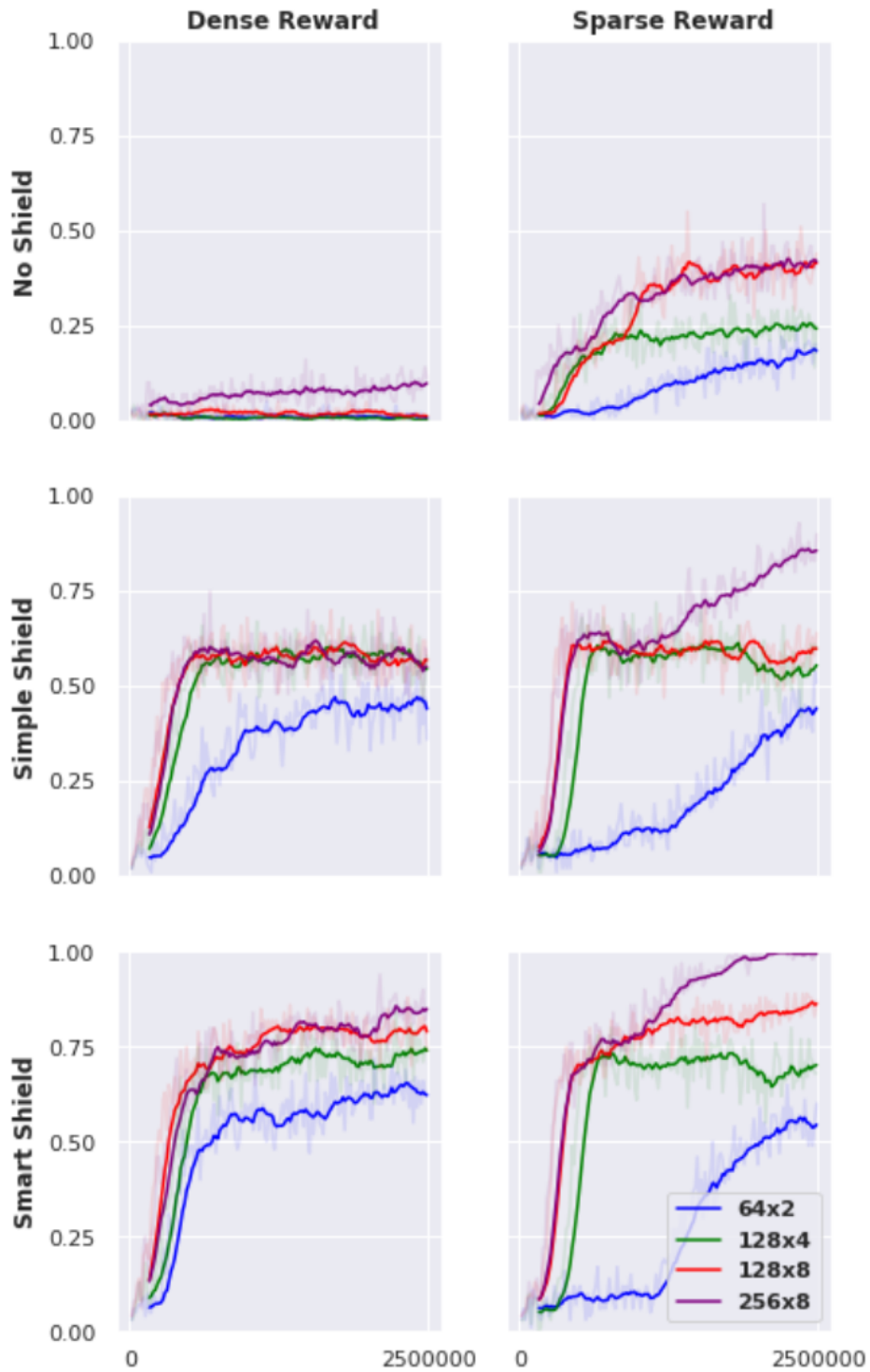


Figure 7.7: Success rates of the PPO agent reaching the goal state in the islands and bridges problem for different shield and reward functions. We also experimented with the size of the policy and value networks (we used separate networks of equal size.)

networks are also needed in order to guarantee success even for such a small environment.

These findings suggest that a shield can be a great advantage in learning tasks with RL that exhibit characteristics like the islands-and-bridges environment. As we described above we believe that the task of in-hand manipulation is such a task and therefore a shield can also be of great use there.

7.4 Constructing a shield for in-hand manipulation

We now describe a method to construct a shield similar in spirit to those described above for the in-hand manipulation problem described in Chapter 7.2.1. We will make use of theoretical grasp analysis in order to derive constraints for the shield to enforce as well as the necessary means to predict future states. To this end we define the state to consist of the pose of the object \mathbf{u} , the joint actuator setpoints \mathbf{q} as well as the contact forces \mathbf{c} .

7.4.1 Grasp stability constraints

As we are concerned with maintaining a stable grasp at all times we chose a set of grasp stability constraints as safety criteria to be enforced by the shield. Specifically, we are concerned with maintaining sufficiently many contacts for force-closure and preventing the contacts from slipping. Thus, we want to ensure that the contact forces at a subset of contacts sufficient for force closure remain within their respective friction cones.

For every such contact i the following describe the constraints that ensure the contact does not break or slip. Subscripts n and t refer to normal and tangential components respectively.

$$c_{i,n} \geq 0 \tag{7.10}$$

$$\|\mathbf{c}_{i,t}\| \leq \mu t_{i,normal} \tag{7.11}$$

Furthermore, we may also want to prevent the object from moving into positions from which

it may be hard to make progress. Therefore we also confine the object pose as part of the shield. We can enforce arbitrary convex constraints on the object pose. For instance, we may confine the objects translational degrees of freedom to a box:

$$x_{min} \leq u_x \leq x_{max} \quad (7.12)$$

$$y_{min} \leq u_y \leq y_{max} \quad (7.13)$$

$$z_{min} \leq u_z \leq z_{max} \quad (7.14)$$

Rotational degrees of freedom are a somewhat more complex. We chose to constrain the orientation of body axes in a global frame. Specifically, we constrain the angle subtended between the projection of the body z -axis \hat{z} into the global xz and yz cardinal planes (\hat{z}_x and \hat{z}_y respectively) and the global z -axis \hat{Z} (all unit vectors).

$$r_{x,min} \leq \text{sgn}((\hat{z}_y \times \hat{Z}) \cdot \hat{X}) \cdot \arccos(\hat{z}_y \cdot \hat{Z}) \leq r_{x,max} \quad (7.15)$$

$$r_{y,min} \leq \text{sgn}((\hat{z}_x \times \hat{Z}) \cdot \hat{Y}) \cdot \arccos(\hat{z}_x \cdot \hat{Z}) \leq r_{y,max} \quad (7.16)$$

In short, the *arccos* term gives us the angle between the two vectors while the *sgn* term tells us if the angle is in the negative or positive sense with respect to the right hand rule. This angle is again bounded to lie within a box.

Thus, given a state we can compute if it satisfies the above stability constraints or not.

7.4.2 Grasp model

Recall that the shield requires the ability to perform a 1-step lookahead. Thus, in order for the above stability constraints to be useful we must be able to predict future states from the current state-action pair. Ideally, we would be able to solve an optimization problem such as that in the

smart shield described above. We could then find optimal actions such that stability is guaranteed at the next step.

However, the agent can only control parameters such as joint positions or joint torques, which in turn affect contact forces and object pose through complex nonlinear relationships. Thus, exactly solving the optimization problem posed by the shield is difficult as there is no closed form analytic expression for the contact forces and object pose in terms of the agent action. We therefore approximate this relationship through linearization, which also allows for efficient computation of a global optimum.

We do this by making use of existing work by Cutkosky et al. [34] analyzing the compliance characteristics of robotic grasps as well as work by Bicchi [23] who studied the distribution of forces resulting from changes in position control setpoints.

Equilibrium: The Grasp Map Matrix $\mathbf{G} \in \mathbb{R}^{6 \times 3m}$ maps the contact forces at the m contacts to the corresponding wrench acting on the object and from (small) object motions to the corresponding contact motions. It therefore expresses object force/torque equilibrium and rigid body motion. The Hand Jacobian $\mathbf{J} \in \mathbb{R}^{3n \times q}$ similarly maps from contact forces to joint torques at the l joints and from (small) joint motions to corresponding contact motions. It expresses joint torque equilibrium and hand kinematics.

$$\mathbf{w} = -\mathbf{G}\mathbf{c} \quad (7.17)$$

$$\boldsymbol{\tau} = \mathbf{J}^T \mathbf{c} \quad (7.18)$$

$$\Delta \mathbf{d} = \mathbf{J} \Delta \mathbf{q} - \mathbf{G}^T \Delta \mathbf{u} \quad (7.19)$$

Calculating contact forces that arise in response to an applied wrench \mathbf{w} is complicated by the fact that, in general, \mathbf{G} will have fewer rows than columns. Therefore it has a nullspace and no unique inverse. This is known as static indeterminacy.

Grasp Stiffness: We do, however, know that if we apply a wrench \mathbf{w} to a grasped object there must

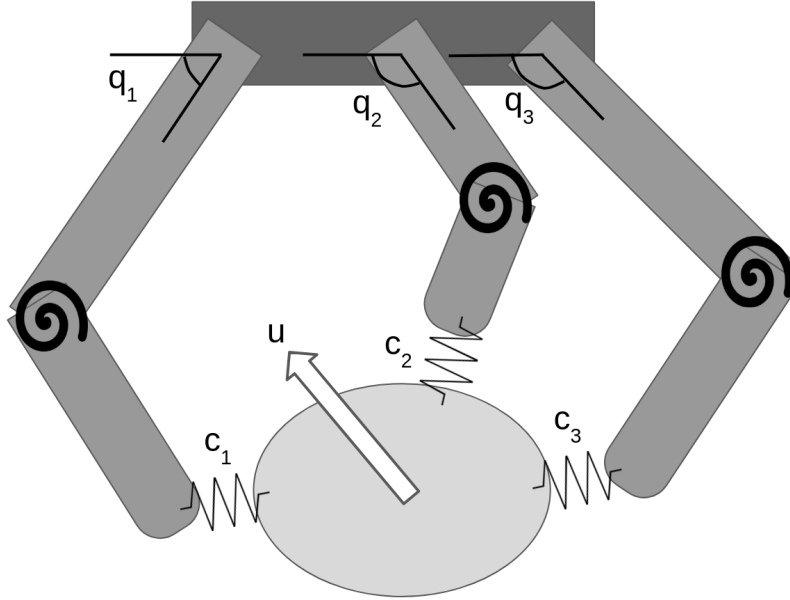


Figure 7.8: Illustration of a grasp with its main sources of compliance. Linear springs at the contacts denote compliance due to soft interfaces between the fingers and the object. Torsional springs denote the compliance due to series elastic actuation as well as the compliance of the low level controller of the actuator.)

arise a unique set of contact forces. Assuming perfectly rigid bodies the problem of computing these contact forces is ill posed but we can resolve the static indeterminacy by taking into account the *compliance* of the grasp. By doing so we are adding constitutive relations to resolve the static indeterminacy.

Using the work of Cutkosky et al. [34] we can derive the compliance in contact frame by constructing the mapping from a change in contact forces $\Delta \mathbf{c}$ to contact motions $\Delta \mathbf{d}$. The main sources of compliance are at the contacts (due to softness of the skin) and in the joints (due to the proportional term of the servo controller as well as any series elastic coupling. See Fig. 7.8.) Assuming linear compliances we can construct diagonal matrices $\mathbf{C}_{contacts} \in \mathbb{R}^{3m \times 3m}$ and $\mathbf{C}_{joints} \in \mathbb{R}^{l \times l}$ containing the compliances of contacts and joints respectively.

Starting from an initial equilibrium position we can now apply a change to the contact forces $\Delta \mathbf{c}$ and compute the resulting contact motion $\mathbf{d}_{contacts}$ due to contact compliance.

$$\Delta \mathbf{d}_{contacts} = \mathbf{C}_{contacts} \Delta \mathbf{c} \quad (7.20)$$

Computing the contact motion \mathbf{d}_{joints} due to joint compliance is only slightly more complex.

$$\Delta \mathbf{d}_{joints} = \mathbf{J} \mathbf{C}_{joints} \mathbf{J}^T \Delta \mathbf{c} \quad (7.21)$$

Due to the linearity of the compliance, overall contact motion is simply the sum of the two components.

$$\Delta \mathbf{d} = \Delta \mathbf{d}_{contacts} + \Delta \mathbf{d}_{joints} \quad (7.22)$$

$$= (\mathbf{C}_{contacts} + \mathbf{J} \mathbf{C}_{joints} \mathbf{J}^T) \Delta \mathbf{c} \quad (7.23)$$

From this we can determine the grasp stiffness — mapping from contact motion to the corresponding change in contact forces — by inverting the overall compliance matrix.

$$\Delta \mathbf{c} = (\mathbf{C}_{contacts} + \mathbf{J} \mathbf{C}_{joints} \mathbf{J}^T)^{-1} \Delta \mathbf{d} \quad (7.24)$$

$$= \mathbf{K} \Delta \mathbf{d} \quad (7.25)$$

Using equation (7.21) we can express the change in contact force as a function of object motion and joint setpoint change.

$$\Delta \mathbf{c} = \mathbf{K} (\mathbf{J} \Delta \mathbf{q} - \mathbf{G}^T \Delta \mathbf{u}) \quad (7.26)$$

Controllable Object Motions: As we only have direct control over the joint setpoint, Bicchi [23] was interested in predicting the motion of the object $\Delta \mathbf{u}$ that will arise when we change the actuator setpoint by $\Delta \mathbf{q}$. Assuming equilibrium and using (7.17) & (7.26)

$$\mathbf{G} \Delta \mathbf{c} = \mathbf{G} \mathbf{K} (\mathbf{J} \Delta \mathbf{q} - \mathbf{G} \Delta \mathbf{u}) = 0 \quad (7.27)$$

which implies

$$\mathbf{G} \mathbf{K} \mathbf{J} \Delta \mathbf{q} = \mathbf{G} \mathbf{K} \mathbf{G} \Delta \mathbf{u} \quad (7.28)$$

and hence

$$\Delta \mathbf{u} = (\mathbf{GKG})^{-1} \mathbf{GKJ} \Delta \mathbf{q} \quad (7.29)$$

$$= \mathbf{F} \Delta \mathbf{q} \quad (7.30)$$

Controllable Internal Forces: Armed with this we can predict the contact forces that will arise when we change the actuator setpoint by $\Delta \mathbf{q}$. Substituting (7.30) into (7.26) we get

$$\Delta \mathbf{c} = \mathbf{K}(\mathbf{J} \Delta \mathbf{q} - \mathbf{G}^T (\mathbf{GKG})^{-1} \mathbf{GKJ} \Delta \mathbf{q}) \quad (7.31)$$

$$= (\mathbf{I} - \mathbf{G}^T (\mathbf{GKG})^{-1} \mathbf{G}) \mathbf{KJ} \Delta \mathbf{q} \quad (7.32)$$

$$= \mathbf{E} \Delta \mathbf{q} \quad (7.33)$$

State prediction: All the relations described above are linearizations that describe the behavior of a grasp with respect to changes in actuator setpoints. Due to nonlinearities such as rolling contacts etc. these linearization are only accurate in a small region around the current state. They do, however allow us to make predictions of future states given a current state-action pair given that the action is sufficiently small. Recall that the components of the state we are interested in with respect to satisfying grasp stability constraints are the contact forces as well as the object pose. We now have the tools to express these parts of the state in terms of the action defined as setpoint changes of the position controlled actuators.

$$\begin{bmatrix} \mathbf{c} \\ \mathbf{u} \end{bmatrix}^{t+1} = \begin{bmatrix} \mathbf{c} \\ \mathbf{u} \end{bmatrix}^t + \begin{bmatrix} \mathbf{E} \\ \mathbf{F} \end{bmatrix}^t \Delta \mathbf{q}^t \quad (7.34)$$

7.4.3 Complete shield formulation

We can now put together the pieces and define the shield function Ψ in (7.2) as a constrained optimization: What action satisfies all shield constraints while minimizing the Cartesian distance from the original action.

$$\text{minimize : } \|\mathbf{a}^t - \tilde{\mathbf{a}}^t\| \quad (7.35)$$

$$\text{such that : (7.10) - (7.16)} \quad (7.36)$$

Of course, in order to allow gaiting we must allow contacts to break occasionally such that fingers can reestablish contact elsewhere. This is why the constraints (7.10) & (7.11) may only be applied to a subset of contacts — we must sometimes exempt a contact from the shield in order allow for contact relocation. We do this as follows:

1. Enumerate all combinations of contact states, where every contact is either shielded or not.
2. Discard all combinations with fewer than 2 shielded contacts as at least two contacts are required for stability.
3. For all remaining combinations check if the selection of shielded contacts by themselves are sufficient for *force closure* (are these contacts sufficient for stability.) Discard all combinations that fail this criterion. This can be done using simple force closure tests [21].
4. Perform the optimization (7.36) for every remaining combination. For all unshielded contacts remove the stability constraints (7.10) & (7.11) and add constraints $\tilde{a}_j = a_j$ for all joints j that make up the kinematic chain of an unshielded contact.
5. Select the result with the lowest value optimal objective. This solution gives us $\tilde{\mathbf{a}}$

Thus, we have computed a safe action $\tilde{\mathbf{a}}^t$ that applies the smallest correction to \mathbf{a}^t such that stability constraints are satisfied. This optimization formulation is an important distinction between

our work and the hierarchical control approach by Li et al. [82]. Their approach relies on a finite number of low level controllers from which the policy chooses, which constrains the possible behaviors to those determined by those controllers. In our case the policy retains all freedom to individually change actuator commands as long as the resulting grasp is stable. It is our intuition that while this may result in a more difficult task it ultimately allows for more dexterous behavior.

We also want to note that the method of enumerating contact state combinations in order to allow for finger gaiting bears similarities to the work by Prattichizzo et al. [38]. In fact it is their proposed *Potential Grasp Stability*, which has inspired us to combine the stability constraints described in Chapter 7.4.1 with such an enumerative approach.

7.5 Future work

Recall that the experimental design described in Chapter 7.2.1 provides us with information of contact position, contact forces, joint positions and joint torques. Thus, we can compute the grasp map matrix as well as the grasp Jacobian and perform an optimization over contact forces as described above. This is true for both the simulated hand as well as its physical counterpart, once it becomes available to us. Natural next steps for us to take include the application of the shield in simulation as well as attempting to transfer the policies trained and described in Chapter 7.2.2 to the real robotic hand we are constructing.

Assuming the islands-and-bridges concept is indeed an accurate representation of the in-hand manipulation task and the shield proves to be an effective tool, there are many further open questions that require investigation. So far we have only considered tasks in which the policy was trained on a single object and is tested on the same object. The concept of *generalization* is central to learning methods and in this case could be applied to a policy that can successfully manipulate previously unseen objects. Note that this could be another instance in which a shield as described above becomes advantageous as the shield is entirely agnostic to the object. A policy could learn general manipulation strategies while the shield provides the intricate feedback control necessary for stability.

We believe that policies can be trained on a variety of objects and thus learn a general structure of the underlying manipulation problem. Partial observability becomes an even larger challenge during such tasks and thus it may be advantageous to make use of LSTM architectures for policy and value networks. This may allow the meta-learning of general in-hand manipulation tasks as the experience collected is encoded in the internal state of the LSTM and can be used to adapt to the specific object.

Considering that the navigation in previously unknown environments bears similarities to maze navigation an interesting avenue of investigation might be the application of RL maze solving algorithms [109][110][111]. Furthermore, finger gaiting bears many similarities with regrasping for object reorientation. Manipulation for regrasping has been studied for decades (see for example [112][113][114][115]) and many different approaches such as regrasp maps [112] or graphs [116][115] have been proposed. These manipulation representations appear to be related to the notion of 'islands and bridges' described in Chapter 7.3 and we expect there to be many other parallels with different aspects of the manipulation theory that may provide valuable insights into the problem of in-hand manipulation.

Chapter 8: Conclusions

8.1 Contributions

In this dissertation we discuss the reasons for the relative obscurity of theoretical grasp analysis within the applied manipulation community. We argue that the most important reason is that none of the existing theoretical approaches capture the passive effects that are the fundamental characteristic of most hands commonly used in practice today. Particularly the effects of nonbackdrivable actuators have not been previously studied. This is despite the fact that this characteristic results in the notion of *passive stability*, which we argue has defined both the design of multi-fingered robotic hands as well as the ways we use them in practice.

We describe the limitations of the existing grasp theory, which prevent the analysis of passive effects as well as alternative approaches from the rigid body dynamics, contact modeling as well as physics simulations communities. We argue that none of these existing approaches allow for the efficient computation of grasp stability taking into account passive effects as they are either too computationally complex or approximate in nature. Thus, we set out to develop our own grasp models and algorithms in order to analyze the stability of grasps with passive effects.

Our first contribution is a grasp model for planar grasps that allows for the computation of contact forces given the *slip state* of the contacts. The state of a contact is defined as either rolling, breaking or sliding in one of two directions. We show that given a valid contact slip state combination stability can be determined by a linear program.

We then show that the number of contact state combinations possible under rigid body motion constraints is quadratic in the number of contacts and describe an algorithm that allows for the enumeration of all such combinations in polynomial time. Thus, we have developed the first algorithm that can determine planar grasp stability taking into account passive effects in polynomial

time. Using an example grasp we show that this method produces physically accurate results and demonstrate its computational efficiency.

Turning our attention to spacial grasps we continue our investigation by describing a system of equations, which we call the *exact problem*. It comprises of the equations defining static equilibrium of a grasp with passive effects due to nonbackdrivable joints and underactuation. As we show many of these governing equations can be cast as constraints in a Mixed Integer Program for which efficient solvers exist. Due to the Maximum Dissipation Principle (MDP) the Coulomb friction law is shown to be non-convex and that it cannot easily be reformulated using piecewise convex decompositions as was done in the planar case.

As we show, a consequence of omitting the MDP from our treatment of static grasp stability is that we introduce unphysical solutions (they violate the law of conservation of energy) that make determination of stability impossible. We thus propose a physically motivated iterative scheme that aims to mitigate the effects of omitting the MDP. Constraining the motion of the grasped object and minimizing at every step the resultant wrench acting on the object approximates the effects of the MDP and thus leads to physically plausible solutions.

This algorithm is the first to enable the stability analysis of spacial grasps with passive characteristics such as nonbackdrivable joints and underactuation. We demonstrate the application of our framework with various grasps using fully actuated as well as underactuated robotic hands. Verifying the predictions made by our algorithm with empirical data we illustrate its practical applicability as a tool both for grasp selection as well as actuator control.

Building on this work we investigate the use of piecewise convex relaxations of the MDP in order to accurately enforce it and obtain solutions to the *exact problem*. We discuss the potential application of existing convex relaxation techniques based on McCormick envelopes and describe an important limitation in that they require knowledge of upper and lower bounds on some variables. Our contribution here is a convex relaxation technique that makes use of the structure of the friction constraint in order to alleviate this limitation.

As our relaxation satisfies all the requirements for the application of tightening methods we

also contribute an algorithm that allows for the successive hierarchical refinement of the convex relaxation in order to obtain solutions converging to those of the *exact problem*. An important advantage of tightening methods such as ours is that it provides strong guarantees: Specifically, we are guaranteed convergence to the solution of the exact problem if one exists. Furthermore, if our algorithm does not find a solution we are guaranteed that none exists. Combined, these two features make our method efficient for problems both with and without exact solutions. It is, to the best of our knowledge, the first time that grasp stability models incorporating Coulomb friction (along with the maximum dissipation principle) have been solved with such high discretization resolution.

We furthermore propose a method of accounting for uncertainties in grasp geometry, specifically contact normals, in order to robustly guarantee stability up to a given magnitude of uncertainty. As this framework allows for multiple queries posed as optimization problems we demonstrate its application not only in the determination of passive stability but also as a tool for computing optimal actuator commands. We investigate the computational performance on a range of algorithmically generated grasps and show that our framework is computationally viable as a practical tool.

Implementations of the grasp models and algorithms presented in this dissertation are publicly available as part of the open source GraspIt! simulator [13].

Having developed tools that fill a gap in the grasp theory with respect to understanding and modeling the passive effects of robotic grasps we turn our attention to recent developments in the robotic manipulation community — specifically the advent of deep reinforcement learning and its application for in-hand manipulation. We argue that parts of the classical grasp modeling theory is indeed applicable to the types of robotic hands considered by practitioners in the learning community. As we believe there are synergistic benefits to be discovered at the interface of classical grasp analysis and reinforcement learning we contribute a method to constrain an RL agent such that it maintains a stable grasp at all times.

We draw parallels to established terms such as 'Safe RL' and 'Shield RL' and derive a shield

using a linearization based on traditional grasp analysis. While this work is highly exploratory we present preliminary results, which we believe to be promising and calling for further research.

8.2 Potential impact

The work pertaining to the analysis of passively stable grasps presented in this dissertation marks a clear theoretical advance. For the first time it is possible to determine the passive behavior of grasps with commonly used robotic hands such as the Barrett and Schunk hands. A potential practical application is in grasp planners, which compute the grasp to be executed by a robot.

Typically, these grasp planners compute a list of candidate grasps and rank them by a quality metric such as the Ferrari and Canny Grasp Wrench Space metric [21]. The grasp quality metrics commonly used by popular grasp planners are concerned with contact locations only and do not reason about contact forces. Thus, they cannot predict actual stability. There already exist grasp quality metrics that take into account hand kinematics and force generation capabilities, but as described in Chapter 3 they make assumptions that limit their applicability to most common robotic hands.

Our frameworks could fill this gap and provide grasp planners with the means to make accurate predictions of stability taking into account not only the hand kinematics but also actuator commands. Thus, our methods provide a further advantage in that they allow for the optimization of actuator commands. Where existing grasp planners only generate grasp geometries, our work can also compute the appropriate actuator commands for a given grasp and task.

We stress that while we have investigated the problem of grasp stability from our perspective as manipulation researchers the models and algorithms in this dissertation are applicable to a much wider class of problems. The stability of arrangements of rigid bodies in frictional contact, some fixed, some free, some constrained by other unilateral or bilateral constraints is an important aspect of many other problems from a variety of fields such as locomotion, robotic construction and the simulation of rigid body structures. We hope that our work may also be of use to researchers in these fields.

In the context of manipulation however, we note that interest in this kind of traditional analytic grasp analysis has decreased over the last decade or so. Modern grasp planning research tends to focus on the applications of machine learning and the popularity of simple two-fingered grippers as well as suction cups has diminished the need for complex quality metrics.

So perhaps there is more progress to be expected in the field of data-driven robotics. Recent results from the deep reinforcement learning community are promising a new breakthrough in truly dexterous multi-fingered manipulation. We hope that our perspective on these problems as analytical grasp stability analysis researchers can provide valuable insights and that our current work of integrating analytical grasp modeling with reinforcement learning will contribute to this progress.

8.3 Challenges

Throughout our work we have found that the accurate modeling of the Maximum Dissipation Principle is perhaps the most complex and difficult aspect of any passive stability formulation. It has thus provided us with many challenges in developing the methods in this dissertation.

While we show a convenient piecewise convex decomposition of the MDP in two dimensions, its treatment only remains of polynomial complexity under some fairly limiting assumptions. We are limited to a single mobile body in the grasp and can thus have to model the hand as a single rigid body; we cannot model the kinematic effects of multi-fingered robotic hands and joint actuation. Accurate treatment of the MDP is necessarily exponential in the number of bodies involved and while our algorithm can be extended to such multi-body problems it cannot retain its polynomial complexity.

For spacial contacts there is unfortunately no exact piecewise convex decomposition of the MDP. Our iterative approach to approximating the MDP — while physically motivated — unfortunately also loses many useful guarantees: It is not guaranteed to converge and if it does is not guaranteed to converge to a physically meaningful solution. As a result we report some outlier results, which are difficult to diagnose, particularly for complex grasps. Furthermore, experimen-

tal validation is difficult due to the difficulty of exactly recreating grasps on a real hand and the uncertainty in many of the physical parameters such as the torque provided by the actuators.

In order to alleviate some of these limitations we turned to convex relaxations of the MDP in order to solve the exact problem. The price we pay is an increased complexity in the grasp model and vastly larger optimization problems. While our algorithm often beats its theoretical worst-case exponential complexity the time taken to answer queries with more than 4 contacts is still significant. This is a major hurdle to the application of our algorithm in practice.

A further limitation is an arguably narrow definition of grasp stability. An initially unstable grasp may - through movement of the fingers and object and hence changes in the grasp geometry - eventually settle in a different stable equilibrium grasp. In such a case our framework can only determine that the initial grasp is unstable and makes no prediction on stability of the final grasp. In order to account for the motion of an initially unstable grasp we would have to model the dynamics of the grasp. Using the currently available dynamics engines to this end comes with its own difficulties.

Our secondary focus has been on the application of traditional grasp analysis to reinforcement learning of in-hand manipulation tasks. While results are preliminary and this work is still ongoing the amount of engineering that has to be performed in order to obtain convincing policies has been significant. This is expected to be even more pronounced once we complete building the physical hand with which we plan on putting our insights into practice. Furthermore, we foresee the discrepancies between the simulation and reality to be a major challenge.

8.4 Future work

We believe we have provided a solid foundation of theoretical work that, for the first time, enables the analysis of passive effects in grasping. There is, however, still room for improvement. An extension of the hyperplane approach to contact state enumeration for spacial grasps is already being investigated [93]. Another interesting and useful extension would be to allow for multiple bodies such that hand kinematics can be accounted for.

A more rigorous validation of our methods for stability determination in three dimensions would be of value, albeit difficult. However, perhaps there are other contact problems that exhibit similar characteristics that are more amenable to empirical validation.

While we believe we described a method to solve the *exact problem* there remain many avenues of investigation in order to improve computational performance. While we used Branch and Bound at every iteration of our tightening approach we did not retain any information of the solution tree between iterations. This means that many convex subproblems are being recomputed at every tightening. Using a solver that allows for warm starting the Branch and Bound process promises great performance gains. An alternative approach might be to cast our relaxation in a formulation that can be solved using existing spacial Branch and Bound algorithms, making the refinement part of the branch and bound process itself.

Ultimately, in this dissertation we have highlighted what we believe to be research topics holding influential results of great practical importance. We believe that there is yet much to be learned about passive reactions in grasping and how to effectively leverage these effects. If we want to move beyond the use of suction grippers for bin picking tasks and achieve robust manipulation with multi-fingered hands we have to develop appropriate tools to model and analyze them. We hope that this field of study sees renewed interest now that industries have evolved, which require large numbers of humans fulfilling menial tasks such as bin picking.

Furthermore, we believe there lies much promise in bringing approaches from the traditional grasping theory to the learning community. Our own endeavors to that end will continue as we plan on continuing along the path outlined in this dissertation. The increasing sensitivity of tactile sensors along with their decrease in price will hopefully drive more practitioners to consider the grasping theory that allows them to analyze the data. To this end we hope the community will continue the development of a new generation of robotic hands, which will provide practitioners with rich tactile and proprioceptive information and become a viable alternative to purely vision-based systems.

If we want to see robots becoming commonplace in human spaces we need to learn to endow

robots with the skills that come to us so naturally. A task as simple as picking an unknown object from a bin without vision is still an open problem in robotics. Perhaps it is unsurprising that the methods that currently appear the most promising and lead to the most human-like robotic behaviors — such as deep reinforcement learning — are those inspired by nature itself. And while roboticists are captivated by these new methods and robots make up more and more ground on their human counterparts we hope that researchers will not lose sight of the analytical models and algorithms.

References

- [1] C. Eppner, S. Höfer, R. Jonschkowski, R. Martín-Martín, A. Sieverling, V. Wall, and O. Brock, “Lessons from the amazon picking challenge: Four aspects of building robotic systems,” in *Proceedings of the Twenty-Sixth International Joint Conference on Artificial Intelligence, IJCAI-17*, 2017, pp. 4831–4835.
- [2] N. Correll, K. E. Bekris, D. Berenson, O. Brock, A. Causo, K. Hauser, K. Okada, A. Rodriguez, J. M. Romano, and P. R. Wurman, “Analysis and observations from the first amazon picking challenge,” *IEEE Transactions on Automation Science and Engineering*, vol. 15, no. 1, pp. 172–188, 2018.
- [3] D. Morrison, A. W. Tow, M. McTaggart, R. Smith, N. Kelly-Boxall, S. Wade-McCue, J. Erskine, R. Grinover, A. Gurman, T. Hunn, D. Lee, A. Milan, T. Pham, G. Rallos, A. Razjigaev, T. Rowntree, K. Vijay, Z. Zhuang, C. Lehnert, I. Reid, P. Corke, and J. Leitner, *Cartman: The low-cost cartesian manipulator that won the amazon robotics challenge*, 2018. arXiv: 1709.06283 [cs.RO].
- [4] E. Ackerman. (2020). “Covariant uses simple robot and gigantic neural net to automate warehouse picking.”
- [5] J. Mahler, J. Liang, S. Niyaz, M. Laskey, R. Doan, X. Liu, J. A. Ojea, and K. Goldberg, “Dex-net 2.0: Deep learning to plan robust grasps with synthetic point clouds and analytic grasp metrics,” 2017.
- [6] A. T. Miller, S. Knoop, H. I. Christensen, and P. K. Allen, “Automatic grasp planning using shape primitives,” in *2003 IEEE International Conference on Robotics and Automation (Cat. No.03CH37422)*, vol. 2, 2003, 1824–1829 vol.2.
- [7] C. Goldfeder, M. Ciocarlie, Hao Dang, and P. K. Allen, “The columbia grasp database,” in *2009 IEEE International Conference on Robotics and Automation*, 2009, pp. 1710–1716.
- [8] D. Berenson, R. Diankov, Koichi Nishiwaki, Satoshi Kagami, and J. Kuffner, “Grasp planning in complex scenes,” in *2007 7th IEEE-RAS International Conference on Humanoid Robots*, 2007, pp. 42–48.
- [9] J.-P. Saut and D. Sidobre, “Efficient models for grasp planning with a multi-fingered hand,” *Robotics and Autonomous Systems*, vol. 60, no. 3, pp. 347–357, 2012, Autonomous Grasping.

- [10] N. Vahrenkamp, E. Koch, M. Wächter, and T. Asfour, “Planning high-quality grasps using mean curvature object skeletons,” *IEEE Robotics and Automation Letters*, vol. 3, no. 2, pp. 911–918, 2018.
- [11] O. M. Andrychowicz, B. Baker, M. Chociej, R. Józefowicz, B. McGrew, J. Pachocki, A. Petron, M. Plappert, G. Powell, A. Ray, J. Schneider, S. Sidor, J. Tobin, P. Welinder, L. Weng, and W. Zaremba, “Learning dexterous in-hand manipulation,” *The International Journal of Robotics Research*, vol. 39, no. 1, pp. 3–20, 2020.
- [12] OpenAI, I. Akkaya, M. Andrychowicz, M. Chociej, M. Litwin, B. McGrew, A. Petron, A. Paino, M. Plappert, G. Powell, R. Ribas, J. Schneider, N. Tezak, J. Tworek, P. Welinder, L. Weng, Q. Yuan, W. Zaremba, and L. Zhang, *Solving rubik’s cube with a robot hand*, 2019. arXiv: 1910.07113 [cs.LG].
- [13] A. Miller and P. Allen, “GraspIt!: A versatile simulator for robotic grasping,” *IEEE Robotics and Automation Magazine*, vol. 11, no. 4, pp. 110–122, 2004.
- [14] F. Jen, M. Shoham, and R. W. Longman, “Liapunov stability of force-controlled grasps with a multi-fingered hand,” *The International Journal of Robotics Research*, vol. 15, no. 2, pp. 137–154, 1996.
- [15] A. Bicchi, “Hands for dexterous manipulation and robust grasping: A difficult road toward simplicity,” *IEEE Transactions on Robotics and Automation*, vol. 16, no. 6, pp. 652–662, 2000.
- [16] F. Reuleaux, *The Kinematics of Machinery*. Macmillan, 1876.
- [17] P. Somov, “Über Gebiete von Schraubengeschwindigkeiten eines starren Körpers bei verschiedener Zahl von Stützflächen,” *Zeitschrift für Mathematik und Physik*, vol. 45, pp. 245–306, 1900.
- [18] K. Lakshminarayana, “Mechanics of form closure,” *ASME Paper No. 78-DET-32*, 1978.
- [19] A. Bicchi and V. Kumar, “Robotic grasping and contact: A review,” in *IEEE International Conference on Robotics and Automation*, 2000, pp. 348–353.
- [20] J. Salisbury, “Kinematic and force analysis of articulated mechanical hands,” Ph.D. dissertation, Stanford University, 1982.
- [21] C. Ferrari and J. Canny, “Planning optimal grasps,” in *IEEE International Conference on Robotics and Automation*, 1992, pp. 2290–2295.
- [22] N. Boneschanscher, H. v. d. Drift, S. J. Buckley, and R. H. Taylor, “Subassembly stability,” in *Proceedings of the Seventh AAAI National Conference on Artificial Intelligence*, Saint Paul, Minnesota: AAAI Press, 1988, 780–785.

- [23] A. Bicchi, “On the problem of decomposing grasp and manipulation forces in multiple whole-limb manipulation,” *Robotics and Autonomous Systems*, vol. 13, no. 2, pp. 127–147, 1994.
- [24] C. Coulomb, *Théorie des machines simples, en ayant égard au frottement de leurs parties et à la roideur des cordages*. Mémoires de mathématique et de physique, présentés à l’Académie royale des sciences, 1781.
- [25] J. Salisbury and B. Roth, “Kinematic and force analysis of articulated mechanical hands,” *ASME Journal of Mechanisms, Transmissions, and Automation in Design*, vol. 105, pp. 35–41, 1983.
- [26] J. Kerr and B. Roth, “Analysis of multifingered hands,” *International Journal of Robotics Research*, vol. 4, no. 4, pp. 3–17, 1986.
- [27] Y. Nakamura, K. Nagai, and T. Yoshikawa, “Dynamics and stability in coordination of multiple robotic mechanisms,” *The International Journal of Robotics Research*, vol. 8, no. 2, pp. 44–61, 1989.
- [28] M. R. Cutkosky and P. K. Wright, “Friction, stability and the design of robotic fingers,” *The International Journal of Robotics Research*, vol. 5, no. 4, pp. 20–37, 1986.
- [29] M. Buss, H. Hashimoto, and J. Moore, “Dextrous hand grasping force optimization,” *IEEE Trans. on Robotics and Automation*, vol. 12, pp. 406–418, 1996.
- [30] L. Han, J. Trinkle, and Z. Li, “Grasp analysis as linear matrix inequality problems,” *IEEE Trans. on Robotics and Automation*, vol. 16, pp. 663–674, 2000.
- [31] S. P. Boyd and B. Wegbreit, “Fast computation of optimal contact forces,” *IEEE Transactions on Robotics*, vol. 23, no. 6, pp. 1117–1132, 2007.
- [32] V. Nguyen, “Constructing stable grasps in 3d,” in *Proceedings. 1987 IEEE International Conference on Robotics and Automation*, vol. 4, 1987, pp. 234–239.
- [33] H. Hanafusa and I. Asada, “Stable prehension by a robot hand with elastic fingers,” in *Proc. of the 7th ISIR, Tokyo*, 1977.
- [34] M. R. Cutkosky and I. Kao, “Computing and controlling the compliance of a robotic hand,” *IEEE Transactions on Robotics and Automation*, vol. 5, no. 2, 1989.
- [35] K. Salisbury, “Whole arm manipulation,” in *Robotics Research: The Fourth International Symposium*, R. C. Bolles and B. Roth, Eds., Santa Cruz, California, USA: MIT Press, 1988, pp. 183–189.

- [36] A. Bicchi, “Force distribution in multiple whole-limb manipulation,” in *Robotics and Automation, 1993. Proceedings., 1993 IEEE International Conference on*, IEEE, 1993, pp. 196–201.
- [37] ———, “On the closure properties of robotic grasping,” *The International Journal of Robotics Research*, vol. 14, no. 4, pp. 319–334, 1995.
- [38] D. Prattichizzo, J. K. Salisbury, and A. Bicchi, “Contact and grasp robustness measures: Analysis and experiments,” in *Experimental Robotics IV: The 4th International Symposium, Stanford, California, June 30 – July 2, 1995*. Berlin, Heidelberg: Springer Berlin Heidelberg, 1997, pp. 83–90.
- [39] J. C. Trinkle and D. C. Zeng, “Prediction of the quasistatic planar motion of a contacted rigid body,” *IEEE Transactions on Robotics and Automation*, vol. 11, no. 2, pp. 229–246, 1995.
- [40] J. J. Moreau, “On unilateral constraints, friction and plasticity,” in *New Variational Techniques in Mathematical Physics*, G. Capriz and G. Stampacchia, Eds. Berlin, Heidelberg: Springer Berlin Heidelberg, 2011, pp. 171–322, ISBN: 978-3-642-10960-7.
- [41] D. E. Stewart, “Rigid-body dynamics with friction and impact,” *SIAM Rev.*, vol. 42, no. 1, pp. 3–39, Mar. 2000.
- [42] R. Palmer, “Computational complexity of motion and stability of polygons,” Ph.D. dissertation, Cornell University, 1989.
- [43] R. Mattikalli, D. Baraff, and P. Khosla, “Finding all stable orientations of assemblies with friction,” *IEEE Transactions on Robotics and Automation*, vol. 12, no. 2, pp. 290–301, 1996.
- [44] M. Erdmann, “On a representation of friction in configuration space,” *The International Journal of Robotics Research*, vol. 13, no. 3, pp. 240–271, 1994.
- [45] R. C. Brost and M. T. Mason, “Graphical analysis of planar rigid-body dynamics with multiple frictional contacts,” in *ISRR*, Cambridge, Mass: MIT Press, 1989, pp. 293–300.
- [46] M. Mason, *Mechanics of Robotic Manipulation*. Cambridge, MA.: MIT Press, 2001.
- [47] J.-S. Pang, J. C. Trinkle, and G. Lo, “A complementarity approach to a quasistatic multi-rigid-body contact problem,” *Computational Optimization and Applications*, vol. 5, no. 2, pp. 139–154, 1996.
- [48] J. C. Trinkle, S. Berard, and J. S. Pang, “A time-stepping scheme for quasistatic multibody systems,” in *(ISATP 2005). The 6th IEEE International Symposium on Assembly and Task Planning: From Nano to Macro Assembly and Manufacturing, 2005.*, 2005, pp. 174–181.

- [49] J. C. Trinkle, J.-S. Pang, S. Sudarsky, and G. Lo, “On dynamic multi-rigid-body contact problems with coulomb friction,” *ZAMM - Journal of Applied Mathematics and Mechanics / Zeitschrift für Angewandte Mathematik und Mechanik*, vol. 77, no. 4, pp. 267–279, 1997.
- [50] D. E. Stewart and J. C. Trinkle, “An implicit time-stepping scheme for rigid body dynamics with inelastic collisions and coulomb friction,” *International Journal for Numerical Methods in Engineering*, vol. 39, no. 15, pp. 2673–2691, 1996.
- [51] M. Anitescu and F. A. Potra, “Formulating dynamic multi-rigid-body contact problems with friction as solvable linear complementarity problems,” *Nonlinear Dynamics*, vol. 14, no. 3, pp. 231–247, 1997.
- [52] J.-S. Pang and J. Trinkle, “Stability characterizations of rigid body contact problems with coulomb friction,” *ZAMM - Journal of Applied Mathematics and Mechanics / Zeitschrift für Angewandte Mathematik und Mechanik*, vol. 80, no. 10, 2000.
- [53] P. Song, J.-S. Pang, and V. Kumar, “A semi-implicit time-stepping model for frictional compliant contact problems,” *International Journal for Numerical Methods in Engineering*, vol. 60, no. 13, pp. 2231–2261, 2004.
- [54] M. Anitescu and G. D. Hart, “Solving nonconvex problems of multibody dynamics with joints, contact, and small friction by successive convex relaxation,” *Mechanics Based Design of Structures and Machines*, vol. 31, no. 3, pp. 335–356, 2003.
- [55] A. Tasora and M. Anitescu, “A matrix-free cone complementarity approach for solving large-scale, nonsmooth, rigid body dynamics,” *Computer Methods in Applied Mechanics and Engineering*, vol. 200, no. 5, pp. 439–453, 2011.
- [56] M. Anitescu and A. Tasora, “An iterative approach for cone complementarity problems for nonsmooth dynamics,” *Computational Optimization and Applications*, vol. 47, no. 2, pp. 207–235, 2010.
- [57] P. C. Horak and J. C. Trinkle, “On the similarities and differences among contact models in robot simulation,” *IEEE Robotics and Automation Letters*, vol. 4, no. 2, pp. 493–499, 2019.
- [58] D. M. Kaufman, S. Sueda, D. L. James, and D. K. Pai, “Staggered projections for frictional contact in multibody systems,” *ACM Transactions on Graphics (SIGGRAPH Asia 2008)*, vol. 27, no. 5, 164:1–164:11, 2008.
- [59] K. G. Murty and S. N. Kabadi, “Some np-complete problems in quadratic and nonlinear programming,” *Mathematical Programming*, vol. 39, no. 2, pp. 117–129, 1987.
- [60] E. Todorov, “Implicit nonlinear complementarity: A new approach to contact dynamics,” in *2010 IEEE International Conference on Robotics and Automation*, 2010, pp. 2322–2329.

- [61] ———, “Convex and analytically-invertible dynamics with contacts and constraints: Theory and implementation in mujoco,” in *2014 IEEE International Conference on Robotics and Automation (ICRA)*, 2014, pp. 6054–6061.
- [62] E. Drumwright and D. A. Shell, “Modeling contact friction and joint friction in dynamic robotic simulation using the principle of maximum dissipation,” in *Algorithmic Foundations of Robotics IX: Selected Contributions of the Ninth International Workshop on the Algorithmic Foundations of Robotics*, D. Hsu, V. Isler, J.-C. Latombe, and M. C. Lin, Eds. Berlin, Heidelberg: Springer Berlin Heidelberg, 2011, pp. 249–266.
- [63] T. Pang and R. Tedrake, “A robust time-stepping scheme for quasistatic rigid multibody systems,” *2018 IEEE/RSJ International Conference on Intelligent Robots and Systems (IROS)*, pp. 5640–5647, 2018.
- [64] J.-S. Pang and J. C. Trinkle, “Complementarity formulations and existence of solutions of dynamic multi-rigid-body contact problems with coulomb friction,” *Mathematical Programming*, vol. 73, no. 2, pp. 199–226, 1996.
- [65] K. Murty, *Linear Complementarity, Linear and Nonlinear Programming*, ser. Sigma series in applied mathematics. Heldermann, 1988, ISBN: 9783885384038.
- [66] M. Erdmann, “An exploration of nonprehensile two-palm manipulation,” *The International Journal of Robotics Research*, vol. 17, no. 5, pp. 485–503, 1998.
- [67] L. Han and J. C. Trinkle, “Dextrous manipulation by rolling and finger gaiting,” in *Proceedings. 1998 IEEE International Conference on Robotics and Automation (Cat. No.98CH36146)*, vol. 1, 1998, 730–735 vol.1.
- [68] Z. Doulergi and L. Droukas, “On rolling contact motion by robotic fingers via prescribed performance control,” in *2013 IEEE International Conference on Robotics and Automation*, 2013, pp. 3976–3981.
- [69] A. Bicchi and R. Sorrentino, “Dexterous manipulation through rolling,” in *Proceedings of 1995 IEEE International Conference on Robotics and Automation*, vol. 1, 1995, 452–457 vol.1.
- [70] M. Cherif and K. K. Gupta, “Planning quasi-static fingertip manipulations for reconfiguring objects,” *IEEE Transactions on Robotics and Automation*, vol. 15, no. 5, pp. 837–848, 1999.
- [71] K. Hertkorn, M. A. Roa, and C. Borst, “Planning in-hand object manipulation with multifingered hands considering task constraints,” in *2013 IEEE International Conference on Robotics and Automation*, 2013, pp. 617–624.

- [72] Y. Bai and C. Liu, “Dexterous manipulation using both palm and fingers,” May 2014, pp. 1560–1565.
- [73] I. Mordatch, Z. Popović, and E. Todorov, “Contact-invariant optimization for hand manipulation,” in *Proceedings of the ACM SIGGRAPH/Eurographics Symposium on Computer Animation*, ser. SCA ’12, Lausanne, Switzerland: Eurographics Association, 2012, 137–144, ISBN: 9783905674378.
- [74] L. U. Odhner and A. M. Dollar, “Stable, open-loop precision manipulation with underactuated hands,” *The International Journal of Robotics Research*, vol. 34, no. 11, pp. 1347–1360, 2015.
- [75] B. Calli and A. M. Dollar, “Robust precision manipulation with simple process models using visual servoing techniques with disturbance rejection,” *IEEE Transactions on Automation Science and Engineering*, vol. 16, no. 1, pp. 406–419, 2019.
- [76] N. Chavan-Dafle and A. Rodriguez, “Sampling-based planning of in-hand manipulation with external pushes,” in *Robotics Research*, N. M. Amato, G. Hager, S. Thomas, and M. Torres-Torriti, Eds., Springer International Publishing, 2020, pp. 523–539.
- [77] Y. Hou, Z. Jia, and M. T. Mason, “Manipulation with shared grasping,” in *Robotics: Science and Systems (RSS)*, 2020.
- [78] H. van Hoof, T. Hermans, G. Neumann, and J. Peters, “Learning robot in-hand manipulation with tactile features,” in *2015 IEEE-RAS 15th International Conference on Humanoid Robots (Humanoids)*, 2015, pp. 121–127.
- [79] J. Schulman, F. Wolski, P. Dhariwal, A. Radford, and O. Klimov, *Proximal policy optimization algorithms*, 2017. arXiv: 1707.06347 [cs.LG].
- [80] H. Zhu, A. Gupta, A. Rajeswaran, S. Levine, and V. Kumar, *Dexterous manipulation with deep reinforcement learning: Efficient, general, and low-cost*, 2018. arXiv: 1810.06045 [cs.AI].
- [81] A. Rajeswaran, V. Kumar, A. Gupta, G. Vezzani, J. Schulman, E. Todorov, and S. Levine, “Learning complex dexterous manipulation with deep reinforcement learning and demonstrations,” in *Proceedings of Robotics: Science and Systems*, Pittsburgh, Pennsylvania, 2018.
- [82] T. Li, K. Srinivasan, M. Q.-H. Meng, W. Yuan, and J. Bohg, “Learning hierarchical control for robust in-hand manipulation,” *2020 IEEE International Conference on Robotics and Automation (ICRA)*, pp. 8855–8862, 2020.
- [83] J. García, Fern, and o Fernández, “A comprehensive survey on safe reinforcement learning,” *Journal of Machine Learning Research*, vol. 16, no. 42, pp. 1437–1480, 2015.

- [84] G. Dalal, K. Dvijotham, M. Vecerik, T. Hester, C. Paduraru, and Y. Tassa, *Safe exploration in continuous action spaces*, 2018. arXiv: 1801.08757 [cs.AI].
- [85] B. Amos and J. Z. Kolter, “Optnet: Differentiable optimization as a layer in neural networks,” in *Proceedings of the 34th International Conference on Machine Learning - Volume 70*, ser. ICML’17, Sydney, NSW, Australia: JMLR.org, 2017, 136–145.
- [86] V. Nguyen, “Constructing force-closure grasps,” *International Journal of Robotics Research*, vol. 8, no. 3, pp. 3–16, 1988.
- [87] S. Ovchinnikov, “Hyperplane arrangements,” in *Graphs and Cubes*. New York, NY: Springer New York, 2011, pp. 207–235, ISBN: 978-1-4614-0797-3.
- [88] A. M. Gleason, L. M. Kelly, and R. E. Greenwood, “Solutions: The twenty-fifth competition,” *The William Lowell Putnam mathematical competition : problems and solutions :1938-1964*, 1980.
- [89] K. Fukuda, S. Saito, A. Tamura, and T. Tokuyama, “Bounding the number of k-faces in arrangements of hyperplanes,” *Discrete Applied Mathematics*, vol. 31, 1991.
- [90] D. Eppstein, “Recognizing partial cubes in quadratic time,” *Journal of Graph Algorithms and Applications*, vol. 15, no. 2, 2008.
- [91] K. Mehlhorn and D. Michail, “Implementing minimum cycle basis algorithms,” in *Experimental and Efficient Algorithms*, S. E. Nikolettseas, Ed., Springer Berlin Heidelberg, 2005, pp. 32–43.
- [92] H. Edelsbrunner, *Algorithms in Combinatorial Geometry*, 1st. Springer Publishing Company, Incorporated, 2012.
- [93] E. Huang, X.-Y. Cheng, and M. T. Mason, “Efficient contact mode enumeration in 3d,” 2020.
- [94] Gurobi Optimization, LLC, *Gurobi optimizer reference manual*, 2018.
- [95] L. Liberti, “Reformulation and convex relaxation techniques for global optimization,” *Quarterly Journal of the Belgian, French and Italian Operations Research Societies*, vol. 2, no. 3, pp. 255–258, 2004.
- [96] G. P. McCormick, “Computability of global solutions to factorable nonconvex programs: Part i — convex underestimating problems,” *Mathematical Programming*, vol. 10, no. 1, pp. 147–175, 1976.
- [97] H. Tuy, *Convex Analysis and Global Optimization*, 2nd. Springer Publishing Company, Incorporated, 2016, ISBN: 3319314823, 9783319314822.

- [98] C. Adjiman, S. Dallwig, C. Floudas, and A. Neumaier, “A global optimization method, *abb*, for general twice-differentiable constrained NLPs — I: Theoretical advances,” *Computers & Chemical Engineering*, vol. 22, no. 9, pp. 1137–1158, 1998.
- [99] M. Tawarmalani and N. V. Sahinidis, “A polyhedral branch-and-cut approach to global optimization,” *Mathematical Programming*, vol. 103, pp. 225–249, 2005.
- [100] A. Miller and H. Christensen, “Implementation of multi-rigid-body dynamics within a robotic grasping simulator,” in *IEEE Intl. Conference on Robotics and Automation*, 2003, pp. 2262–2268.
- [101] E. M. L. Beale and J. J. H. Forrest, “Global optimization using special ordered sets,” *Mathematical Programming*, vol. 10, no. 1, pp. 52–69, 1976.
- [102] C. Meeker, M. Haas-Heger, and M. Ciocarlie, “Computing an intuitive teleoperation mapping empirically and algorithmically,” *IEEE Transactions on Robotics*, 2019 (submitted).
- [103] T. Bretl and S. Lall, “Testing static equilibrium for legged robots,” *IEEE Transactions on Robotics*, vol. 24, no. 4, pp. 794–807, 2008.
- [104] B. Wu and B. Ghanem, “Lp-box admm: A versatile framework for integer programming,” *IEEE Transactions on Pattern Analysis and Machine Intelligence*, pp. 1–1, 2018.
- [105] P. Piacenza, K. Behrman, B. Schifferer, I. Kymissis, and M. Ciocarlie, “A sensorized multicurved robot finger with data-driven touch sensing via overlapping light signals,” *IEEE/ASME Transactions on Mechatronics*, vol. 25, no. 5, pp. 2416–2427, 2020.
- [106] E. Todorov, T. Erez, and Y. Tassa, “Mujoco: A physics engine for model-based control,” in *2012 IEEE/RSJ International Conference on Intelligent Robots and Systems*, 2012, pp. 5026–5033.
- [107] J. C. Trinkle, A. O. Farahat, and P. F. Stiller, “First-order stability cells of active multi-rigid-body systems,” *IEEE Transactions on Robotics and Automation*, vol. 11, no. 4, pp. 545–557, 1995.
- [108] M. Alshiekh, R. Bloem, R. Ehlers, B. Könighofer, S. Niekum, and U. Topcu, “Safe reinforcement learning via shielding,” *CoRR*, vol. abs/1708.08611, 2017. arXiv: 1708.08611.
- [109] T. Mannucci and E. van Kampen, “A hierarchical maze navigation algorithm with reinforcement learning and mapping,” in *2016 IEEE Symposium Series on Computational Intelligence (SSCI)*, 2016, pp. 1–8.

- [110] P. Mirowski, R. Pascanu, F. Viola, H. Soyer, A. J. Ballard, A. Banino, M. Denil, R. Goroshin, L. Sifre, K. Kavukcuoglu, D. Kumaran, and R. Hadsell, *Learning to navigate in complex environments*, 2017. arXiv: 1611.03673 [cs.AI].
- [111] P. Mirowski, M. K. Grimes, M. Malinowski, K. M. Hermann, K. Anderson, D. Teplyashin, K. Simonyan, K. Kavukcuoglu, A. Zisserman, and R. Hadsell, “Learning to navigate in cities without a map,” in *Proceedings of the 32nd International Conference on Neural Information Processing Systems*, ser. NIPS’18, Montréal, Canada: Curran Associates Inc., 2018, 2424–2435.
- [112] R. Alami, T. Simeon, and J.-P. Laumond, “A geometrical approach to planning manipulation tasks. The case of discrete placements and grasps,” in *The fifth international symposium on Robotics research*, H. Miura, Ed., MIT Press, 1990, pp. 453–463.
- [113] M. A. Farooqu, T. Tanaka, Y. Ikezawa, T. Omata, and K. Nagata, “Sensor based control for the execution of regrasping primitives on a multifingered robot hand,” in *Proceedings 1999 IEEE International Conference on Robotics and Automation (Cat. No.99CH36288C)*, vol. 4, 1999, 3217–3223 vol.4.
- [114] S. A. Stoeter, S. Voss, N. P. Papanikolopoulos, and H. Mosemann, “Planning of regrasp operations,” in *Proceedings 1999 IEEE International Conference on Robotics and Automation (Cat. No.99CH36288C)*, vol. 1, 1999, 245–250 vol.1.
- [115] W. Wan, M. Mason, R. Fukui, and Y. Kuniyoshi, “Improving regrasp algorithms to analyze the utility of work surfaces in a workcell,” in *Robotics and Automation (ICRA), 2015 IEEE International Conference on*, 2015, pp. 4326–4333.
- [116] Hong Zhang, K. Tanie, and H. Maekawa, “Dextrous manipulation planning by grasp transformation,” in *Proceedings of IEEE International Conference on Robotics and Automation*, vol. 4, 1996, 3055–3060 vol.4.